2-2014

Chemistry of 6-Monobrominated Indigo, MBI

Hiroko Ajiki
Graduate Center, City University of New York

CHEMISTRY OF

6-MONOBROMINATED INDIGO, MBI

By

Hiroko Ajiki

A dissertation submitted to the Graduate Faculty in Chemistry in partial fulfillment of the requirements for the degree of Doctor of Philosophy, The City University of New York

2014

This manuscript has been read and accepted for the Graduate Faculty in Chemistry in satisfaction of the dissertation requirement for the degree of Doctor of Philosophy.

Prof. Lou Massa

Date

Chair of Examining Committee

Prof. Maria Tamargo

Date

Executive Officer

Prof. John Lombardi

Prof. Klaus Grohmann

Prof. Sasan Karimi

Supervisory Committee

THE CITY UNIVERSITY OF NEW YORK

Abstract

Chemistry of 6-Monobrominated Indigo (MBI)

By

Hiroko Ajiki

Advisor: Prof. Lou Massa

6-monobrominated indigo, MBI, is a component of a historically important and the most expensive colorant, Tyrian Purple. The colorant is remarkably stable under the sun, in the air and after extensive washing with water. The color is still vivid after thousands of years. Even though it has such a high stability, MBI and Tyrian Purple have color changes from purple to blue upon temperature changes. This color change has been known for long to certain people, but the mechanism of the color change was unknown.

Tyrian Purple also has recently attracted interests for applications towards semiconducting material due to its ambipolar property and high stacking structure and towards its biomedical applications.

Though other chemicals in the colorant have been studied and analyzed well, MBI is the least studied and understood chemical. The full investigation of the chemistry of MBI has been conducted and reported in this study.

Acknowledgments

I would like to express my deepest gratitude to my thesis advisor, Prof. Lou Massa, for introducing me to the problem, for his guidance, encouragement, financial support through all the years of my graduate program, also to have introduced the importance of collaborating with many people for one problem.

I would also like to thank my Committee Members, Prof. John Lombardi, Prof. Klaus Grohmann and Prof. Sasan Karimi for their time, constructive criticisms, and helpful comments toward my project from different point of views.

I would like to thank Dr. Federica Pozzi, Dr. Marco Leona and other people at the Department of Scientific Research of the Metropolitan Museum of Art, for the help with experiments and instruments for Raman spectroscopy and uv-vis spectroscopy analysis in the lab.

I would like to thank Dr. Lulu Huang at NRL for the support for the DFT calculation.

Prof. Steve Greenbaum at Hunter College, Dr. Paul Sideris and Dr. Subhasish Chatterjee at City College for the help with 13C solid NMR analysis for the instruments in their labs.

I would like to thank Prof. Roger Lalancette at Rutgers University and Dr. Lou Todaro for their time to help me learning about crystallography.

I would like to thank Mr. Uesaka and the Scientific Research Division at Juraku Corp. and TOBA SEA FOLK Museum for their time and sharing the precious information and data with me.

I would like to thank Mr. Sonjae Wallace for checking my English for this thesis.

Prof. Zvi Koren to have introduced the problem to us.

Prof. Keith Ramig and Ms. Olga Lavinda for their contributions to synthesis of MBI, and to them and Dr. Jacopo Samson for the TEM experiments, and Dr. David Szalda for his contribution to the crystallography analysis.

I would like to thank Prof. Seojoo Jang at Queens College and his lab members, Mr. Mirali Devi, Dr. Daniel Montemayor and Dr. Eva Rivera for their help and for the professor’s financial support in the very last time of my program.

To my old friends, Stephanie Liu, Mari Yoh, friends in Japan, my landlord, Ms. May Hsu, and my former supervisor at RIKEN, Ms. Mayumi Yoshida, I would like to show gratitude for their all-time support in many ways through the years.

Lastly, I would like to show the gratitude to my family in Japan for all the support and help they have provided me.

Table of Contents

PART II: Color Properties of MBI

PART III: Discussion and Conclusion

List of Tables

List of Figures

1. Introduction

1.1. MBI: What is the problem, Why it is interesting, Who is interested

Tyrian purple or Royal purple is a historically important and highly expensive colorant. It is extracted from certain snails' hypobranchial gland and is said to take 2000 – 10,000 snails to make only 1g of Tyrian purple[1–6]. 6-monobrominated indigo (MBI) is a component of this dye and has not yet been fully studied compared to other components[2,3]. Also, it is known to have a color change from purple to blue upon heating[7]. The color change is observed with wool fabrics dyed with MBI and heated in hot water and also with hot air gun. At around 60 degree in Celsius, the color changes from purple to blue[8]. The reversibility of the color change of pure MBI has not been observed. Although, the reversible color change with Tyrian purple has been observed and recorded[9]. The mechanism of this color change is still unknown and has been a mystery for color chemists for long[10].

Tyrian purple is an amazingly stable colorant and remains vivid even after multiple washing and thousands of years[1,2,4,11–14]. Yet there exists the color change with Tyrian purple by itself upon heating also, which has been known for long, but has not been fully studied. The colorant is very stable upon the exposure to the air, to the sun, and also upon washing with water. This remarkable high stability to the air and to the sun as well as having 2 electron donors and 2

acceptors sites within its system recently draw high attention toward the application as an ambipolar semi-conducting material in the solar energy field[15–19] and more efficient synthesis procedures have been filed for patents in the last several years[20–22]. Some researchers are interested in its biomedical applications too[23–25]. Also, the color change of Tyrian purple has been observed as reversible by Juraku Corporation[9]. Recently, Zvi Koren found that a certain sea snail with purple glands contains significantly high percentage of MBI[26]. Since Tyrian purple has been very precious and thereby a symbol of wealth and power to many people and cultures including the Jews, Roman Emperors[27], and such, the dye has been used in many historically important things, such as textiles, art objects, bibles, manuscripts which also can be important evidence throughout the history[28]. Studying and analyzing MBI can provide clues to identify and re-evaluate these valuable objects for their zoological and geographical origins and authenticity[26] as well as the recent interesting applications.

1.1.1. Historical Importance

Different names have been used to call Tyrian Purple because it has been used in many countries, cultures and for such a long time. Tyrian Purple may be the most famous name. The next most common name probably Royal Purple[4]. In Japan, it is called Kai-Murasaki (snail purple) and/or Teiou-Murasaki (Imperial Purple)[4].

Figure 1.1. Byzantine Emperor Justinian I, wearing Tyrian purple, 6th-century mosaic at Basilica of San Vitale, Ravenna, Italy

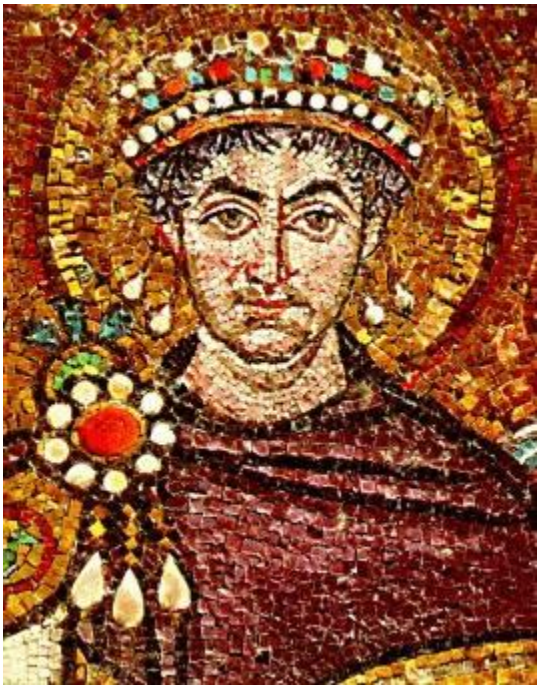

The first evidence of this colorant usage is dated as old as BC 1600 in the ancient Phoenician[4]. The actual dying methods with Tyrian purple used in the historical objects are not well-known despite the fact that there are some records. It is noted that most of these methods do not work as

expected if they are reproduced. It is considered that because the colorant is very expensive and its color was considered to be very important, the traders did not report the actual methods when they were asked[4,14]. And there exists time when the Tyrian Purple industry was diminished in the Mediterranean around AD 1453 when Turkish troops entered Constantinople and the Byzantine Empire (the Eastern Roman Empire) was demolished, until its usage has been restored in other parts of the world around 1900, when an American anthropologist discovered that same types of sea snails exist in Mexico and have been used for dying threads, which might have contributed to the lack of information of actual methods with Tyrian Purple in the past[4].

1.1.2. The Color and Snails

The Tyrian purple is extracted from the purple glands of certain types of sea snails. There have been found about 78 types of these sea snails in the world and 65 types among them exist in Japan[4]. There are several types of snail known to be used commonly in Mediterranean, Central America[27], and Japan. In the Mediterranean, common types are: *Murex trunculus*, *Murex brandaris*（シリヤツブリ）, and *Purpura haemastoma*. These shell mounds have been found in the Mediterranean. In Mexico and Peru, the common types are: *Concholepas peruviana*（アワビモドキ） and *Purpura patula*（ヒメサラレイシ）(Figure 1.2) [4].

Figure 1.2. Common snails shells used for snail-purple dyeing: Murex brandaris, Concholepas peruviana and Purpura patula (from left to right)

Japan is not a well-known country for the snail purple usage and in fact, they usually make purple colors from plants sources[4,29]. But in 1994 by using 3-D fluorescence spectrum analysis for the determination of the natural dyestuffs used for an ancient coloring cloth without damage of the cloth, Mr. Ujo Maeda found that fabrics and bracelets found in the Yoshinogari remain in Saga-prefecture in Japan, which is dated to be about 2000 years old have used snail purple, instead of plants-source purples, which was then considered to be the only source used for purples used in Japan in past[29]. This was a big sensation to Japanese and it is the first record of snail purple usage in Japan up to now. The shell mounds of these snails with holes in the shells have been found in other areas of Japan also. The hole is located where the purple glands can be removed from. Although, it is not certain if these holes and snails were used for snail purple dying, or for just consumption of snails and to remove the bitter-taste glands. Also, people in certain areas do use snail purple for ritual purposes in Japan[4,13]. In Shima in Mie-prefecture, professional female divers (Ama-san), who dive for pearls, marine snails, fishes, and such use snail purple to write ritual symbols, called Doman and Seiman, on their long handkerchiefs (Tenugui) and wrap their heads when they dive. Since they dive into the sea up to around 5 m

without an oxygen tank and with the simplest tools (see Appendix B.), this diving job can be very dangerous; these symbols are meant to protect them from evil spirits in the sea[4,30,31]. Ishigami-shrine (石神神社) in Shima uses these symbols for its Omamori (charm) and dyes the symbols with snail purple[31]. In Okinawa, also divers/fishers use snail purples to write their family's crests on the towel and wrap their head when they go to the sea[4]. Tyrian Purple, as well as Tekhelet blue, which is another type of snail-dye, also have been used often for ritual purposes in the Western cultures. Biblical Hebrew describes about the snail dyeing and the colorant being used for the garments of the High Priest[32]. In Peru, the ritual fishing mesh was dyed with Tyrian Purple (Figure 1.3)[4].

Figure 1.3. The ritual fish mesh from Peru (~2 m x 6 m size, about the 1st A.D. old). Owned by Juraku Corp., Japan.

After Mr. Tsuneo Yoshioka, a Japanese chemist and textile-dying artist introduced snail purple dying method with Juraku Corporation to Japan widely in the late 1960's, it has been used in expensive kimonos too[4] (see Appendix B.). The common snail types used (and eaten) in Japan are: *Rapana thomasiana (アカニシ), Thais clavigera (イボニシ), and Thais inteostma (クリフレイシ)*[4]

The color dyed with Tyrian purple is extraordinary stable. We can still see the manuscripts, paintings and fabrics whose colors are still vivid for years. Some of them are already thousands of years old. It is said that the color becomes even more vivid upon washing with water[3,4]. It's been said it is even more beautiful and shines under the moon lights[29]. Ujo Maeda said the fabrics dyed with snail purple reflect blue tones under sunset lights whereas fabrics with plant-purple reflect red tones. And this was when he realized those fabrics from the Yoshinogari remain are not dyed with plants[29].

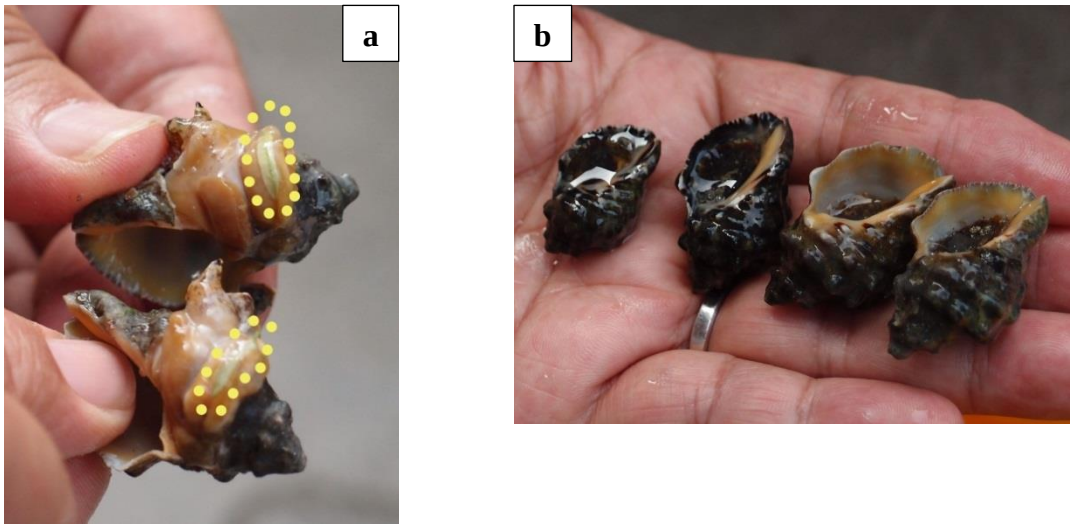

Figure 1.4. (a) Purple glands to be used for snail-purple dying are in yellow circles. Note how small they are. (b) Thais clavigera (left) and Thais Inteostma (right) used for dying at TOBA Sea Folk Museum (Umi no Haku Museum)

Purple color always attracts people from all over the world. It is considered as a royal color in many countries and in many cultures and religions. “Born in purple” means someone is born in a very wealthy family. In Asia, purple color is worn by high priests[14]. In Japan, purple was once declared by Emperor Suiko in AD 604 as the highest color out of 12 levels that shows the officials ranks in the occupation (Kanni-Junikai)[14]. It’s said that purple attracts people so much because it has the effect of stabilizing hormone balance, reducing nerve pain and psychological stress and Tyrian purple is being said to have the strongest effect of these[33]. Patricia Valdez found that in general, short wavelength colors are considered to be pleasant and in fact, blue-purple and red-purple, which are the colors of snail purple are colors considered to be pleasant in their psychological experiments. Valdez also found that although hue/wavelength does not have very strong effect tendency on emotions, blue-purple and red-purple are pleasant colors while they are also considered as the least arousal and dominant colors. The brightness has more effect than hues on the emotions according to the experiments[34]. Tyrian purple is famous of being very bright and vivid. Almost all the people I showed the sample dyed with snail purple said the color is very calming and bright when “purple” is not usually bright colors. When I saw a manuscript dyed with Tyrian Purple at the Library of Mr. J. Pierpont Morgan in New York, which is more than thousand years old, I was shocked how vivid and beautiful the color is. It was actually shining. Then I realized why some people have been obsessed with this color. While I was taking Raman spectra of various fabrics dyed with MBI and DBI, some of the fabrics were much shinier and brighter and looked almost metallic, compared to indigo under the microscope (Figure 1.5). The color being pleasant as well as being bright may be the strong point of snail purple. The beauty of color, the mysterious color change from fluorescent creamy yellow to

green to purple during the dying process as well as the amazing stability of color attracted people in the past and its esteem value once had Aristotle claimed that Tyrian Purple is more valuable than gold[6,35,36].

Figure 1.5. Dyed wool fabrics under the microscope: On the left (Indigo), center (MBI), right (DBI)

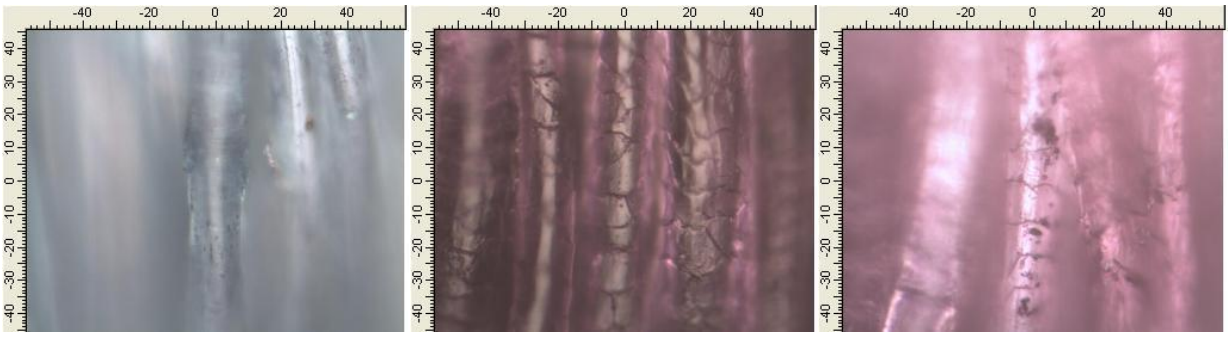

The colorant is extracted from purple glands of snails. In Mediterranean, the snail's shell was broken and the purple gland was removed. They grinded the purple glands, which was fluorescent whitish-yellow/green color at that point. This becomes purple once it is exposed under the sun (see Appendix B). This ground gland extract is very sticky and hard to handle, so people in the past invented several methods to work with it easily and more efficiently. Also, since thousands of snails are needed to make just a small amount of the colorant, it leads to the extinction of these snails in the Mediterranean. In Mexico and Peru, snails are not killed. They breathe on to the snail and wait for the snail to secret the milk. Then they rub the threads into the milk and return the snails into the sea. This is done at the rocky shores at full moon nights during November to March except for during festivals. Even for experienced people, this is a dangerous job[4].

Snails use the milk from the purple glands to protect themselves from other shell fishes such as oysters by making them numb. During the period of spawning, snails insert the fluids into their eggs to protect, therefore the color looks different if snails are caught and dyed during this period[4].

It is said that Hercules found that his dog eating these snails and the mouth of the dog turned purple later. In Japan, some of the snails of these types are edible and is said that people found that their fingers becoming purple after they removed the bitter-taste glands for consumption. The purple stain remains more than a week[4].

1.1.3. Use of the color in the past

Tyrian purple started being used in Phoenicia as early as in 1600BC. It was one of the major trading for them and the Phoenicians are famed in Classical Greece and Rome as ‘traders in purple’. The garments colored with Tyrian purple became status symbols for the Greek elite. The colored garments were highly controlled in Byzantine. Caesar wore the garment. Cleopatra dyed the sails of the ship which she took to Tarsos. Augustus limited wearing Tyrian purple only to emperors when he became the first emperor in the Roman Empire. Nero forbade the selling and wearing of Tyrian purple and executed those who did not follow. During AD 300 to 500, Tyrian Purple had been used in writing bibles, which is assumed to be used only by hierarches, as well as for Silver Books, whose papers were dyed with Tyrian Purple and written with silvers. The Tyrian purple industry continued until around when Eastern Roman Empire was demolished in 1453 AD with the over-hunting of snails for dying [4]. The Jewish rabbis still use Tyrian purple to color their tassels.

1.1.4. The Color in the modern time & its Chemistry

After Friedlander discovered a synthesis of 6, 6'-dibromoindigo (DBI) and separated DBI from snail purple in 1909, many chemistries coming from snail have been found. These chemical discoveries are quite new compared to its history[2,3].

The components of Tyrian Purple have been analyzed to be: DBI, MBI, indigo, and indirubins with some contaminations with other chemicals [3]. The phenomenon of the ground gland being whitish-yellow becoming purple has been found to be the reduction and oxidation of pre-cursors, leuco-forms of brominated indigotins[3].

Prof. Zvi Koren from Shenkar College in Israel discovered a particular snail with significantly high MBI contents % and he brought the color problem to us when Koren was doing his sabbatical research at Hunter College, CUNY with Prof. Lou Massa. This information can be utilized to find the source of Tyrian purple used in the past. Also, he observed the color change when he dyed wools with MBI from purple to blue upon heating in hot water.

The reversible color change from purple to blue upon heating with steam iron has been observed and recorded by the Scientific Research Division of Juraku Corporation with snail purple, but pure MBI has not been tested. Once the fabrics become cool again, the color changes back to purple with wool and cotton, but not with silk[9].

Our first hypothesis was that this change was due to the change in crystal structure before and after the heating. Therefore, by analyzing its crystal structures we can solve the reason for the color change by solving the atoms' positions change. This turned out to be not true; we found the crystal structures did not change[37].

Up to recently, the chemistry of DBI and Indigo has been well studied and is quite well known, including their crystal structures, and synthesis [3]. Yet the chemistry of MBI is not well known. Its synthesis was reported by Clark and Cooksey [2], but its crystal structure was unknown until our group recently analyzed[37]. We started from synthesizing MBI by ourselves to crystalize and obtain the crystal structure, which turned out to be much more complicated than expected. Also, during the process, I found that the MBI's purple color that we observe is different from the actual color that each MBI molecules has and MBI has even more interesting color properties.

1.2. Goal

This study is focused on MBI among all the other components of Tyrian Purple because it is the least understood chemical in the colorant and is the chemical, whose components vary and is present at very high percentage in one kind of snail[12,26,38]. There is a mystery associated with a temperature caused color change in MBI. By these techniques: synthesis, crystallization, Raman spectroscopy, uv-visible absorption and reflectance analysis, NMR and crystal structure analysis

with theoretical calculations, I want to finally determine whether the color change is inherited from its electronic and/or structural changes and where the differences in the observed color are inherited from.

The search for an answer to the color change has been long and difficult. There has been no obvious answer. Professors Zvi Koren and Lou Massa at first speculated the color change was associated with a geometrical change of structure that would be shown by crystallography. That turned out to not be the case. We began to study the molecule by all the other experimental techniques available to us. Finally some experimental hints began to indicate the color change might be related to the size of clusters. At that point the power of quantum calculations could be brought to bear on the problem. In the following chapters I relate the steps I traveled along the experimental and theoretical journey to a better understanding of the properties of MBI. The result is perhaps the best understanding now of MBI.

PART I

Preparations and Identifications of 6-Monobrominated Indigo, MBI

2. Synthesis

2.1. Synthesis

The systematic name of 6-monobromoindigo (MBI) is 6-brmo-2-(3-oxo-2, 3-dihydro-1*H*-indol-2-ylindene)-, 3-dihydro-1*H*-indol-3-one, $C_{16}H_9BrN_2O_2$, and its structure is as in Figure 2.1. One bromine atom is attached to its 6-position of indigo molecule.

Figure 2.1. The structure of MBI

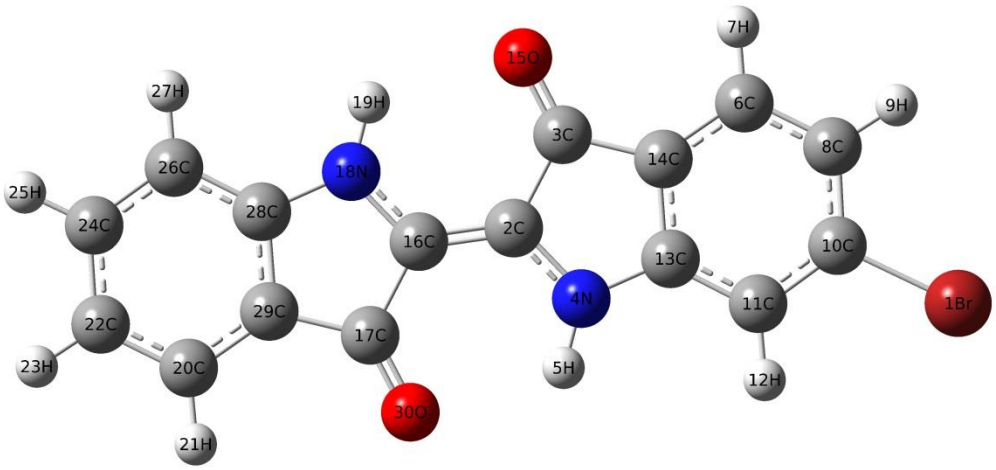

Since MBI is not commercially available, I tried to obtain MBI by purchasing from a synthesis company. After so many inquiries, I found only one company that agreed to synthesize MBI for us. The purchased product sent to us was analyzed by Koren with HPLC and was determined to

be not MBI, but was mostly 6-monobromo indirubin with small percentages of MBI, DBI and indigo. Therefore, I needed to synthesize MBI by myself using the previously published synthesis procedure[2].

2.1.1. Cooksey's Synthesis Procedures & Modifications

For the first trial, I followed the Cooksey's synthesis exactly[2]. The protocol is in 2 steps (Figure 2.2 & 2.3). The first step is to heat the mixture of 6-bromoisatin (1.0g, 4.4 mmol) and PCl5 (1.0g, 4.8mmol) in chlorobenzene ($30cm^3$) under nitrogen gas at 98-102ºC for 4 hrs. The second step is to cool the solution and add 3-acetoxyindole (716 mg, 4.2 mmol) to the solution and let it stand overnight. Then dilute the violet reaction mixture by ethanol (30cm x 3) and filter out. Wash the residue with ethanol (2 x $30cm^3$). The dark blue solid will be left.

Figure 2.2. The first step of synthesis of MBI

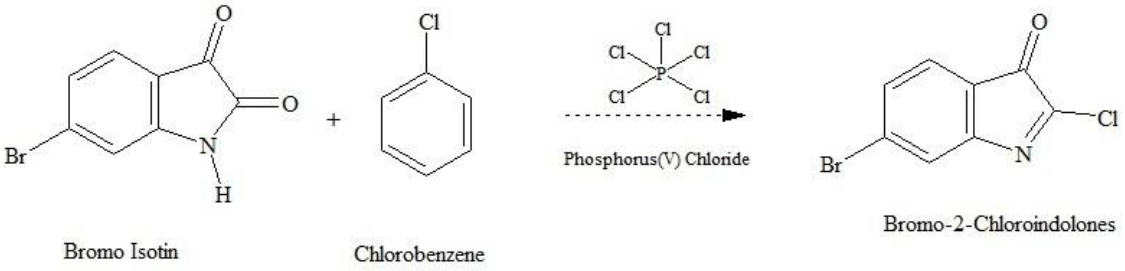

Figure 2.3. The second step of synthesis of MBI

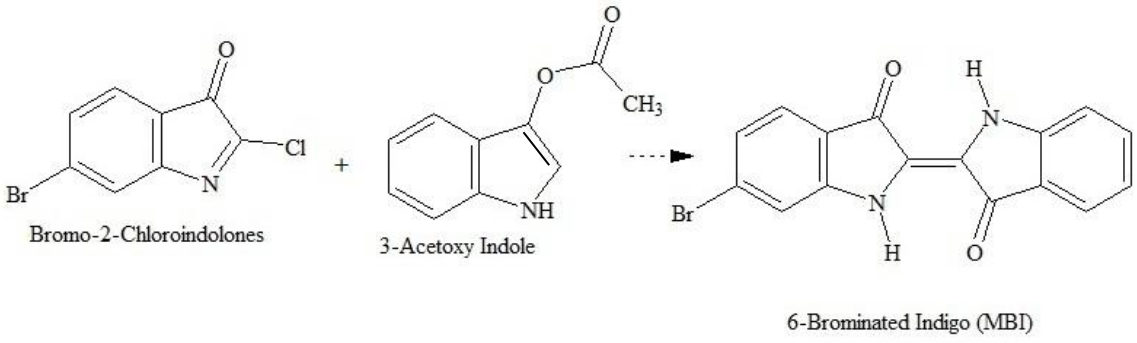

The final product, 6-mono-bromoindigo has bi-product(s), which was difficult to remove. Also, the products from this trial did not form good crystals. Most of them became smeared when they dried (Figure 2.4 & 2.5).

Figure 2.4. the Cooksey's method (Ethyl Benzoate): No crystals were obtained.

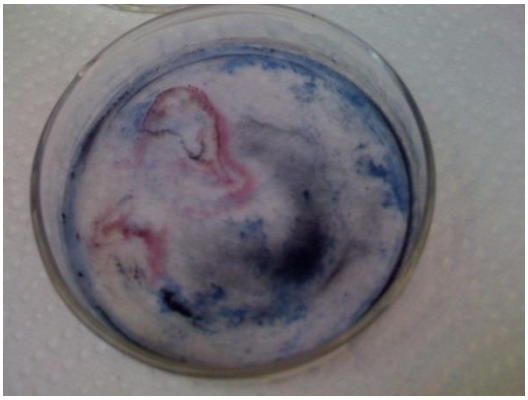

Figure 2.5. with DMSO: crystals were not large enough to give good diffractions.

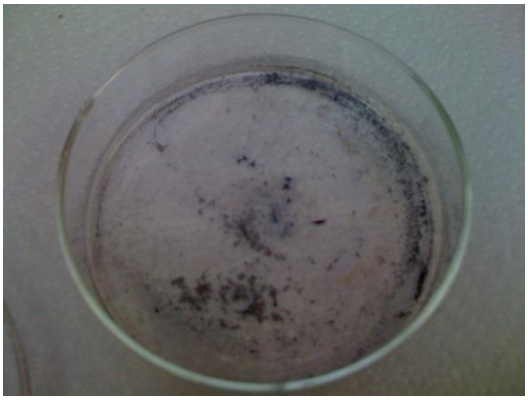

Therefore, I tried several different solvents to crystalize the sample. The best solvent was dimethyl sulfoxide but still the final crystal was not good enough to give good single crystal x-ray diffraction.

From the 2nd trial synthesis, I started to work with Prof. Sasan Karimi. According to the advice from Prof. Sasan Karimi, for the 2nd trial, the precursor, 2-chloro-6-bromo-3H-indol-3-none was isolated before proceeding further in order to increase the purity of the products to form better crystals.

The published synthesizing procedure of the target compound was not found, but instead, the procedure for 2-chloro-3H-indol-3-none [39–41] was used to isolate the target compound. Although, one of the papers mentioned that 2-chloro-3H-indol-3-none decomposes readily at room temperature, therefore it was not expected to be an easy process. The compound of our interest is

expected to be more stable, but it may not be stable enough to be isolated. This product did not form solids after the filtration.

Figure 2.6. 2-chloro-6-bromo-3H-indol-3-none

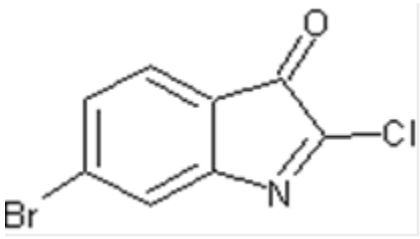

Figure 2.7. 2-chloro-3H-indol-3-none

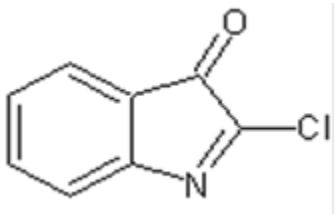

After heating the sample for 4 hrs as in the Cooksey's protocol, the yield of the produced target compound was analyzed as about 30% of the starting material so that the synthesis was modified to increase the yield by: (1) using benzene instead of chlorobenzene, (2) changing the heating hours from 4 hrs to 12 hrs, and (3) adding more PCl5 (50% more) and benzene (about 90% more).

At the 4th hours of heating, 2 N-H peaks were confirmed, one of them was from the initial compound and was being reduced, and the other was possibly a new product, which I assume as a bi-product and was increasing.

At the 6th hours of heating, these 2 peaks' integration reversed and the initial compound's peak was increased. It may be because of the protons switched back and forth. The reaction was

proceeded for additional 6 hours to determine how the products will be. But after the additional 6 hours of heating, other peaks appeared which show the product of the interest.

This 3rd trial's product did not form crystals or solids after the filtration.

The 4th trial was made by purchasing the pre-cursor, bromo-isotin from a company as well as with the following modifications to the original Cooksey's synthesis:

(1) Temperature used was 107ºC for the oil bath instead for 98-102ºC The actual temperature of the solution was assumed to be around 104ºC.
(2) The solution was filtered with vacuum and washed with an excess of methanol.
(3) Lights were turned off when the sample was weighed with a scale and aluminum foil was used to cover the funnel while filtrating.

While washing the sample with methanol, I realized how insoluble MBI is in methanol. The filtrate became much clearer at the end, but was still very reddish-purple. Although, the last filtrate seemed to be more bluish compared to the initial one when seeing the flask from its bottom, the filtrate seemed to be more reddish when seeing from its top or from its side. The initial filtrate was reddish-purple from any angle.

We tried to further purify the sample by the Soxhlet extractor, which was invented by Franz von Soxhlet in 1879 (Figure 2.8) [42]. This is typically used for the sample, which has a limited solubility with a solvent and its impurities are soluble in that solvent. The sample is placed in a thimble made from thick filter paper, which is connected to the round bottom flask with the solvent. The top of the thimble is connected to a condenser. The solvent is heated to reflux and

goes in the distillation path of the thimble. Then it goes into the thimble with a small chamber. The chamber is slowly filled with the solvent. When it gets almost full, the chamber released the solvent back into the round bottom flask through the siphon arm so that the chamber will become empty and finishes one cycle of purification. This process can be repeated automatically for many times[42].

We used this piece of apparatus because the particle size of the sample was very fine and it clogged gravity filtration systems and took hours to filter even once.

0.051g from the crude MBI from the 4th trial was purified by using the Soxhlet extractor with distilled methanol.

The methanol first appeared very purple in the chamber (Figure 2.9), which is supposed to be blue or colorless once the sample is purified.

The first purification took about 30 min and approximately 10 min thereafter. The purification system was left running until we saw a difference in the color of methanol.

The Soxhlet extraction was left running for about 70 hours and 30 min until the color of methanol became almost colorless. The product was weighted as 38mg after drying with nitrogen gas. Its purity was analyzed to be about 70% purity of the target product by Photo Diode Array Detector analysis (HLPC-PDA) by Prof. Zvi Koren, but did not crystalize large enough to obtain a good crystal structure. It was considered to be difficult to purify further also because of the possible decomposition of the compound upon the heating for long period of time.

The 5th trial was performed by Prof. Keith Ramig and Ms. Olga Lavinda at Baruch College, CUNY. They used the precursor that Prof. Lou Massa purchased from a company (TCI America), which was different from the company Prof. Sasan Karimi and I used.

The precursor, 6-bromoisatin was obtained from TCI America and other chemicals were purchased from Alfa Aesar.

Its purity was determined to be 93.4% by HLPC-PDA and the crystal structure was also determined with using this sample[37].

We later determined the purity of the two pre-cursors used and found the one they used is much higher purity than the one I used.

This tells us that the purity of the precursor is significantly important to start with because purification of the final product is much harder.

Figure 2.8. The Soxhlet extraction system

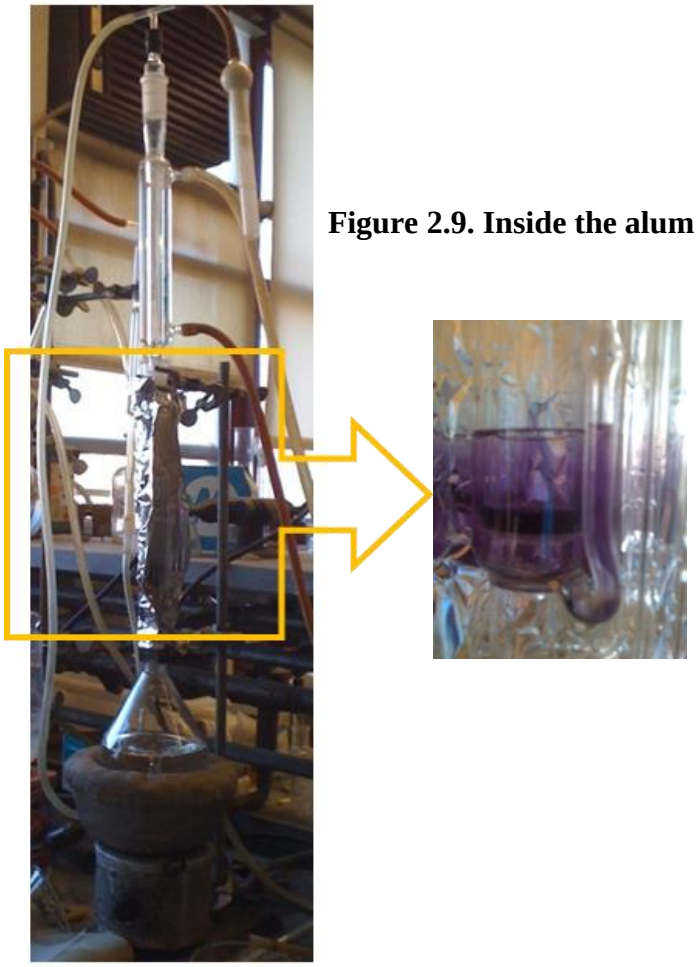

Figure 2.9. Inside the alum foil

Figure 2.10. After some cycles of the purification

Figure 2.6. Before starting the purification

Figure 2.12. After the completion of the purification

2.2. HPLC-PDA Analysis of the Compound and its Purity

2.2.1. HPLC-PDA Analysis

High performance (or pressure) liquid chromatography (HPLC) is a widely used separation technique to separate chemicals by using the distribution constant fundamental between the mobile and stationary phases. Yet, the fundamental is not easily measured, so instead, the technique measures the retention time of analytes. The retention time is the time that the analyte spends in the column and is a function of the distribution constant [43]. By using these time differences, analytes can be separated to purify. We used this technique to analyze if the synthesized sample is actually MBI, and also, its purity.

2.2.2. Experiments

The purity of the sample used for x-ray single crystal analysis was determined to be 93.4% using Photo Diode Array Detector analysis (HLPC-PDA) by Dr. Zvi Koren [26,38,44–46]. The samples used for the analysis were extracted in DMSO at 100 ºC for 5 minutes. A gradient water/methanol mobile phase was used with RP-18 XBridge column in the all-Waters chromatographic system with injected volume of 20 microliters. Retention times and the PDA-produced UV-Vis spectra

with standard dye components are compared for the analysis. The wavelengths used was 600 nm and 540 nm.

2.2.3. Results

The purity of the synthesized MBI is analyzed to be 93.4%. (Figure 2.13) and the major impurities are indigo, DBI and 6-monobromoindirubin (Figure 2.14).

Figure 2.13 shows the identification of the sample as MBI by its retention time at around 18 minutes at 600 nm. Figure 2.14 shows the further analysis for the impurities at 540 nm, which shows the main impurities are indigo (4.5%), 6, 6-dibrominated indigo (DBI), and then 6-monobromoindirubin.

Figure 2.13

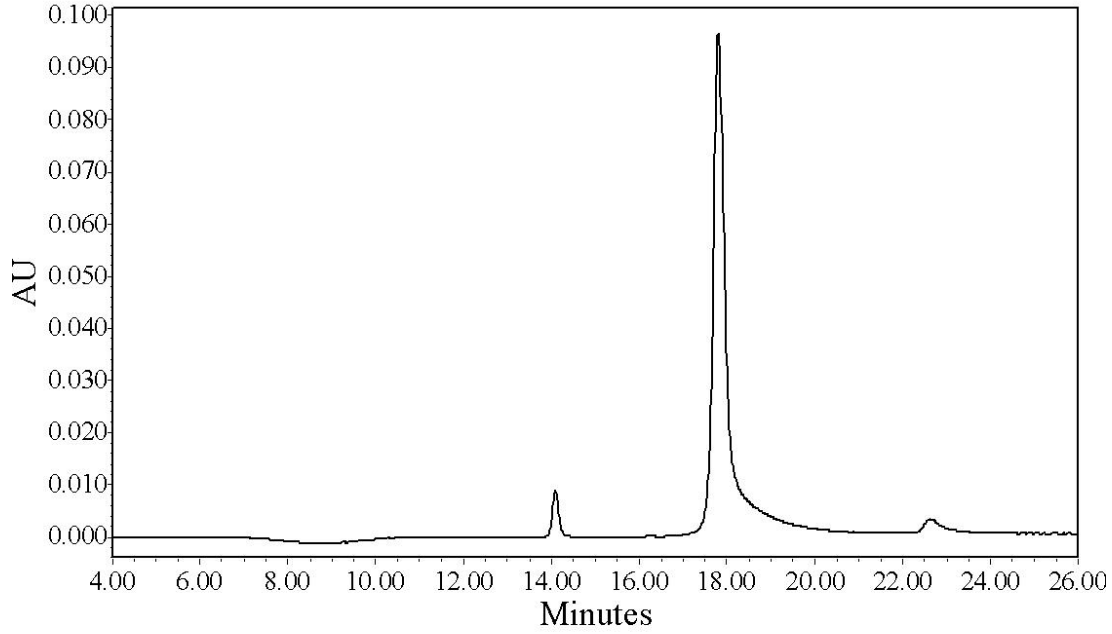

Figure 2.14

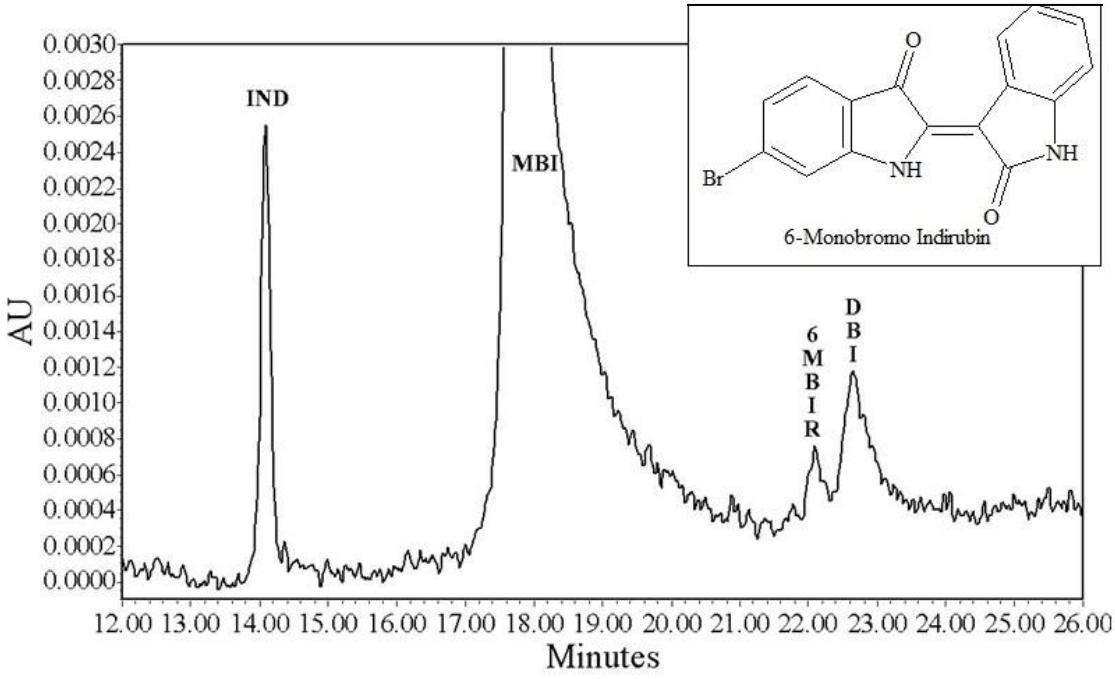

2.3. X-Ray Single Crystal Crystallography Analysis

2.3.1. X-Ray Crystallography

X-ray diffraction crystallography technique is based on the measurement of diffractions of electromagnetic radiation and is used for determination of atomic and molecular structure of a crystal. When x-ray is shone and passes through a crystal, it reacts with electrons in the atoms to produce scattering. When the x-ray is scattered in a crystal, constructive and destructive interference are produced, hence diffraction occurs. The constructive interference occurs only when the angle of the incident x-ray satisfies Bragg equation [43]:

$$n\lambda = 2d \sin\theta$$

Equation 2-1

where n is any integer, λ is the wavelength of the beam, d is the spacing between diffracting planes, and θ is the incident angle [47].

Single crystal x-ray diffraction crystallography technique was used to study the crystal structure of MBI and was determined for the first time [37].

2.3.2. Experiments

The sample was recrystallized using ethyl benzoate (100 cm x 3 times) by Prof. Keith Ramig and Ms. Olga Lavinda using the MBI sample which they had synthesized. The crystal structure was determined by Dr. David Szalda from Baruch College at the National Brookhaven Laboratory [37]

Below is the set-up used for the analysis (Table 2.1. Crystallography **set-ups**).

Table 2.1. Crystallography set-ups

Data Collection[37]	
Bruker APEXII CCD area detector diffractmeter	415 measured not refined
Absorption correction: multi-scan (SADABS; Bruker, 2005)	2180 independent reflections
T_{min} = 0.513	1558 reflections with $I > 2\text{sigma}(I)$
T_{max} = 0.745	R_{int} = 0.056

Szalda et al., D. J. Acta Crystallogr. Sect. C 2012, 68, 160 –

2.3.3. Results

Below is the summary of the MBI crystal data (Table 2.2. MBI crystal data):

Table 2.2. MBI crystal data

Cryatal Data (Szalda et. al[37])	
C16H9BrN2O2	V = 641.8 (3) A^3
M_r = 341.16	Z = 2
Monoclinic, *Pc*	Mo *Kalpha* radiation
a = 12.347 (3) A	miu = 3.21 mm^{-1}
b = 4.6558 (12) A	T = 173 K
c = 11.607 (3) A	0.25 x 0.10 x 0.02 mm
beta = 105.856 (8)°	

Szalda et al., D. J. Acta Crystallogr. Sect. C 2012, 68, 160 –

The crystal structure of MBI is disordered with one Br atom on one ring in the unit, which makes it asymmetric with a pseudo-inversion center [37]. The bond lengths and stacking of MBI units are similar to those in indigo and DBI, but due to the disorder, all the atoms are shifted equally by 0.34 Å (Figure 2.15) and the Br atom is 0.28 Å out of the mean plane, where DBI's Br atoms are only 0.09 Å out of the plane[37,48–52]. Also, the distance of C-Br in MBI is 0.08 Å, which is 0.26 Å

shorter than DBI[50]. But the major difference between MBI and among the two structures is the interactions made by the Br atom (or the atom on 6-positions). The Br atoms in DBI interact with the neighboring two Br-atoms with the two C6-Br6···Br angles of 92.6º and 167.6º, while the Br atom in MBI interacts with a neighboring hydrogen atom 6-position in one molecule and carbon atom at C6B position in another molecule (Figure 2.16) [37].

Figure 2.15. The positions of the atoms in the ring differ by 0.34 Å due to the Br atom.

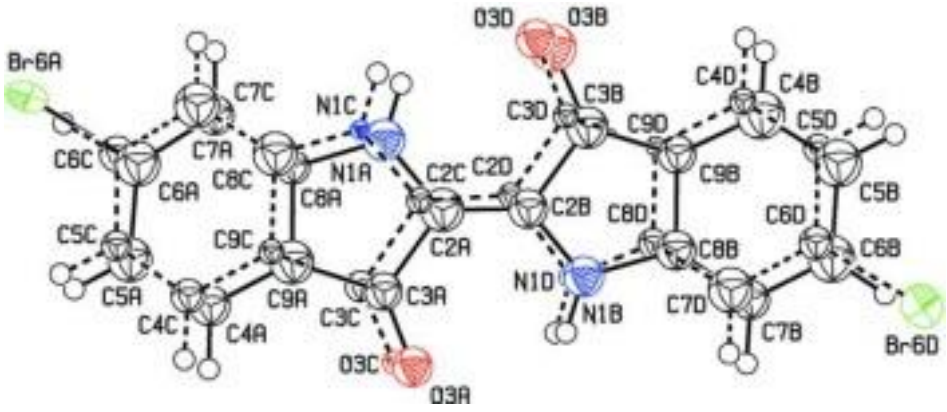

Szalda et al., D. J. Acta Crystallogr. Sect. C 2012, 68, 160 – 163.

Figure 2.16. How the Br atom interacts with neighboring atoms

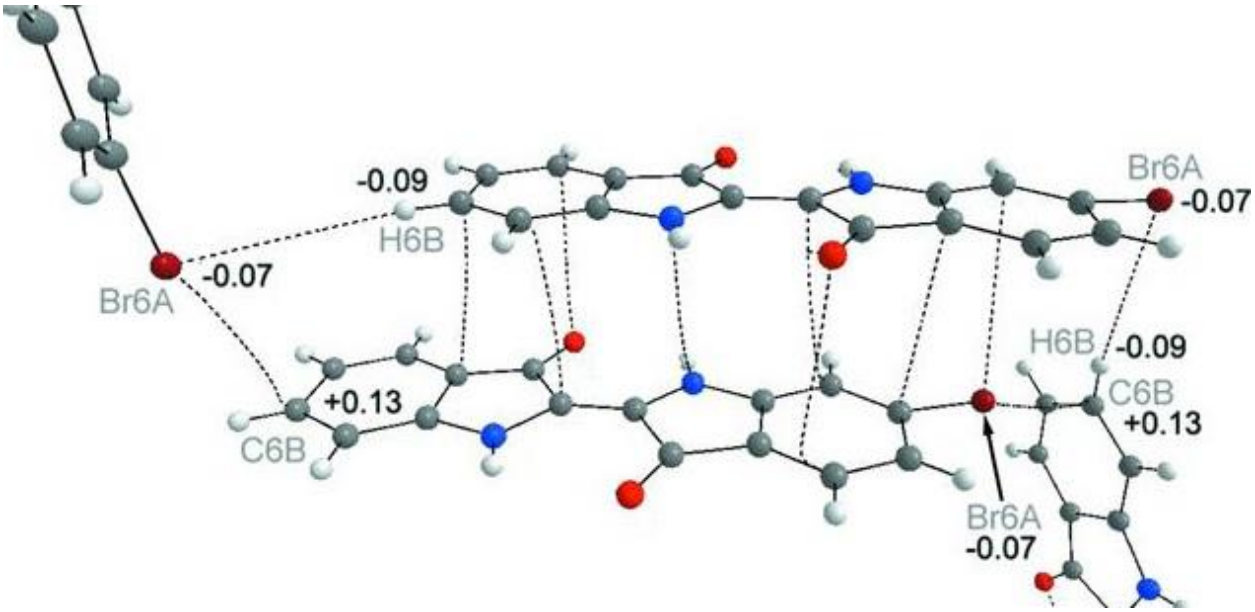

Szalda et al., D. J. Acta Crystallogr. Sect. C 2012, 68, 160 – 163.

Raman Spectroscopy Analysis

3.1. Raman Spectroscopy

Raman spectra of MBI and indigo were obtained to further analyze their structure and structural differences between them.

Raman spectroscopy is a spectroscopic technique to observe vibrational, rotational, and other low frequency modes in a system. Raman spectra are acquired by irradiating a sample with a powerful laser source of visible or near-IR monochromatic radiation of $h\upsilon_{ex}$. When the inelastic scattered radiation is of a lower frequency than the excitation radiation, it is called Stokes scattering. This occurs when a molecule in the ground vibrational level ($\upsilon = 0$) can absorb a photon of energy $h\upsilon_{ex}$ and reemit a photon of energy $h(\upsilon_{ex} - \upsilon_v)$, where $h\upsilon_v$ is the energy difference between the ground vibrational level and vibrationally excited states ($\upsilon = 0$ and $\upsilon = 1$). When the scattered radiation is higher than hv_{ex}, it is called anti-Stokes scattering. This occurs when molecules in a vibrationally excited states ($\upsilon = 1$) are excited and produce a Raman signal of energy $h (\upsilon_{ex} + \upsilon_v)$. These scatterings will be present on both sides of elastic scattering of Rayleigh scattering, which occurs with the emission of a photon of the same energy as the excitation photon $h\upsilon_{ex}$. Stokes scattering will be in the lower frequency region and anti-Stokes scattering in the higher frequency region. The magnitude of Raman frequency is the difference

from the Rayleigh lines. Therefore, the magnitude of Raman shifts is independent of the wavelength of excitation beams used [43].

The results obtained have similarities with FTIR and often are combined with the results from FTIR to study the structure of molecules, but the advantages over FTIR are the following:

- Carbon materials analysis is possible so that it is often used for fullerenes and nanotubes analysis
- Carbon-carbon information can be obtained so that it is useful for backbones information of molecules
- Non-destructive analysis is possible so that it is useful for valuable artifact, gemstone, and historical properties analysis
- No special material's cell is needed for analysis so that any format of analysis is possible
- Analysis of aqueous solutions are easy because of the Raman scattering of H_2O is rather small and OH-band is very sharp
- Analysis of any physical states, solid, liquid, and gas are possible

Although, one must be careful about the strength of laser beams to be used for analysis because the sample may be burnt if inadequate strength of laser beam is used. This becomes especially important when organic solvents are used [43].

MBI and indigo carry 2 benzene rings, which are expected to give strong Raman signals. Also, MBI is expected to give extra peak due to its lower symmetry (C1) compared to indigo (C2h), which comes from one heavy Br atom attached to its 6 position.

3.1.1. Experiments

The MBI sample used was prepared and its crystal structure was previously analyzed [37]. Prof. John Lombardi and Dr. Marco Leona arranged that Raman Spectra could be obtained using instrumentation available in the Department of Scientific Research of the Metropolitan Museum of Art[35]. All the spectra were acquired in the dispersive mode using a Bruker Senterra Raman apparatus, excitation at 785nm and 488nm, an Olympus 100x long working distance microscope objective, a CCD detector, and holographic gratings providing a resolution of 3-5 cm-1 (1200 rulings/mm for the 785nm laser, 1800 rulings/mm for the 488nm laser). For measurements at 785nm excitation, a continuous wave diode laser was employed as the exciting wavelength. Measurements were taken collecting 1 scan with an integration time of 30 s, and the lowest output laser power available within the equipment in these experimental conditions, namely 1 mW, was selected in order to avoid sample damages. Measurements at 488nm were obtained using a Spectra Physics Model 2020 BeamLock Ar+ laser, with an output power of 0.25 mW. In this latter case, the spectra were obtained as the result of one scan with an integration time of 1000 s, in order to improve the signal-to-noise ratio.

3.1.2. Theoretical Calculations

Density Functional Theory (DFT) calculations were performed by Dr. Lulu Huang at NRL using Gaussian 09 (G09)[53] to obtain the theoretical Raman spectral information of MBI and indigo. The G09 program computes Raman spectra by calculating the polarizability derivatives of molecules. The polarizability derivatives are calculated with respect to nuclear Cartesian coordinates, and then were converted to derivatives with respect to mass-weighted normal coordinates at a stationary point of the geometry [54–58]. The crystal coordinate of MBI used for the initial geometry optimization was determined by David Szalda [37]. The exchange correlation functional and orbital basis functions used for a minimum geometry of MBI were Becke, Three-parameter, Lee-Yang-Parr (B3LYP) [59,60] and 6-31G (2d, 2p)[61,62]. A total of 84 vibrational frequencies (3N-6) have been calculated with the same quantum method and the basis functions.

3.1.3. Results

The Raman spectra of MBI and indigo are very similar despite the initial expectations for large differences, and look identical at first glance. Yet with careful inspection of spectra, differences in the region of lower wavelengths can be identified. MBI has more peaks in these lower wavelengths regions. These extra peaks are expected due to the lower symmetry of MBI (C1) than the symmetry of indigo (C2h). For the Raman spectra of MBI and indigo excited at 785 nm in the range of 300 – 1900 cm-1, there exists one dominant peak by a single line at 1580 cm-1 (for MBI) and 1572cm-1 (for indigo) with two much weaker lines at higher wavelengths at 1625 and 1700 cm-1. These lines have been assigned to C=O stretching modes for indigo [63]. The dominant intense line is assigned to C=C stretch of central bond.

In order to make a detailed assignment of Raman spectra of MBI and indigo, we multiplied the wavenumbers scale of the calculated by a scale factors of 0.958, which has been found to give excellent results in the past as well as in this case [64–66]. The results are shown in the Table 3.1. The results show an exact correspondence of the spectra features with expectations in the relative intensities of several lines and small wavenumbers shifts especially at lower number wavelengths. However, since the Raman spectra of MBI and indigo have strong similarity, the further comparisons of DFT and experimental spectra of indigo were carried to ensure and explain the small spectra differences by DFT calculations. The indigo spectra calculation was carried at the same level of theory as the MBI. The Figure 3.1 shows the comparison of the calculations results

of MBI and indigo in the region 400 – 1200 cm-1. The Figure 3.1 shows the DFT results and experimental Raman spectra of MBI and indigo. As you can see, the DFT calculated results show a very good match with experiments. Moreover, the small, but observable differences can be seen in the DFT calculations too. For example, the 1046 cm-1 line appear in both DFT and experiments sets, with no counterpart in indigo spectra. Likewise, the same is true for the 894, 716, 619, 576, and 516 cm-1 lines. For indigo, the 1149 and 599 cm-1 lines are observed and have no counterpart in MBI spectra. Other lines are common to both spectra with slight shifts for both calculated and experiment. As expected with the lower symmetry of MBI respect to indigo, more lines are observed than indigo.

We summarized the spectral measurements in indigo and MBI in Table1, with comparison to the recent work by Tomkinson et al [63]. These assignments of normal modes were done by using the visual comparison of normal modes displayed in GaussView[53]. Each Raman signal can be animated by GaussView and visually be checked and compared for its modes. The normal modes in the first column in Table 1 are obtained from visual inspection of the GaussView output. The 364 cm-1 line is assigned to C-Br stretching, and we have used the assignments of a work by Karapanayiotis et al.[67] on 6, 6’ dihalogen analogues of indigo for comparison as well. In Figure 3.5, we show a comparison of the Raman spectra of MBI at two different excitation wavelengths. The upper trace is at 785 nm and the lower is at 485 nm. Note that these two wavelengths lay on either side of the optical resonance at 616 nm. The most important differences are shown in the arrows. The several lines between 1200 and 1400 cm^{-1} change somewhat in intensity, and these are assigned as CH in-plane rocking motions. In addition, the two lines above 1600 cm^{-1} increase drastically in intensity at 488 nm. These are C=O stretch modes. The line at 940 cm^{-1} in 488 nm

does not appear at all in the 784 nm spectrum and is assigned to a CH out –of-plane rock. This assignment is to mode #46 of the (scaled) DFT calculation, which predicts a very low Raman activity. This is consistent with its extreme weakness at 785 nm, but not with the relative intensity observed at 488 nm.

Figure 3.1. Comparison of Raman spectrum of 6-monobromoindigo (MBI) with that of indigo at excitation of 785 nm

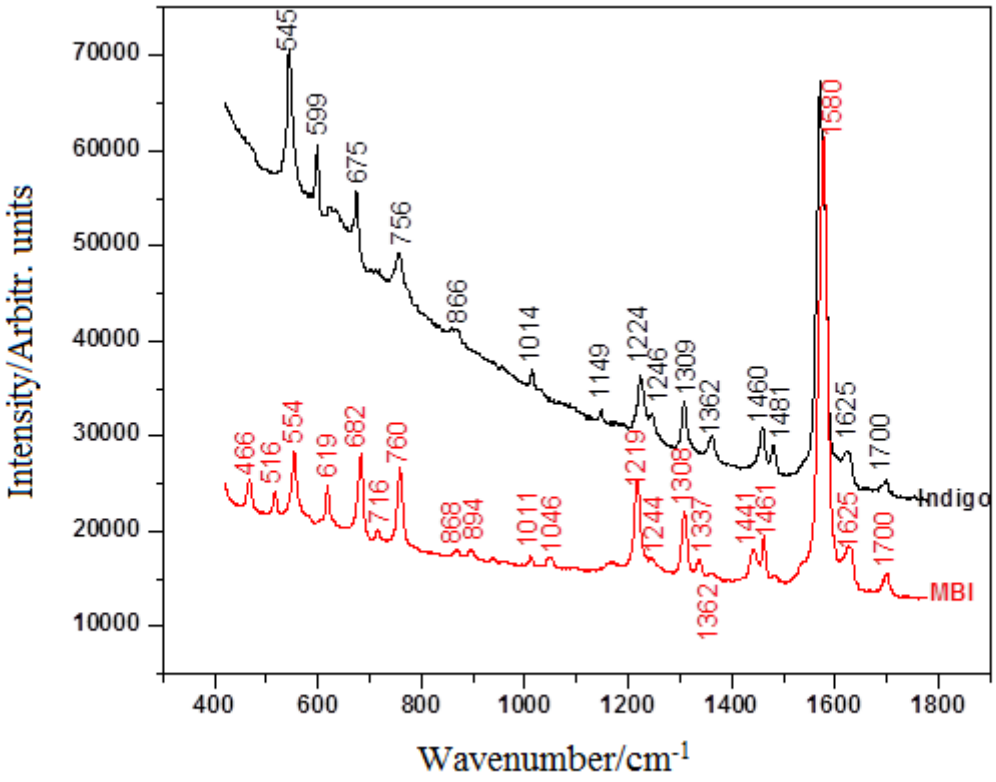

Ajiki, H.; Pozzi, F.; Huang, L.; Massa, L.; Leona, M.; Lombardi, J. R. Journal of Raman Spectroscopy 2012, 43, 520–525.

Figure 3.2. Comparison of Raman spectrum of 6-monobromoindigo (MBI) at 785 nm with that calculated by Density Functional Theory (DFT). The wavenumber scale of the DFT results was shifted by a factor of 0.958 to obtain the best fit.

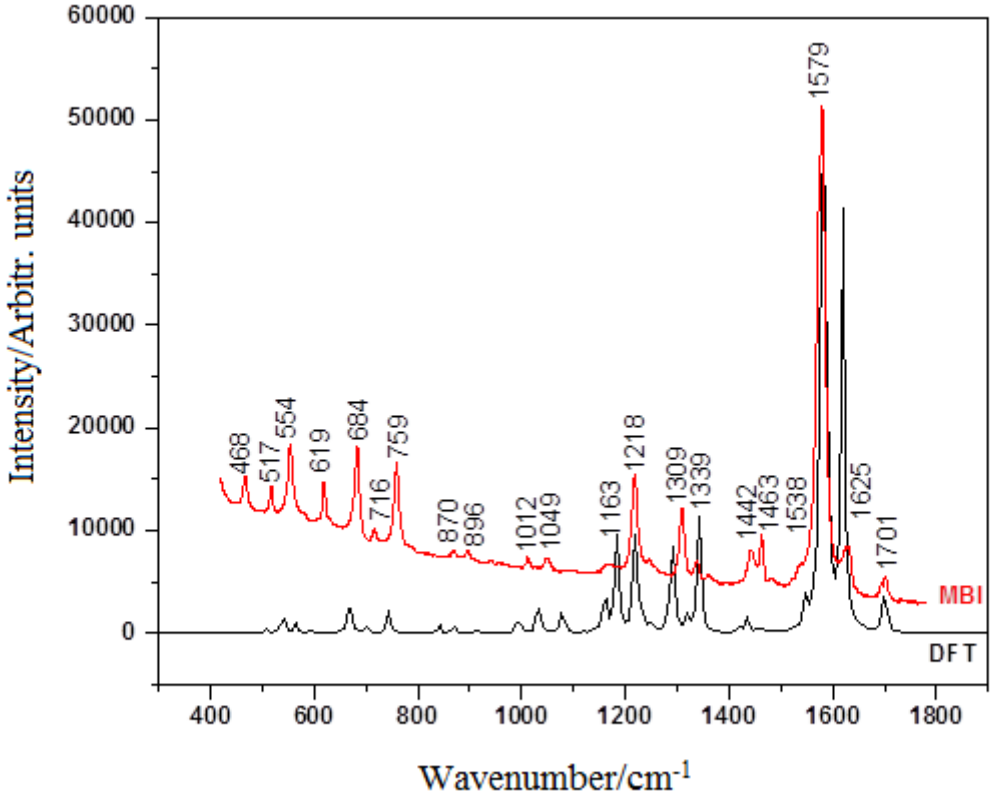

Ajiki, H.; Pozzi, F.; Huang, L.; Massa, L.; Leona, M.; Lombardi, J. R. Journal of Raman Spectroscopy 2012, 43, 520–525.

Figure 3.3. Comparison of DFT calculations (unshifted) for 6-monobromoindigo (MBI) and indigo

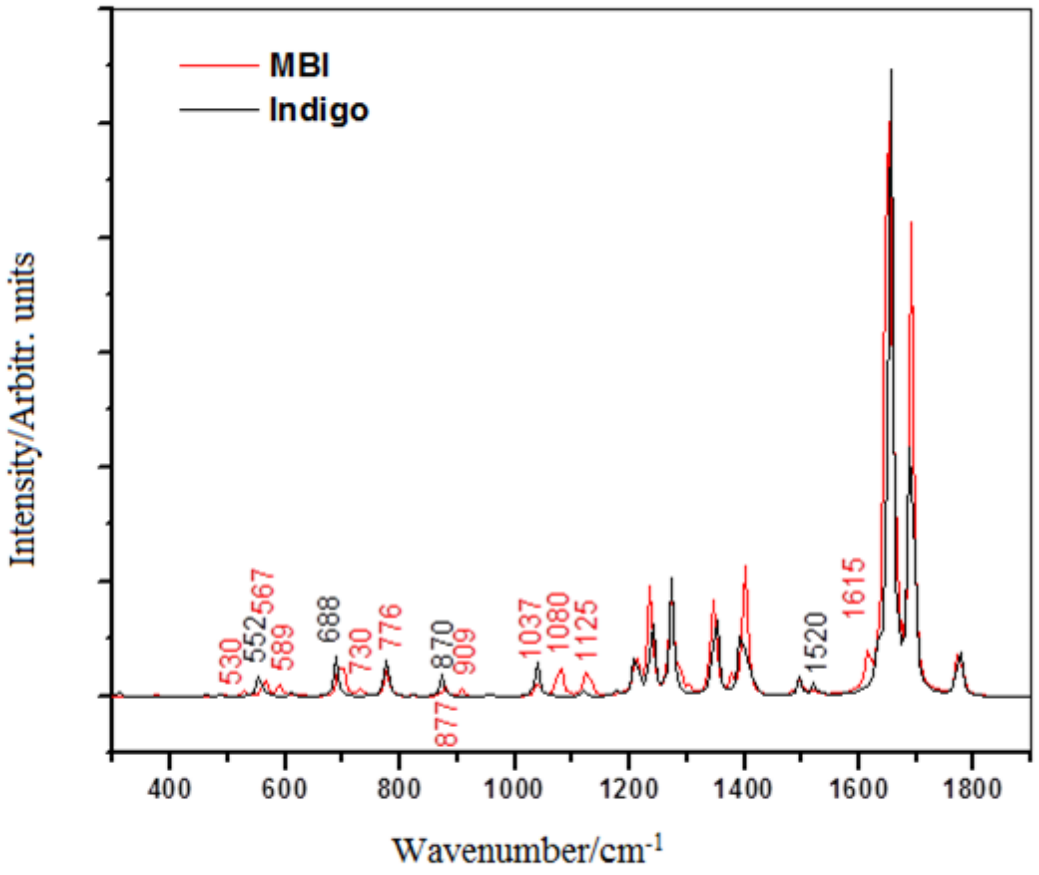

Ajiki, H.; Pozzi, F.; Huang, L.; Massa, L.; Leona, M.; Lombardi, J. R. Journal of Raman Spectroscopy 2012, 43, 520–525.

Figure 3.4. Detailed comparison of the DFT (upper) and experimental Raman spectra (lower) for 6-monobromoindigo (MBI) and indigo. The arrows highlight the correspondences between calculation and observation for those lines not common to the spectrum of both MBI and indigo

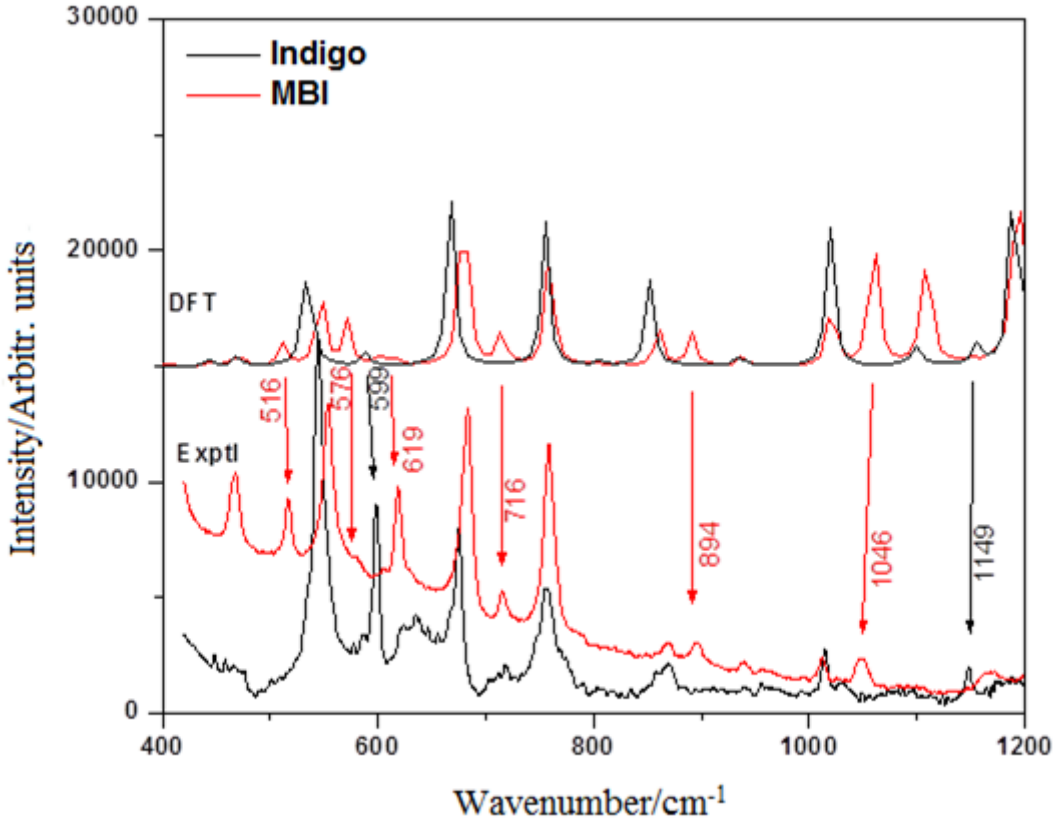

Ajiki, H.; Pozzi, F.; Huang, L.; Massa, L.; Leona, M.; Lombardi, J. R. Journal of Raman Spectroscopy 2012, 43, 520–525.

Figure 3.5. Comparison of Raman spectra of 6-monobromoindigo excited at two laser wavelengths. The top trace is at 785 nm and the bottom is at 488 nm. The most important differences are shown by arrows

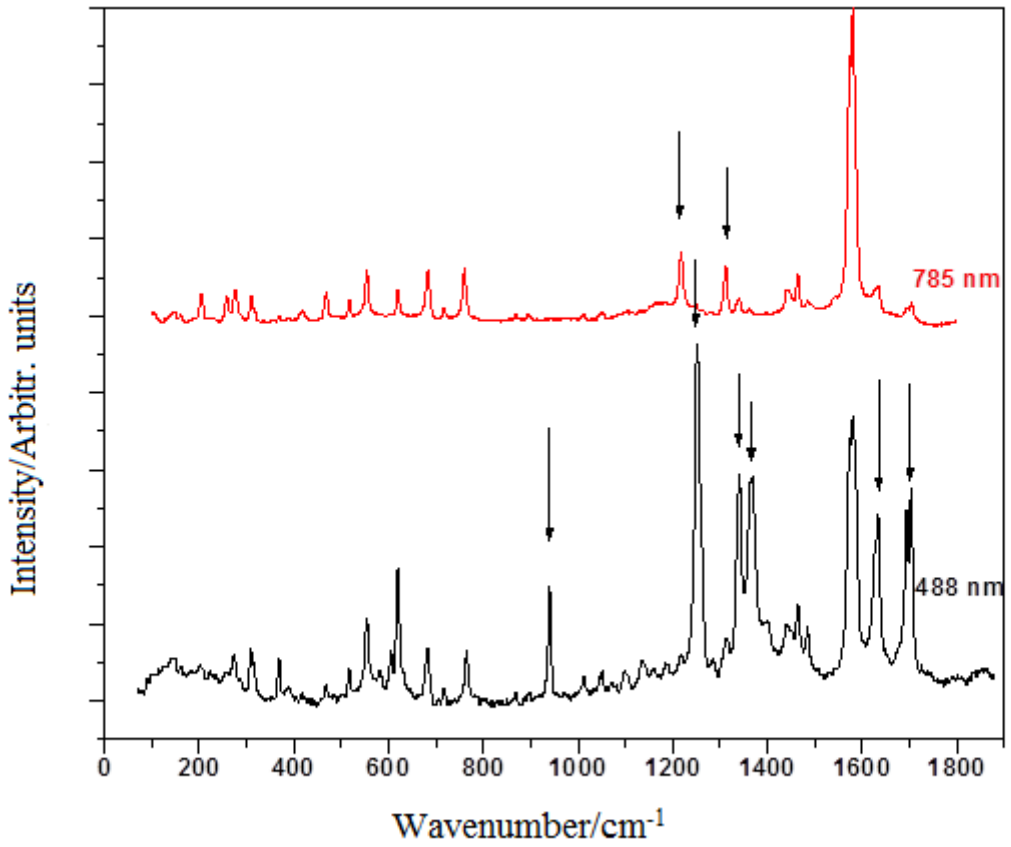

Ajiki, H.; Pozzi, F.; Huang, L.; Massa, L.; Leona, M.; Lombardi, J. R. Journal of Raman Spectroscopy 2012, 43, 520–525.

Table 3.1. Summary of DFT calculations and spectral measurements on indigo and MBI in comparison to the work by Tomkinson et al.[63]

	MBI	**DFT**	**Indigo**	***DFT***	**Reference**[63]		
		Mode #		***Mode #***	**Mode #**		
OC-C-CH stretch (Br)	267	13					
C=O stretch (Br)	304	14	302	*12*			
C-Br stretch	364	15					
	466						
CH, NH rock oop	516	22					
CH, CO rock	554	23	545	*20*	26	A_g	544
CC-C-C-CN stretch			599	*25*	51	B_g	598
C-C-C, CC-CO-CC stretch	619	25					
CH, CO ip rock	682	29	675	*26*	24	A_g	674
HN-CC-CO stretch	716	31					
C-NH-C=C-NH-C ip bend	760	34	756	*32*	23	A_g	758
C-C str, C-N str	868	41	866	*37*	22	A_g	868
C-C str, C-N str	894	42					
CH rock oop	940(*)	46					
C-C-C stretch--Benzene ring	1011	47					
CO-C=C-CO stretch (out of phase)			1014	*47*	20	A_g	1015
C-C-C stretch--Benzene ring	1046	48					
CH, CO ip rock	1125	50	1149	*53*	18	A_g	1147
CH ip rock	1219	57	1224	*56*	16	A_g	1224
CH ip rock	1244	60	1246	*59*	15	A_g	1248
NH-C=C-NH rock	1308	62	1309	*61*	14	A_g	1310
NH-C=C-NH rock	1337	63					
CH ip rock	1362	65	1362	*62*	13	A_g	1365
C-C-C stretch--Benzene-Br- ring	1441	66					
C-C-C stretch--Benzene-Br- ring	1461	67	1460	*65*	11	A_g	1460
CH rock oop			1481	*66*	10	A_g	1482
C=C stretch	1580	71	1572	*70*	8 & 9	A_g	1582
C=O in phase stretch	1625	73	1625	*72*	7	A_g	1625
C=C stretch, C=O in-phase stretch	1700	75	1700	*74*	6	A_g	1701

(*) Observed only with 488 nm excitation

Ajiki, H.; Pozzi, F.; Huang, L.; Massa, L.; Leona, M.; Lombardi, J. R. Journal of Raman Spectroscopy 2012, 43, 520–525.

Figure 3.6. Instruments with adjustable table (x-y planes) for samples at the Metropolitan Museum of Arts

Figure 3.7. The instrument from below (MET)

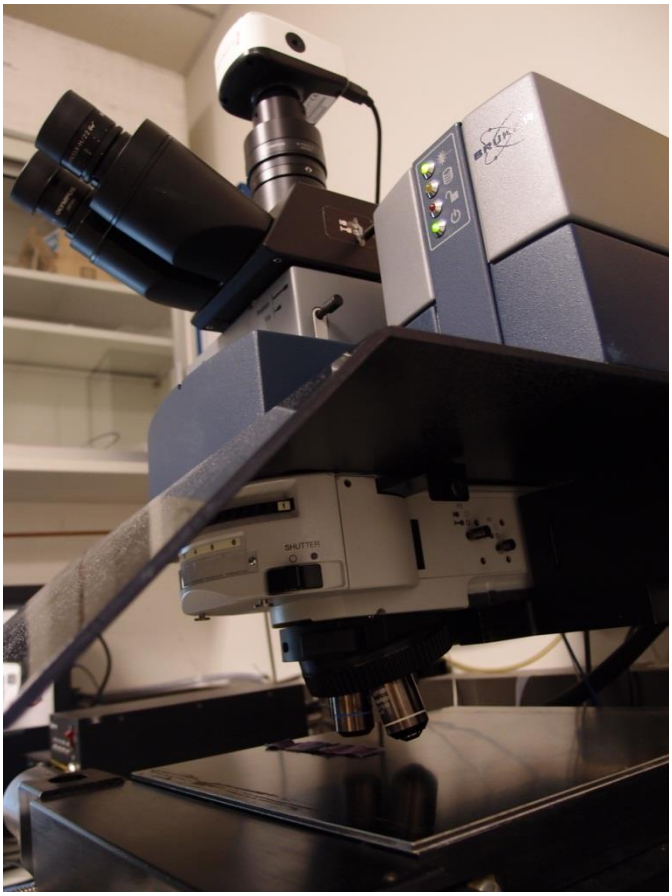

Figure 3.8. The interface of the software (MET)

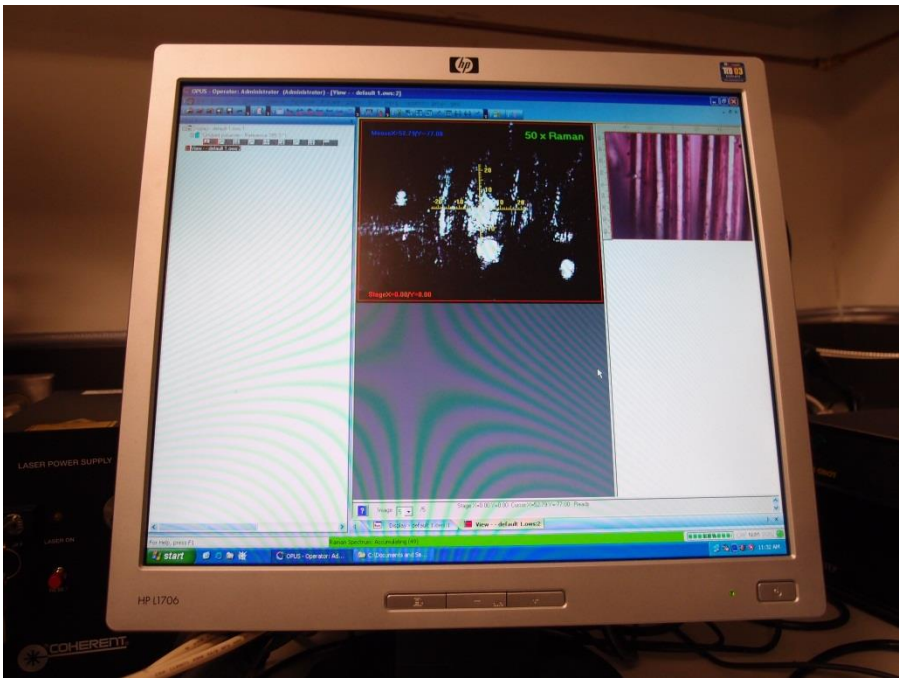

4. 13C Solid NMR Analysis

4.1. 13C Solid NMR.

Nuclear Magnetic Resonance (NMR) spectroscopy involves the measurement of absorption of electromagnetic radiation in the radio-frequency region of ~ 4 to 900 MHz. Unlike other techniques used in this study, such as Raman, UV, and visible spectroscopies, the energy change of nuclei of atoms are involved in the absorption process, rather than its outer electrons. Because of this, the analyte has to be placed in an intense magnetic field[43]. NMR analysis can be used for both qualitative and quantitative determination of species.

W. Pauli proposed in 1924 that certain atomic nuclei have the properties of spin and magnetic moment and hence it will lead to splitting into different energy levels upon the exposure to a magnetic field [43,68]. During the early period of development of NMR, chemists became aware that this energy difference can be correlated to the structural differences of molecules because the absorption of radio-frequency (RF) radiation is influenced by the environmental factor of molecules. The samples in an intense magnetic field are irradiated with periodic pulses of RF energy and these excitation pulses cause signals, which decay in between the pulses. These time-domain signals are converted to frequency-domain signals by Fourier transformation to give a spectrum[43].

When a nucleus with a spin quantum number of ½ is placed in an external magnetic field of Bº, the difference in energy ΔE between the two states after the splitting is given by

$$\Delta E = E_{-1/2} - E_{+1/2} = \frac{\gamma h}{4\pi} B^{\circ} - \left(-\frac{\gamma h}{4\pi} B^{\circ}\right) = \frac{\gamma h}{2\pi} B^{\circ}$$

Equation 4-1

Where the potential energy E of a nucleus in these states, or quantum states is given by

$$E = -\frac{\gamma m h}{2\pi} B^{\circ}$$

Equation 4-2

And the energy for the two states, m = +1/2 state and m = -1/2 are given by

$$E_{+1/2} = -\frac{\gamma h}{4\pi} B^{º}$$

Equation 4-3

$$\mathrm{E}_{-1/2} = \frac{\gamma h}{4\pi} B^{º}$$

Equation 4-4

This transition between the energy states can be correlated to the absorption or emission of electromagnetic radiation of a frequency v_0 that corresponds to ΔE. Then, the frequency of the radiation required to bring about the transition is obtained by substituting $\Delta E = hv_0$ into Equation 4.1.

$$v_0 = \frac{\gamma B^{\circ}}{2\pi}$$

Equation 4-5

4.1.1. Experiments

The first analysis with 13C solid state NMR was taken with the 70% pure MBI, the 93% pure MBI [37,69], and pure indigo; the first one is from my synthesis, the second one from Lavinda and Ramig's synthesis and the last one purchased from Sigma-Aldrich. The system set-up I used for the analysis was the following: JMTl 7 T magnet and a Varian S Direct Digital Drive spectrometer with Varian Apex 3.2 mm probe for the carbon spectra at spin speed of 17000/sec, with magic angle of 50.4 °, which was available at Prof. Steve G. Greenbaum lab at Physics Dept. of Hunter College, CUNY. The samples were measured at room temperature, as well as at ~60 ºC for MBI.

The second analysis was taken with the pure MBI[37,69] from Lavinda and Ramig's synthesis and the pure indigo, from Sigma-Aldrich. The system set-up used by Dr. Subhasish Chatterjee was the following: 13C CPMAS (cross-polarization magic angle spinning) measurements on the 750 MHz (1H frequency) Bruker spectrometer with 15 kHz magic angle spinning frequency at ~25 ºC, which was available at NYSBC of City College, CUNY.

Theoretical NMR shielding tensors were predicted using Density Functional Theory (DFT) calculations. The crystal coordinates[37,52] of MBI and indigo were first optimized with Density Functional Theory (DFT) [70–72] method with B3LYP functional with 6-31G(2d, 2p) basis set. Then the optimized structures are used for the calculations of NMR shielding tensors with the same level of method, functionals, basis sets and the Gauge-Independent Atomic Orbital (GIAO) [73–77]method using G09[53]. The reference used for the data analysis was TMS (tetramethylsilane: $Si(CH_3)_4$ with GaussView[53].

4.1.2. Results

The spectra of indigo and MBI taken at Hunter College look very similar with lots of noise (Figure 4.1 and Figure 4.2), and almost identical with broadening of peaks at first glance even after running the instrument over night to intensify the signals. The spectra of MBI at room

temperature and at 60º C look identical except with higher noise with 60º C, which is considered to have been caused from the heating (Figure 4.1). Because of the magnet availability, the samples were not able to be analyzed further at the lab, so that they were brought and further analyzed at the NYBSC. The second analysis also shows almost identical data with broadening of peaks. The difference between indigo and MBI may be difficult to be clearly detected by 1-D NMR analysis that we carried.

The peaks are still very broad (Figure 4.3) and thus it may not be appropriate to talk about the difference at this point, but with careful inspection of the spectra, in the first analysis of indigo and MBI, one can find subtle differences in the peaks at around 125 ppm and 135 ppm. The peak heights of these are switched in between indigo and MBI. In addition, the small peak around 118 ppm might be the difference between MBI and indigo also. Yet because of the noise present in the spectra, further refinement of data will be needed to confirm if these are coming from the structural differences in indigo and MBI.

When these experimental resonance peaks are compared with DFT calculation results, assignments of carbon atoms of indigo and MBI were possible (Table 4.1 and Table 4.2). The broadening of the first peak at 110.89 ppm with MBI seems to be resulted from the splitting of peaks of C26 and C11. C11 is the next carbon attached to Br-atom and C26 is the carbon at the same position in the other side of the ring. Another significant difference is in the third peak at around 131.81 ppm. For indigo, this peak is assigned to carbons at the 6-position. For MBI, one of these carbons is attached to bromine atom, namely C10. For MBI, this peak is assigned to C24,

which is another 6 position, but without bromine atom and on the other side of the ring. According to the calculation results, C10-peak is shifted to the left side, closer to the next peak. With the experimental spectra, the width of the fourth peak is about the same, but shows the decrease in the intensity and increase in the intensity in the fifth peak. Also, the 6th peak at around 185.91 ppm, which is assigned to carbons with oxygen atoms, show broadening as peak is splitting with MBI.

The assignment of 13C NMR CPMAS resonance peaks of indigo was compared to the previously published data with Domenech et al.[78,79]. Most of the assignments are in agreement, except for 3 carbons. These carbon atoms are C1 (C_q) , C3 (C_q) and C4 (CH).

Note that the labeling of carbon atoms is different between MBI and indigo, simply because of the crystal structures used for the theoretical calculations.

Figure 4.1. Spectra of 70% pure MBI, indigo, pure (93%) MBI

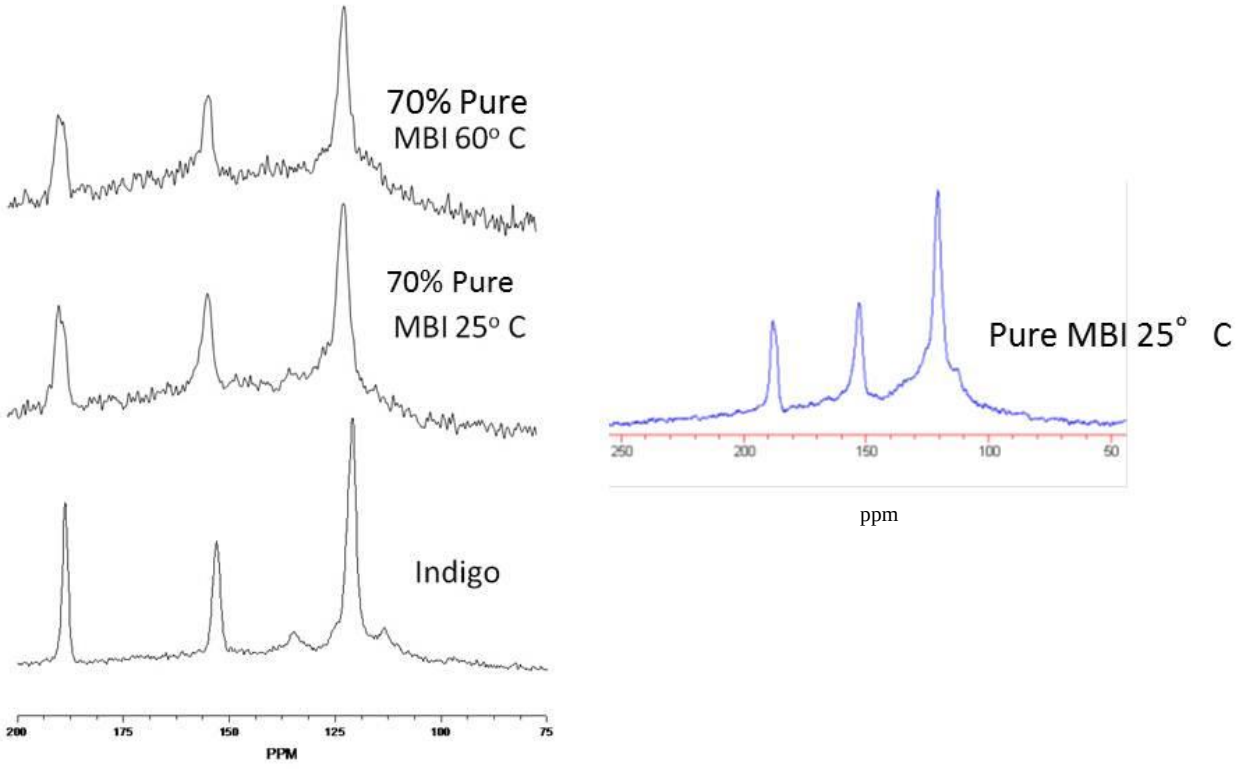

Figure 4.2. Spectra of indigo and pure MBI from the first analysis

LINE	PPM	WIDTH	AREA	FRACTION LORENTZIAN
1	188.724	99.68	14496101	0.956
2	152.988	137.36	14206018	0.956
3	138.547	6972.31	91577664	0.956
4	125.121	195.62	1660712	0.974
5	121.038	175.46	35870564	0.956
6	113.163	328.24	6364441	0.956
7	134.650	311.62	5107036	0.976

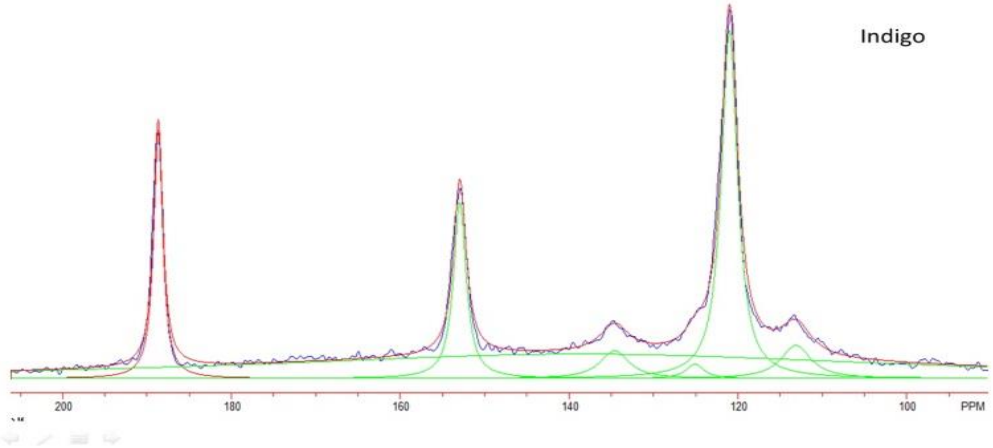

LINE	PPM	WIDTH	AREA	FRACTION LORENTZIAN
1	187.691	221.39	5103287	0.339
2	152.873	213.05	5349335	0.670
3	153.132	6738.13	88120952	0.932
4	125.465	687.82	5193827	0.954
5	120.718	244.04	13259490	0.850
6	112.908	264.26	962383	0.900
7	133.356	780.74	2519250	0.970
8	186.311	39.25	237331	1.000
9	190.458	34.35	115864	1.000

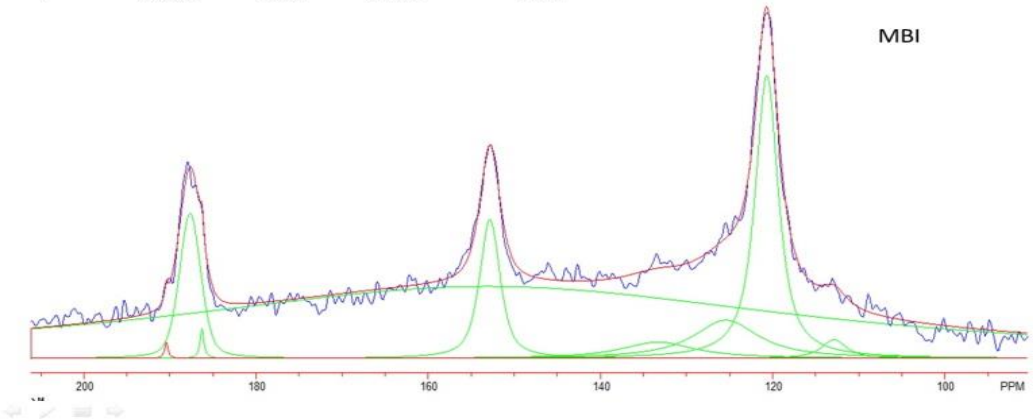

Figure 4.3. Spectra of indigo and MBI from the second analysis

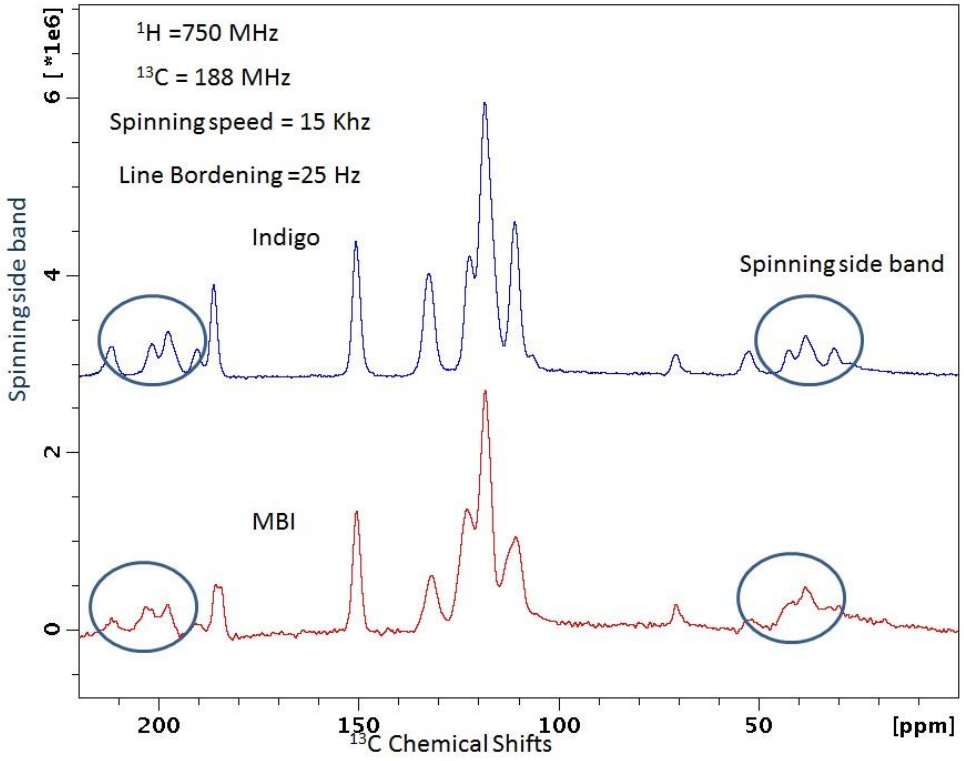

Indigo

No.	(ppm)	(Hz)	Height
1	111.04	20947.1	0.5293
2	118.50	22354.0	1.0000
3	122.30	23071.2	0.4381
4	132.54	25002.3	0.3607
5	150.82	28450.6	0.4873
6	186.21	35126.5	0.3214

MBI

No.	(ppm)	(Hz)	Height
1	110.89	20919.5	0.3496
2	118.50	22354.0	1.0000
3	123.03	23209.2	0.5303
4	131.81	24864.4	0.2457
5	150.52	28395.4	0.5169
6	185.91	35071.4	0.1936

Figure 4.4. Indigo NMR Assignments

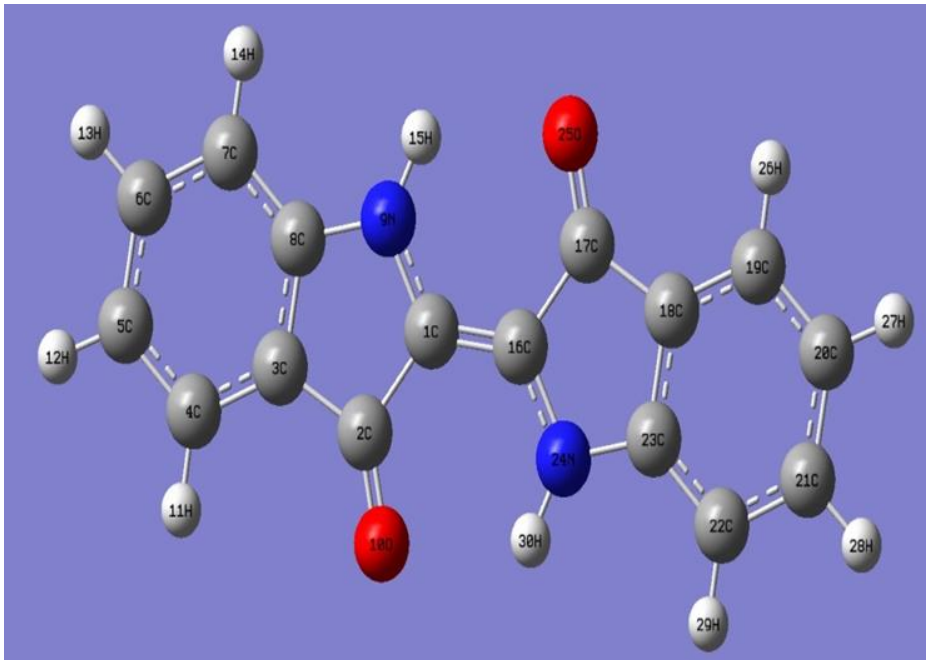

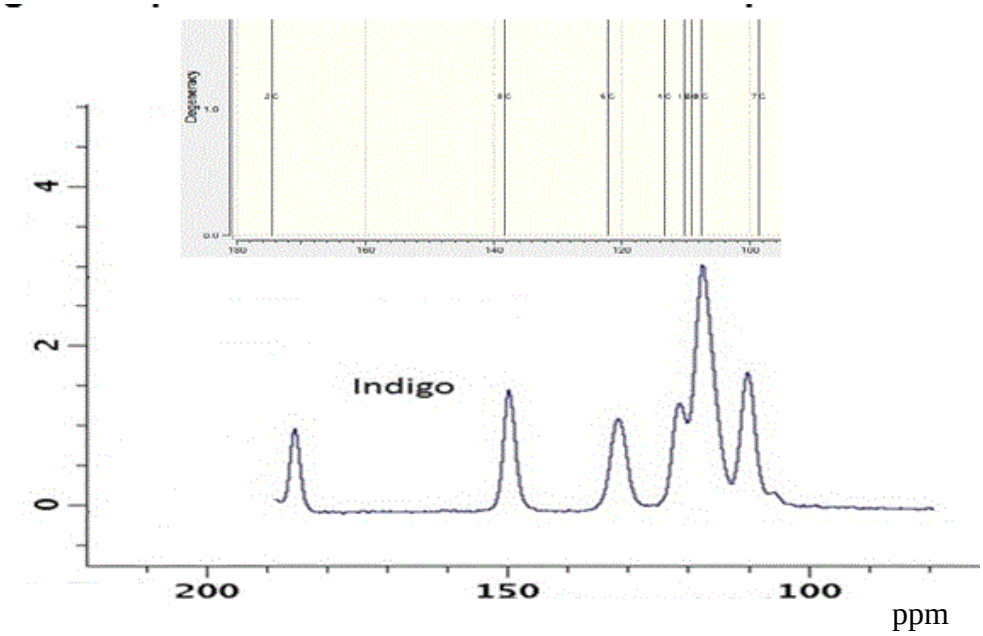

Figure 4.5. Comparison of DFT calculation and experiment

Table 4.1. Indigo NMR Peaks Assignments

Peaks (ppm)	Carbon Atom (Ajiki)	Carbon Atom (Domenech et al[78])
111.0	7(22): CH	7(22), 3(18)
118.5	1(16): C=O, 3(18): C_q 5(20): CH	4(19), 5(20)
122.3	4(19): CH	1(16)
133.5	6(21): CH	6(21)
150.8	8(23): C_q	8(23)
186.2	2(17): C_q	2(17)

*The red atoms are not in agreement

Figure 4.6. MBI NMR Assignments

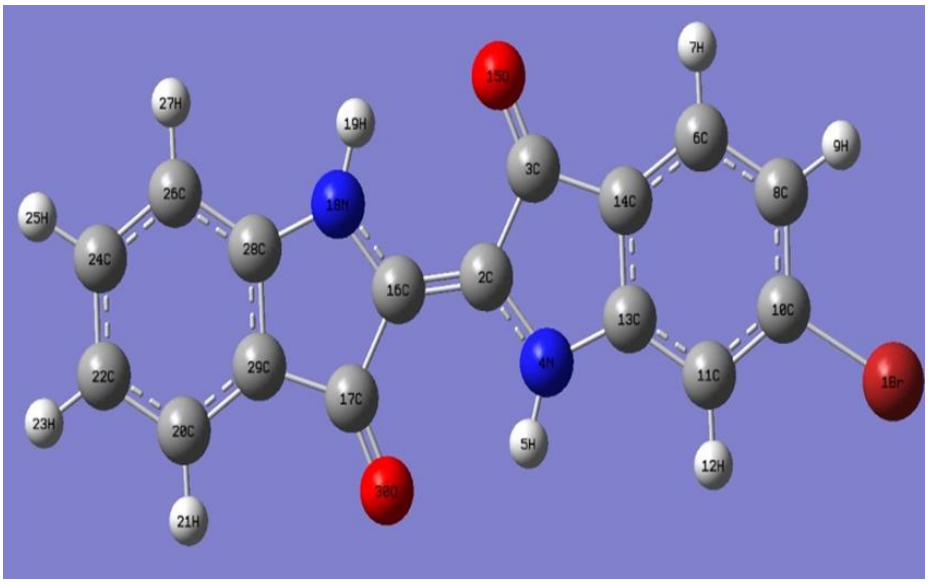

Figure 4.7. Comparison of DFT Calculation and Experiment

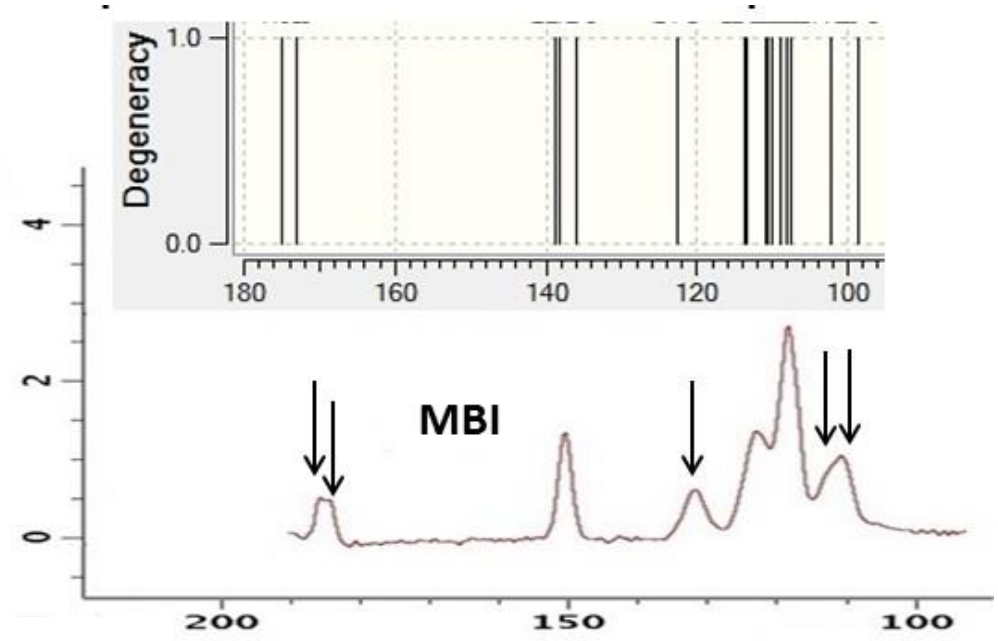

*The arrows show the differences from indigo

Table 4.2. MBI NMR Peaks Assignments

Peaks (ppm)	Carbon Atom (Ajiki)
110.9	26: CH
113	**11: CH**
118.5	6(18): CH 2(29): C_q 16(8): C_q
123.0	6(20): CH
131.8	**24: CH**
150.5	10: CH 13: C_q 28: CH
185.9	3: C=O
188	**17: C=O**

*The red carbons corresponds to the significant peaks to MBI

PART II

Color Properties of MBI

5. UV-Visible Absorption and Reflectance Spectroscopy Analysis

5.1. Ultraviolet-visible Absorption/Reflectance Spectroscopy

Ultraviolet (UV) (200 – 390 nm) and visible (Vis) (390 – 800 nm) spectroscopy is routinely used in analytical chemistry for the quantitative analysis of different samples. The common samples are in solution state, but solid and gas phase determinations are also possible. The technique excites the ground electronic state molecules to higher excited electronic states and measures these transitions. Because many molecules absorb uv-vis light, uv-vis absorption spectroscopy measures the percentage of radiation absorbed by the sample at each wavelength. A sample was scanned for a designed range of wavelength and the absorbance is recorded. The technique is often used in organic chemistry because highly conjugated systems absorb uv-vis light well and the common solvents such as ethanol do not absorb uv-vis light so that they will not interfere the analysis.

The most important information that can be obtained from uv-vis spectroscopy is the maximum absorbance, λ_{max}. Molecules containing π-electrons and non-bonding electrons can absorb energy and get excited to higher energy anti-bonding molecular orbitals [43]. Since this energy difference is

$$\Delta E = hv = hc/\lambda$$

Equation 5-1,

where *h* is Planck constant and *c* is the speed of light, it is inversely proportional to the HOMO-LUMO energy gap.

Therefore, the smaller the energy difference between HOMO and LUMO, the longer the absorbance wavelength becomes and vice versa.

Uv-vis absorption technique is widely used to quantitatively determine concentrations of solutions and absorbed wavelengths of different analyses because the observed colors are supposed to be the complementary color of the absorbed wavelengths (**Figure 5.1**).

The other important information is the absorbance intensity, which can be described by Beer's Law, which can be used to determine solutions' concentrations. The technique uses Beer's law:

$$\boldsymbol{A = \varepsilon bc}$$

Equation 5-2

where $\boldsymbol{A}$ is the absorbance of a medium, $\boldsymbol{\varepsilon}$ is a proportionality constant called the molar absorptivity, $\boldsymbol{b}$ is the path length of the sample cell in cm and $\boldsymbol{c}$ is the concentration of the sample in g/L so that $\boldsymbol{\varepsilon}$ is in the unit of L/mol·cm.

The absorbance of a medium is also defined by the equation:

$$\boldsymbol{A = -log_{10}T = log\,(P_0/P)}$$

Equation 5-3

where ***T*** is the transmittance of the medium,

$$\boldsymbol{T = P/P_0}$$

Equation 5-4

where $\boldsymbol{P_0}$ is the initial power of the beam shone from the instrument and ***P*** is the resulted power of the beam passed through a medium that has a thickness of ***n*** cm and concentration ***c*** of an absorbing species [43].

For reflectance analysis, it measures the differences in the intensity of light reflected from a sample (***P***) and of light from a reference material for the calibration ($\boldsymbol{P_0}$). The ratio $\boldsymbol{P/P_0}$ is called the reflectance and is usually expressed as a percentage [80]. For our analysis, each undyed fabric was used for the calibrations.

In this study, only the visible region was used for the analysis because our interest is the color, and reflectance data was collected instead of absorbance data for the fabrics. The reflectance analysis is often used for solid samples with special diffusing accessories (Barellina) which enable us to collect data without destroying the solid samples. The technique is used for characterization of optical and electronic properties of solid samples. The accessory allows the

collection of the reflection of incoming beam instead of absorbance of the beam. Our samples were solid (dyed fabrics) so that the visible reflection spectroscopy was chosen for the purpose.

Also, MBI dyed carbon nanotube's transmission electron microscopy (TEM) analysis data was obtained to determine the atomic positions of molecules on carbon nanotubes and the effect of temperatures towards the aggregation of particles

5.1.1. Visible Absorption and/or Reflection vs. Color

Photons of different wavelengths make the electromagnetic spectrum (EM) [81]. A small region in this EM is called “visible” regions and our eyes can detect colors with lights in this region. The region is roughly from 400 to 700 nm (see Figure 5.2). Each wavelength corresponds to a certain color and when all the wavelengths in this region are mixed together, we see “white light”, or no color.

Colors are created substantively or additively. If some light with a certain wavelength is “emitted”, our eyes and brains detect and signal the color of that wavelength. For example, if 600 nm light is emitted from a light bulb, then we see red color. This is additive.

If any wavelengths are absorbed by some substances when white light is shined, the resulted color is the mixture of all the other wavelengths colors. The resulted color is often called the complementary color of the absorbed color. This is shown in the color wheel in Figure **5.1**. For example, if any substance absorbs 530 nm wavelengths, which is the green region, the resulted color is its complementary color of red, so we observe red color. This is subtractive.

The wavelengths and frequency are inversely proportional as in the Equation 5-1, so if the wavelength of some light is in the short wavelength region, then the frequency of the light is higher, and therefore the energy of the light is high also. An example is uv light, whose wavelength is very low, lower than visible region light and around 300 nm. As we know, the energy of uv light is very high.

5.1.2. Experiments

TEM data was obtained in the procedure described by Dr. Jacapo Samson [69]. For the reflectance analysis, the fabrics were prepared in the procedure described in the published article[69] by Olga Lavinda, Sasan Karimi, and Kieth Ramig by using multi-fabrics strips (Figure 5.18 & 5.19). MBI used was prepared by them[37,69] and indigo was purchased from Sigma Aldrich. I analyzed these fabrics and solutions at the Department of Scientific Research of the Metropolitan Museum of Art. All the solution samples were prepared in the concentration of 1×10^{-4} M for each solution at the museum for the analysis.

The data collections and system set-ups that I used are the following. Uv-vis absorption and visible reflectance spectra were obtained using the instrumentation available in the Department of Scientific Research of the Metropolitan Museum of Art. All the solution data was collected with a Varian Cary 50 Bio UV-Vis spectrophotometer using a quartz cuvette with path length of 1.0 mm. The sample, insoluble in water and most organic solvents, was dissolved in solvents in an ultrasonic bath for the analysis. For fabric samples, the data was collected in dual-beam mode using a Varian Cary 50 Bio UV-Vis spectrophotometer equipped with a Barrelino remote diffuse reflection probe by Harrick Scientific for fabrics and a xenon flash lamp. The scan range was 200-800 nm with a maximum scan rate of 120 nm/s. Spectra of undyed fabrics were taken before each measurement and used as a calibration reference. The data were processed using Cary WinUV and Origin softwares.

5.1.3. Results

The λmax for the MBI solutions are 616, 659, and 665 nm for DMSO, chloroform (CHCl3), and dimethylformamide (DMF) solutions (Fig 2, 3 and 4). The previously reported values are 607 nm for DMSO[44].

The indigo spectra were reported as 615 nm[44], 605 nm [2] in DMSO and 613 nm in DMF [2]. The λ_{max} of experimental gaseous phase of indigo are 320ºC and 385ºC have been also reported as 546 nm and 539 nm respectively [2], both indicate the color of indigo at gaseous phase is red [6,7].

TEM results with carbon nanotubes show the size of particle becomes smaller upon heating. In other words, the size of aggregation becomes smaller when the color becomes blue from purple (Figure 5.7). They found that upon the heating, the molecules become smaller chunks [69]. The color did not return to the original purple color, but stayed to blue. The most populated size before heating is at around 12.5 nm, with the second populated size of ~27.5 nm and ~ 3nm in size. After the heating, the biggest particle size at 27.5 nm and the smallest size at from 0 to 2 nm completely disappeared, instead, the new populated peak at the size of ~5 nm appeared with the slight shift and decrease of the previously most populated peak at 12.5 nm. These results show the aggregation of MBI becomes smaller when its dyed wool fabrics heated in hot water and its color becomes blue from purple.

The visible reflectance results with all 13 different fabrics show the trend of reddening from blue in indigo, to MBI, and to DBI (see Figure 5.18, Figure 5.19, Figure 5.8, Figure 5.18, and Figure 5.19 for the pictures of actual fabrics used).

For the different passes samples and different concentration samples, as the passes progressed and/or solutions were diluted, they show the trend of becoming bluer or "loses red-components" in all colorant (Figure 5.11, Figure 5.12, & Figure 5.13).

When heated, most of the fabrics show the color change towards bluer colors in indigo and MBI. However this trend is opposite in DBI, which changed to redder colors (see Figure 5.8). This color change is very significant and can readily be observed in wool fabrics (Figure 5.6 & Figure 5.8).

All the samples have strong reflections around 400 – 500 nm, which is purple – blue region. This is in the agreement with the purple color that we observed with the dyed fabrics.

The two main absorbed peaks around 510 – 530 nm and 650 nm appear and disappear upon heating.

The observed color of MBI is purple on fabrics, such as wool and is changed to blue upon heating. The observed color of indigo is indigo blue on fabrics. These observed colors indicate that these molecules absorb long wavelengths (around 610 nm and in orange regions), which is not typical and unique for these fairly small molecules. The DFT calculated maximum absorption for both molecules from their crystal structures results in around 530 nm, which

indicate the absorbed color is green, and therefore the observed color is red (see Ch. 6 & 7).

Figure 5.1. Color wheel shows complementary colors (observed colors) of absorbed colors. It starts around from 390 nm with purple and ends around at 800 nm with red. The complementary color is on the other side of the circle. Ex. When 700 nm is the wavelengths absorbed (i.e. λ_{max} = 700 nm), then its complementary color is green, therefore we observe green color. Note the color and wavelengths vary slightly depending on references[81–85].

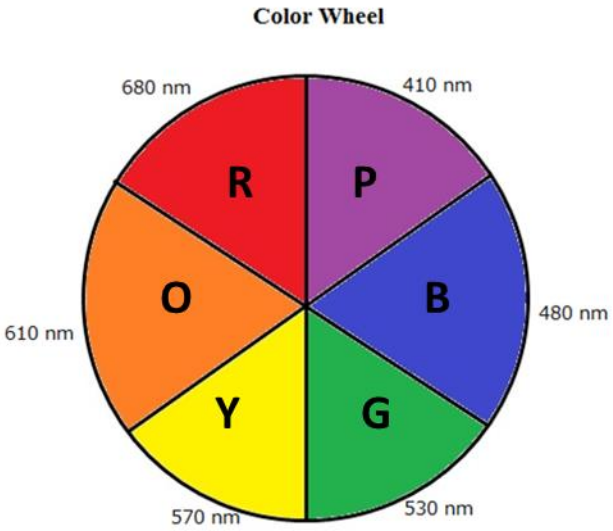

Figure 5.2. Electromagnetic spectrum of visible region, from~390 to ~800 nm

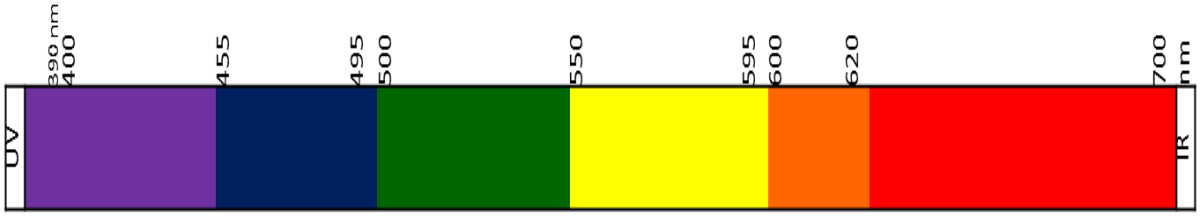

Table 5.1. Summary of absorbed colors and observed colors. In order to have purple colors of MBI, wavelengths in yellow regions have to be absorbed.

Absorbed Color (nm)	*Observed Color*
Purple (~390)	Yellow
Blue (~455)	Orange
Green (~497)	Red
Yellow (~550)	**Purple**
Orange (~597)	Blue
Red (~622)	Green

Figure 5.3. MBI of 1 x 10^{-4} M in DMSO solution. The absorption maximum is at 616 nm, which may be compared to indigo in DMSO [86] in which the absorption maximum is at 619 nm. The transition is assigned to the lowest lying pi - pi* transition.

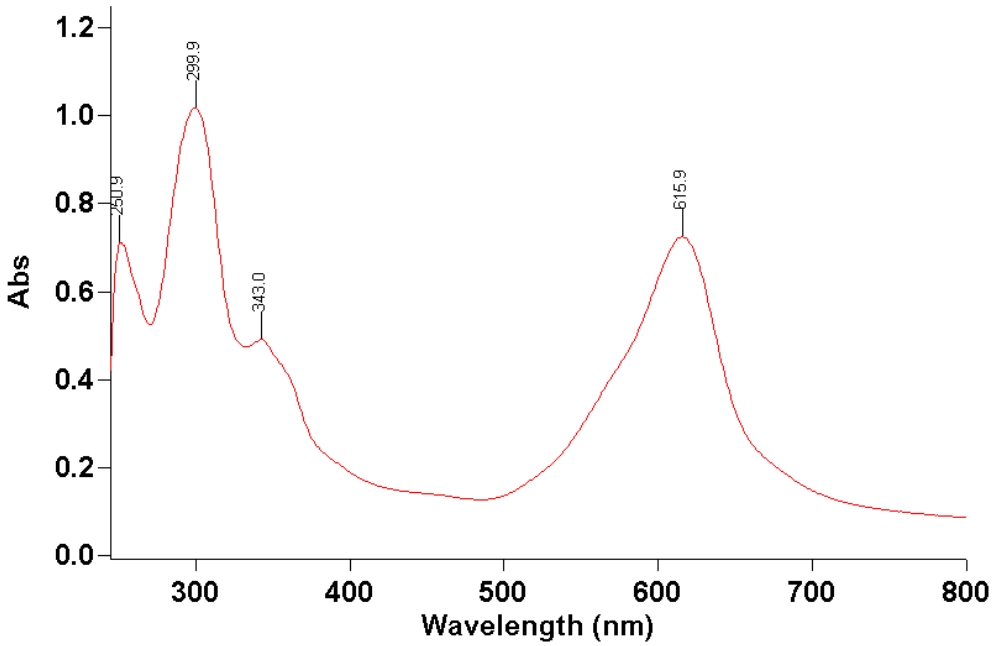

Figure 5.4. MBI of 1 x 10^{-4} M in $CHCl_3$ solution (unlabeled shoulders: 243, 362, 601 nm)

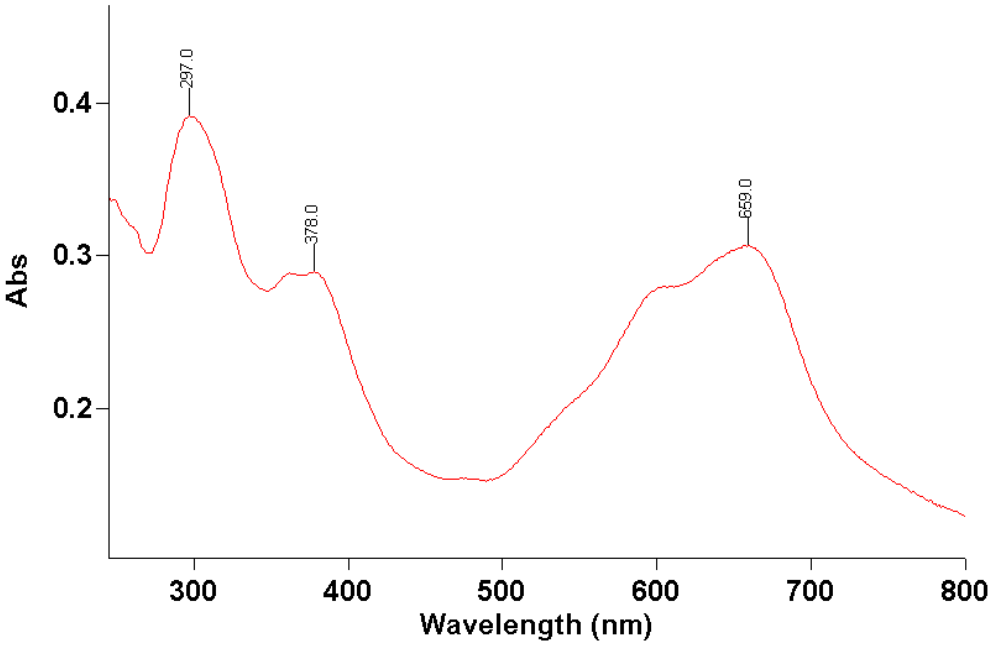

Figure 5.5. MBI of 1 x 10^{-4} M in DMF solution (unlabeled shoulders: 362, 601 nm)

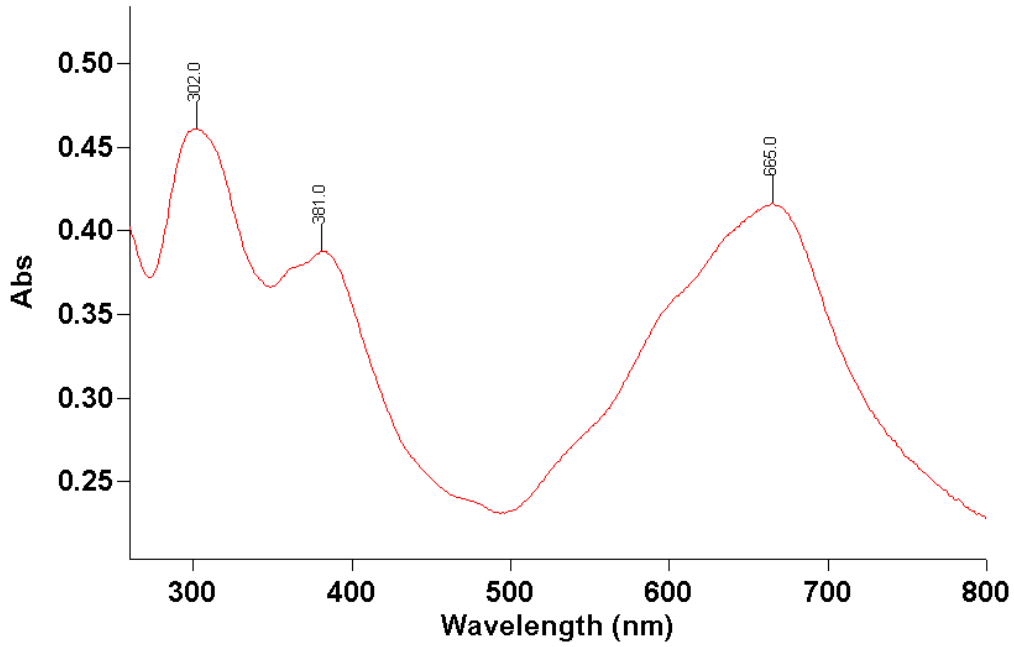

Figure 5.6. The color change of MBI upon heating on wool fabrics. The color changes from purple before heating to blue after heating to around 60ºC.

Before Heating **After Heating ~60ºC**

Purple **Blue**

Fabrics prepared by Prof. Keith Ramig and Ms. Olga Lavinda. The picture is taken by H. Ajiki.

Figure 5.7. TEM analysis of MBI dyed carbon nanotubes before heating and after heating [2]. The populated size becomes smaller upon heating. The disappearing and appearing peaks of populations are marked with arrows.

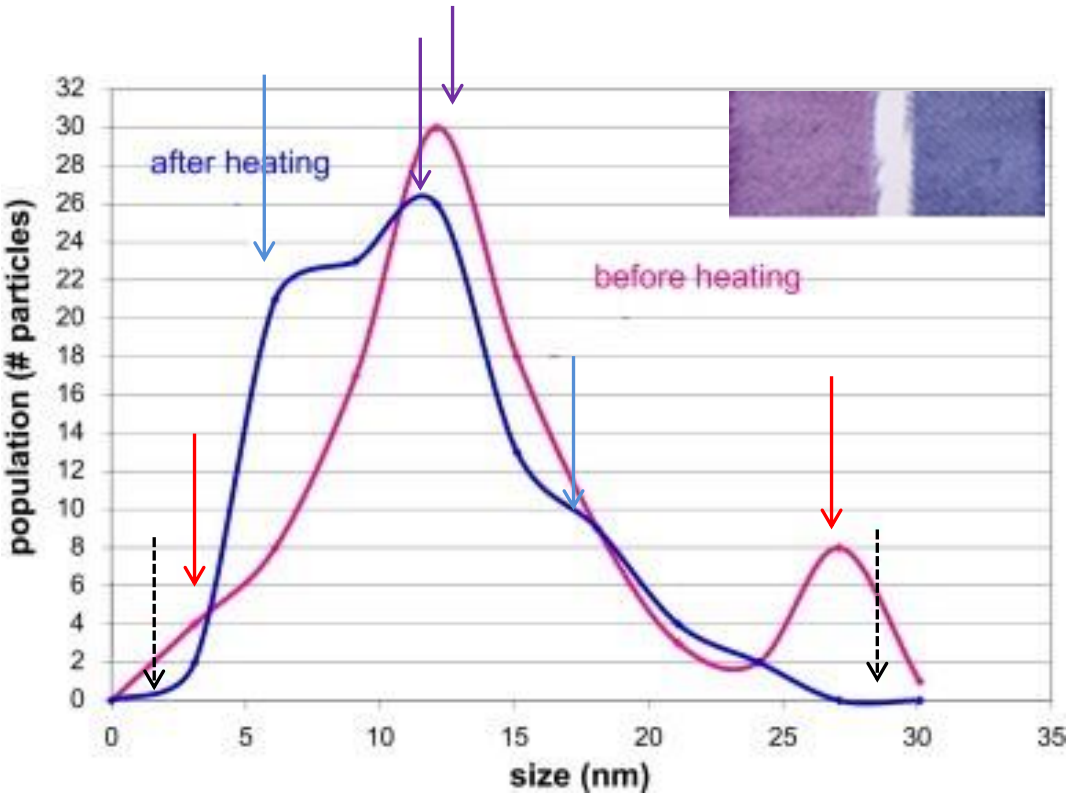

Lavinda, O.; Mironova, I.; Karimi, S.; Pozzi, F.; Samson, J.; Ajiki, H.; Massa, L.; Ramig, K. Dyes Pigm. 2013, 96, 581–589.

Figure 5.8. Wool parts from the dyed multi-fabric strips, which were used for the reflectance analysis in this study. Top: MBI (from left to right: Pass 1, Pass 2, Pass 3 and Heated), Middle: Indigo (same order), Bottom: DBI (same order). Note the heated color changed to bluer colors with MBI and indigo. The heated color changed to redder color with DBI.

Fabrics prepared by Prof. Keith Ramig & Ms. Olga Lavinda. Pictures taken by H. Ajiki

Figure 5.9. The complete reflectance data of wool fabrics. The numbers from 1 to 3 correspond to the degree of passes, 1 to the first pass, 2 to the second pass and 3 to the third pass. Heated samples are same pass with the first pass, but heated in hot water.

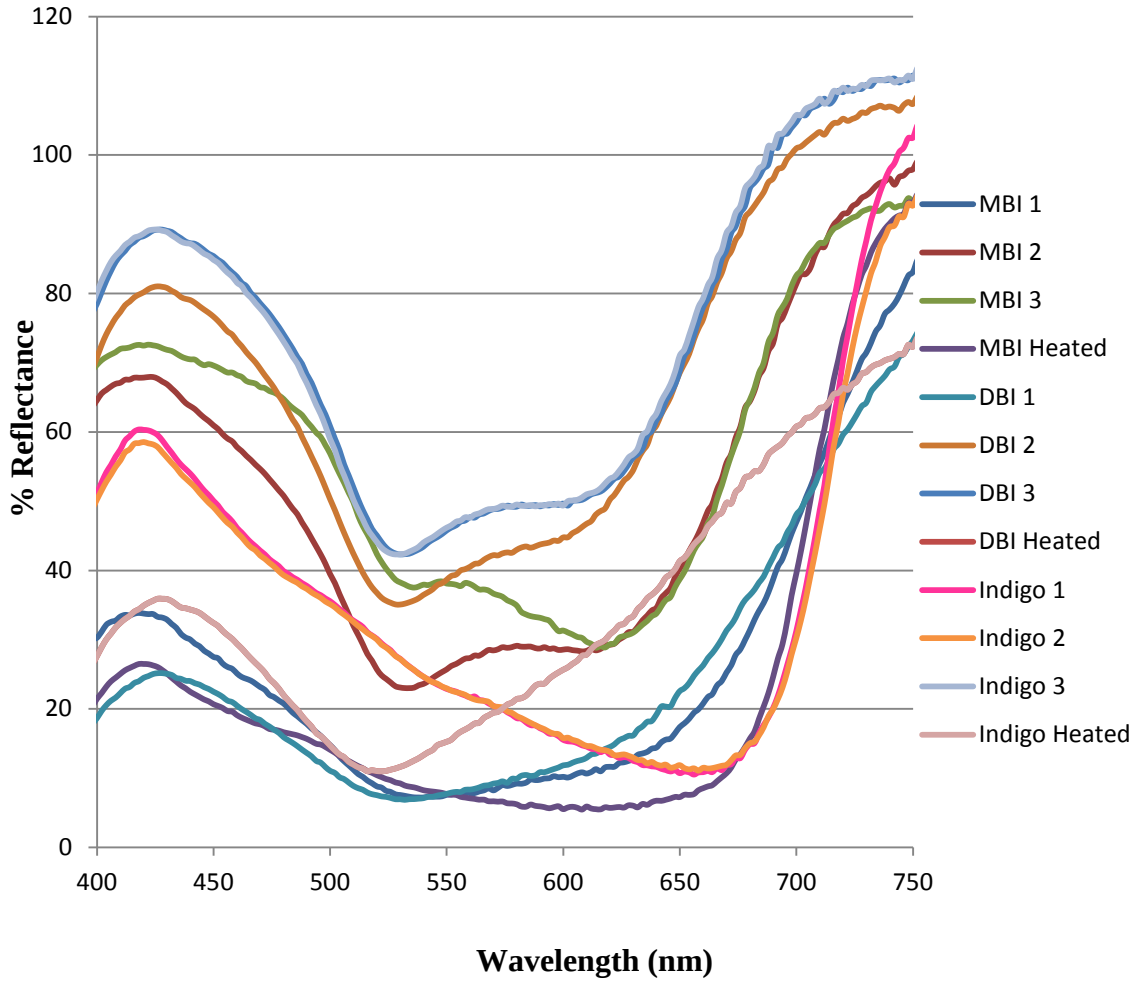

Lavinda, O.; Mironova, I.; Karimi, S.; Pozzi, F.; Samson, J.; Ajiki, H.; Massa, L.; Ramig, K. Dyes Pigm. 2013, 96, 581–589.

Figure 5.10. Visible reflectance charts of wool fabrics with MBI and indigo.

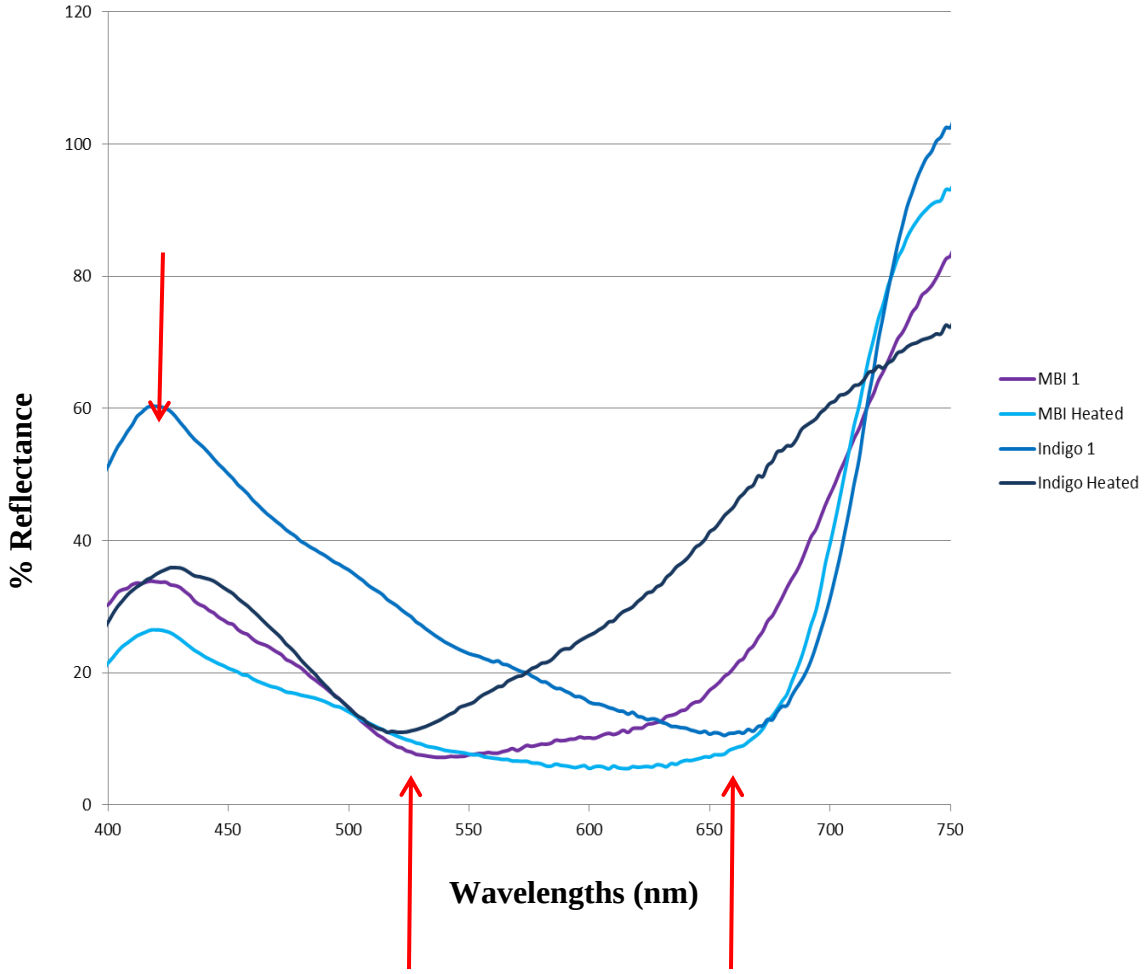

Lavinda, O.; Mironova, I.; Karimi, S.; Pozzi, F.; Samson, J.; Ajiki, H.; Massa, L.; Ramig, K. Dyes Pigm. 2013, 96, 581–589.

Figure 5.11. Visible reflectance charts of wool fabrics with MBI Pass1, 2, 3, and Heated samples

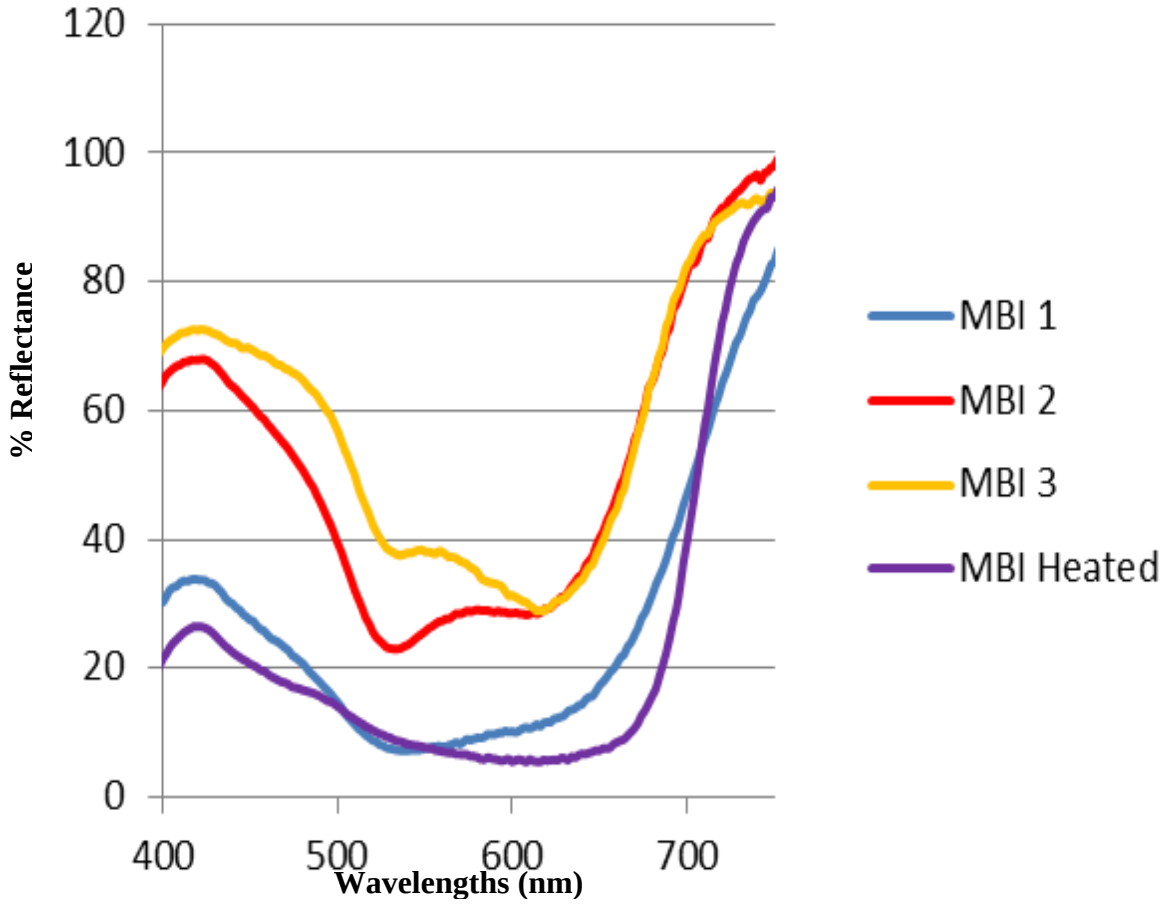

Lavinda, O.; Mironova, I.; Karimi, S.; Pozzi, F.; Samson, J.; Ajiki, H.; Massa, L.; Ramig, K. Dyes Pigm. 2013, 96, 581–589.

Figure 5.12. Visible reflectance charts of wool fabrics with Indigo Pass1, 2, 3, and Heated samples

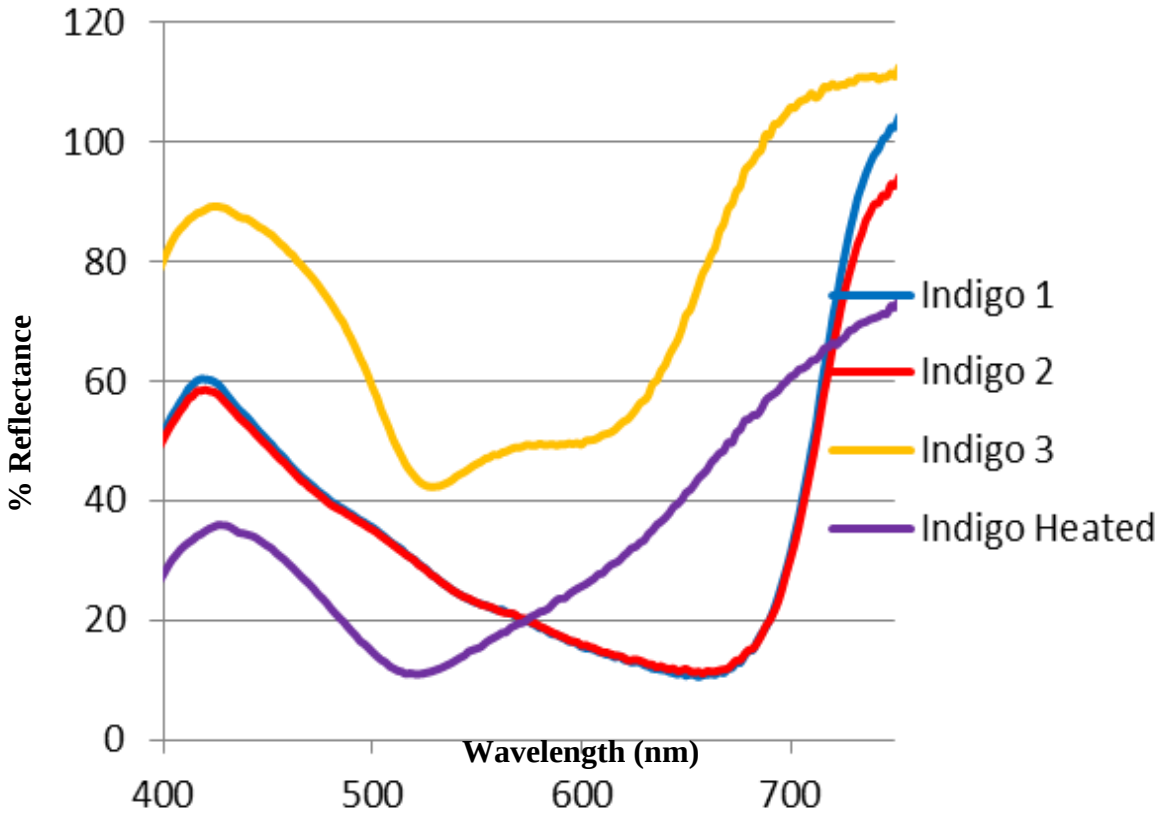

Lavinda, O.; Mironova, I.; Karimi, S.; Pozzi, F.; Samson, J.; Ajiki, H.; Massa, L.; Ramig, K. Dyes Pigm. 2013, 96, 581–589.

Figure 5.13. Visible reflectance charts of wool fabrics with DBI Pass1, 2, 3, and Heated samples

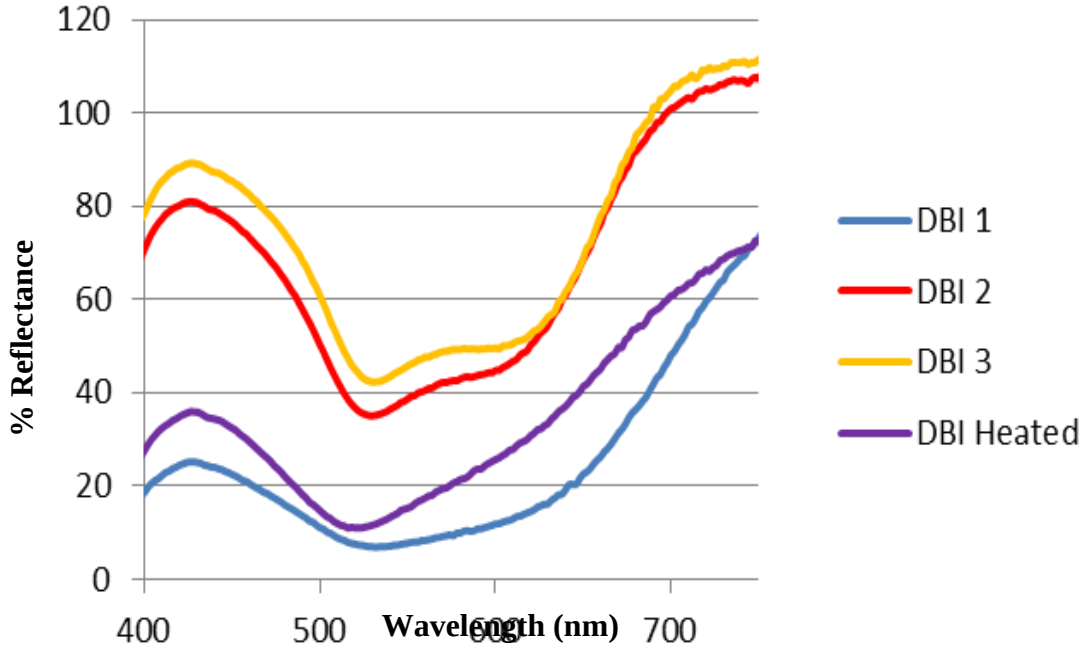

Lavinda, O.; Mironova, I.; Karimi, S.; Pozzi, F.; Samson, J.; Ajiki, H.; Massa, L.; Ramig, K. Dyes Pigm. 2013, 96, 581–589.

Figure 5.14. Instrument with a diffuser and samples at the Metropolitan Museum of Arts

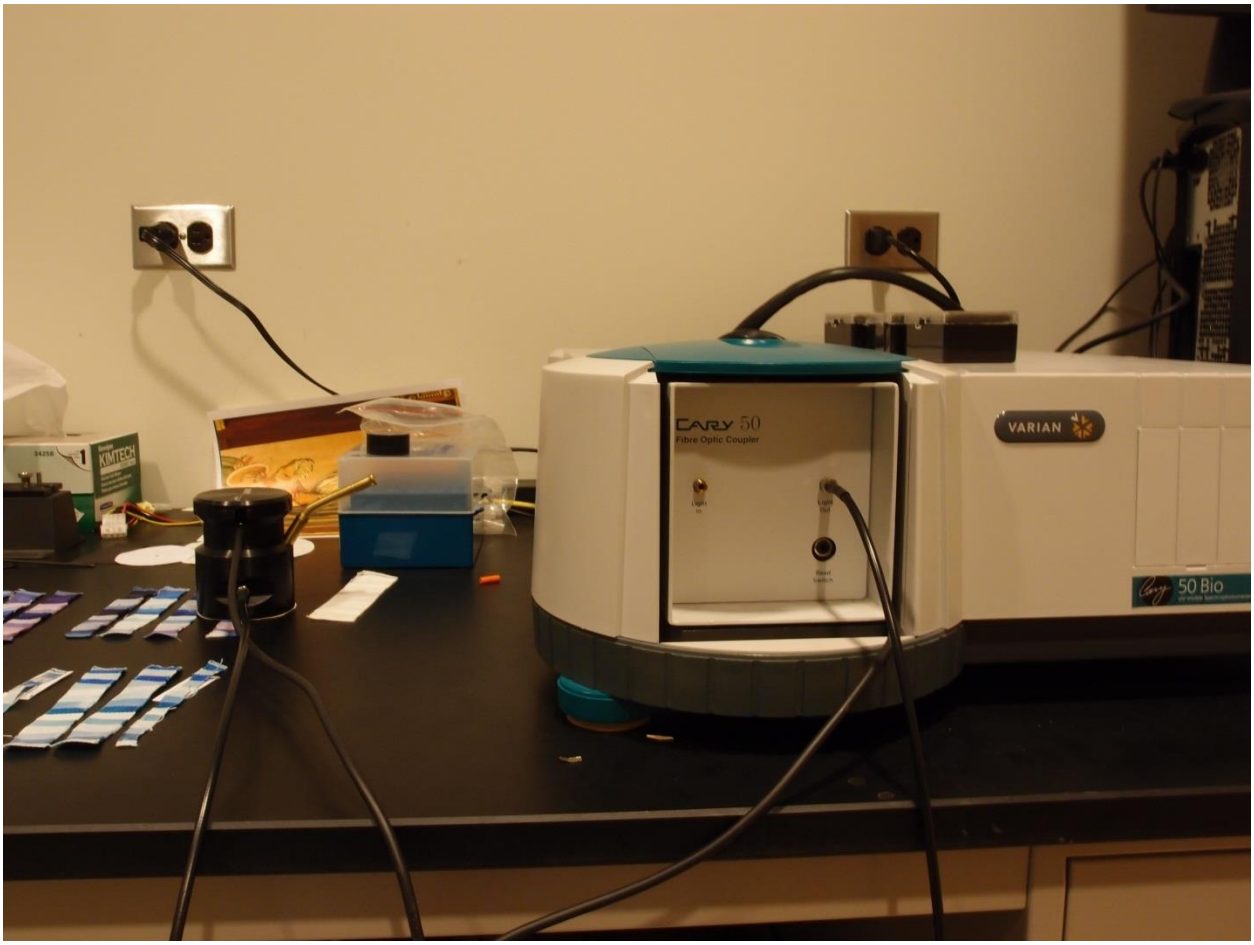

Figure 5.15. The diffuser

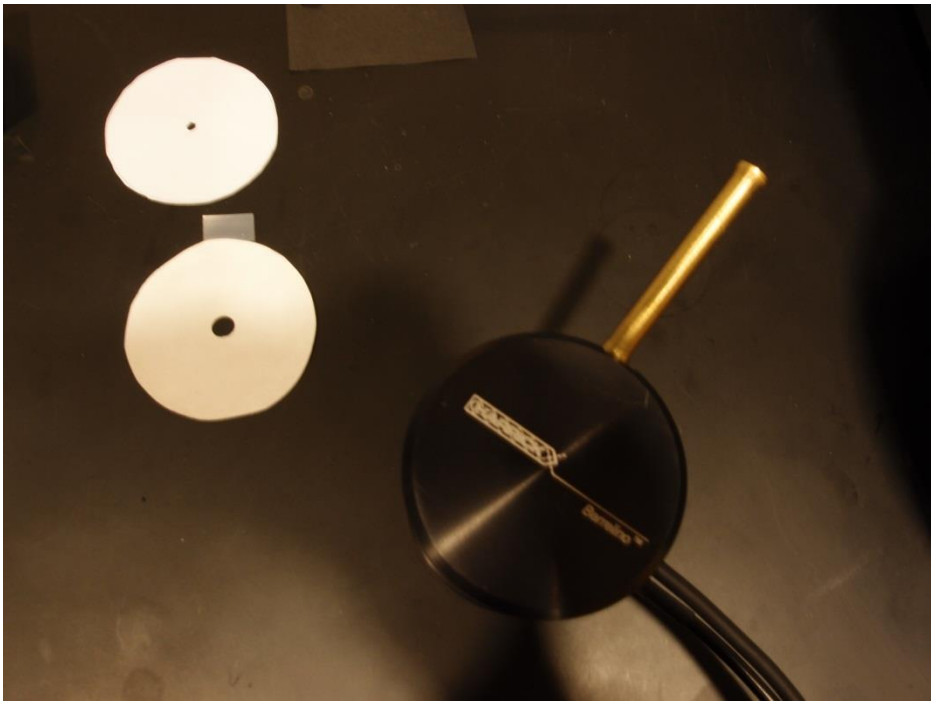

Figure 5.16. The diffuser from the bottom

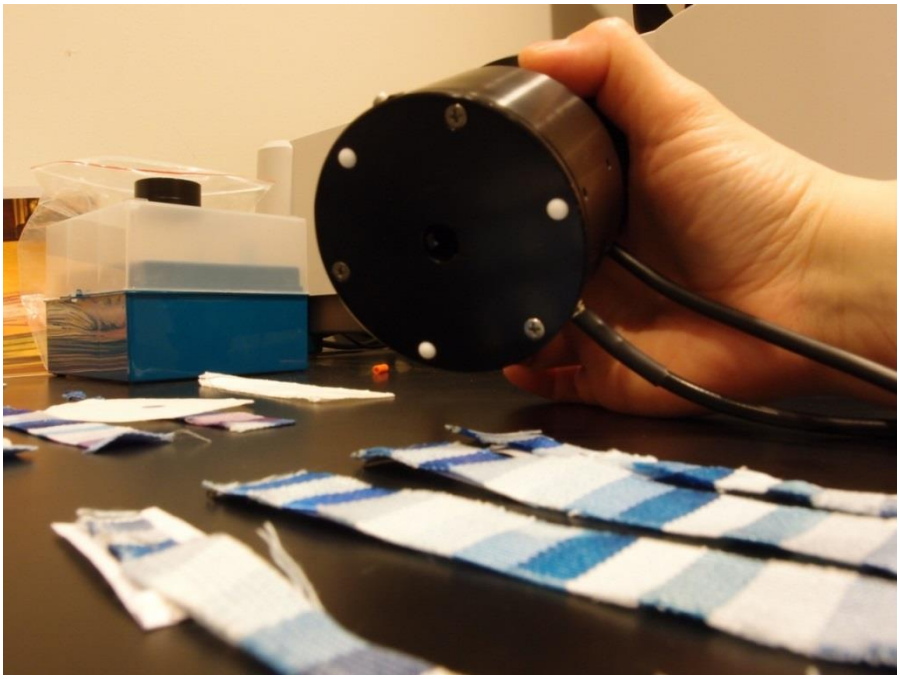

Figure 5.17. Actual fabric samples used with the diffuser

Figure 5.18. Dyed multi-fabrics with indigo on the left and MBI on the right

Fabrics prepared by Prof. Keith Ramig and Olga Lavinda. The picture taken by H. Ajiki.

Figure 5.19. Dyed multi-fabrics with DBI

Fabrics prepared by Prof. Keith Ramig and Olga Lavinda. The picture taken by H. Ajiki.

6. Quantum Chemical Analysis

6.1. Theoretical Calculations

Quantum mechanical calculations have been utilized for this study of MBI.

All the theoretical calculations employed in this study have been performed with Density Functional Theory (DFT) method using Gaussian 09[53], except when it is mentioned so.

In DFT, the total energy of a system is expressed as a functional of the charge density. Within Kohn-Sham formulation of density functional theory, the electronic energy is separated into[87]:

$$E = E^T + E^V + E^J + E^X + E^C$$

Equation 6-1

where E^T and E^V are the kinetic and external potential energies, E^J is the classic Coulomb repulsion of electrons of density ρ, and E^X and E^C are the exchange functional and correlation functional parts and the electron-electron repulsion energy, also treated as a functional of the density ρ. One can realize that this equation is very similar to Hartree-Fock (HF) equation, and in fact, within the Kohn-Sham formulation of DFT, HF equation can be regarded as a special case of DFT[88,89], where E^X is given by:

$$\frac{-1}{2}\sum_{j=1}^{n} \mathrm{K}_j$$

which is the exchange energy resulting from the quantum nature of electrons being fermion.

And at the same time, when E^C has to be zero for this case.

E^X, the exchange functionals are usually given in the form of integrals of some function of the density and possibly the density gradient[89]:

$$E^X = \int f(\rho_\alpha(r), \rho_\beta(r), \nabla\rho_\alpha(r), \nabla\rho_\beta(r))dr$$

Equation 6-2

With DFT, an electron density, ρ(r), which will be defined by a 3-dimensional coordinate, r = (x, y, z) will be very important. Hohnenberg and Kohn proved that if we can obtain the ρ(r), we can in principle obtain the molecule's electronic energy at its ground state[70,71,87,90].

For the electronic structures of molecules at the ground states, time-independent DFT is used. Time-independent Kohn-Sham Equation looks like:

$$(-\frac{1}{2}\nabla^2 + \mathrm{v_{KS}}(\mathbf{r}))\ \varphi i(\mathbf{r}) = \varepsilon\, i\ \varphi i(\mathbf{r})$$

Equation 6-3

where $\mathrm{v_{KS}}$ = Kohn-Sham potential and ε_i = Orbital energy of the corresponding Kohn-Sham orbital, φi

The density for an N-particle system is:

$$\rho(\boldsymbol{r}) = \sum_{i=1}^{N} |\varphi i(r)|^2$$

Equation 6-4

This density gives the probability of finding an electron at the location[91–93].

For the calculation of transition to excited states, time-dependent density functional (TD DFT) method is used.

$$(-\frac{1}{2}\nabla^2 + v_{KS}(\mathbf{r}, t))\ \varphi i(\mathbf{r}, t) = i\frac{\partial}{\partial t}\varphi i(\mathbf{r}, t)$$

Equation 6-5

This is a simple excitation method. It excites only one electron from its ground state and creates several possible electron orientations[90]. There are options with Gaussinan 09[53] to calculate Singlets, Triplets, and Singlets and Triplet in 50-50[88] for electrons states, but only Singlets option was used for this entire study.

I have performed geometry optimizations of monomers, dimers and solution states of MBI, indigo and DBI, whose results showed these indigoids' colors differ depending on its phase. These calculations and results can be found in Appendix A.

.

6.2. Single Point Energy, Excitation Energy of Clusters, and Color Properties

Single point calculations of different size of clusters of MBI were performed to see the effect of other MBI molecules in a highly ordered environment. A single point energy calculation is performed on a single, fixed point on the potential energy surface of the molecule to predict the energy and related properties with a specific geometric structure[94]; here I used previously published crystal structures[37,52,95].

6.2.1. Calculations

The single point energy calculations were performed with DFT B3LYP 6-31G(2d,2p) and the excitation energies were obtained with TDDFT B3LYP 6-31G(2d,2p) with Gaussian 09[53].

The molecular geometries were taken from the crystal structure of MBI[37].

The calculated cluster structures contains from 1 to 6 MBI molecules in each cluster system. For some structures, namely, 2, 3, and 5-molecule ones, more than one coordinates were used for calculations simply due to the more freedom of placing the additional molecules from the last structure (see Figure 6.1. Monomer: crystal to Figure 6.9. 6-molecule cluster: crystal).

Figure 6.1. Monomer: crystal

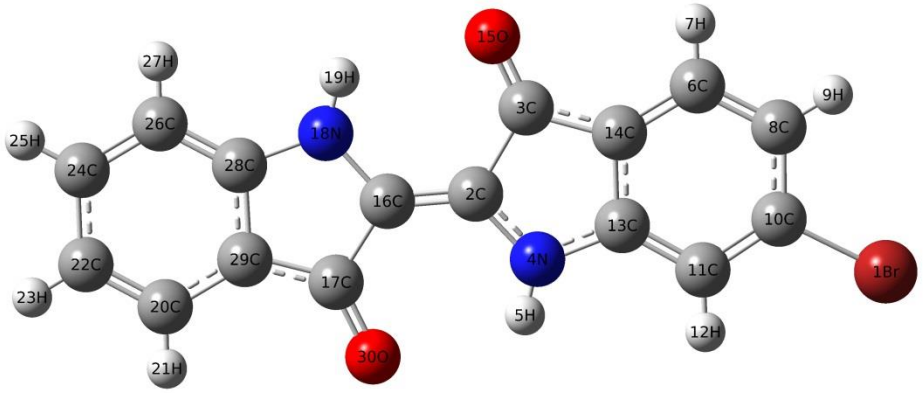

Figure 6.2. Dimer, parallel: crystal

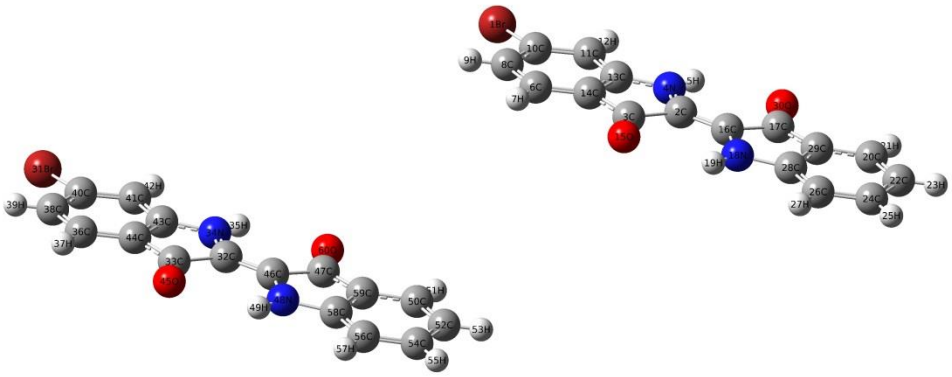

Figure 6.3. Dimer, cross: crystal

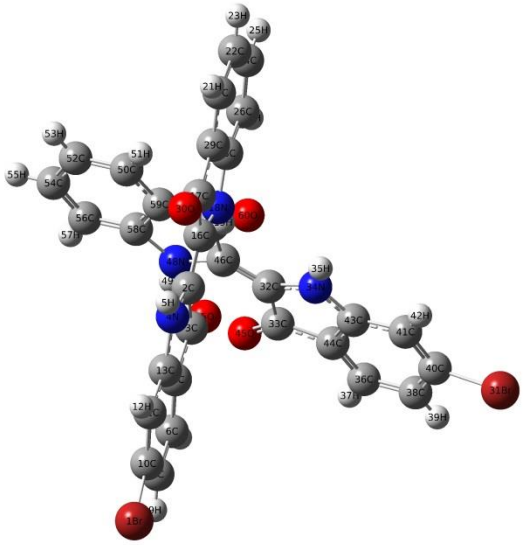

Figure 6.4. Trimer I (less crossing): crystal

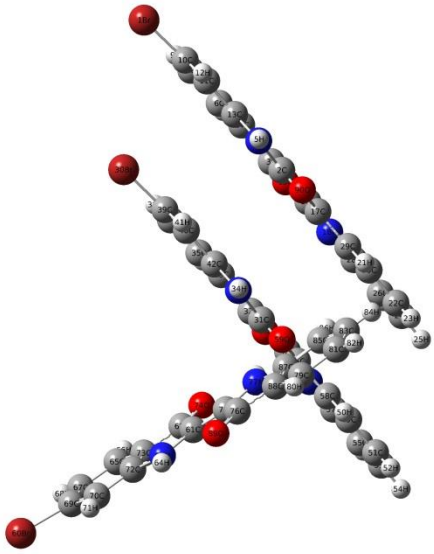

Figure 6.5. Trimer II, more crossing: crystal

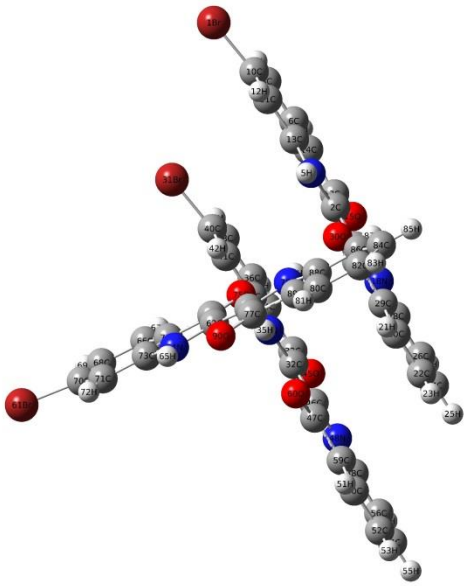

Figure 6.6. 4-molecule cluster: crystal

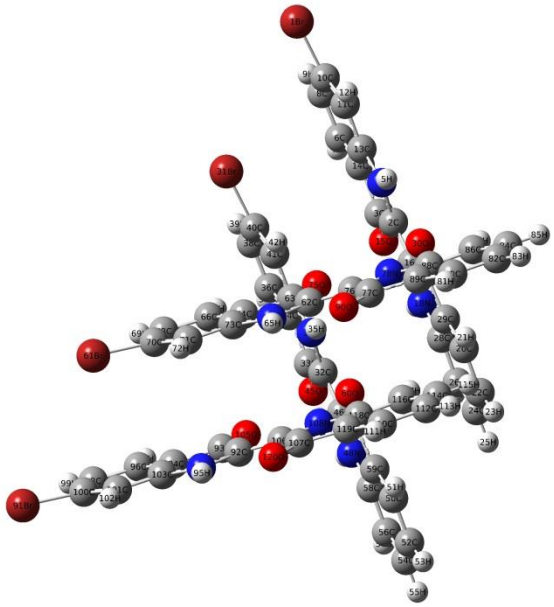

Figure 6.7. 5-molecule, I (center), cluster: crystal

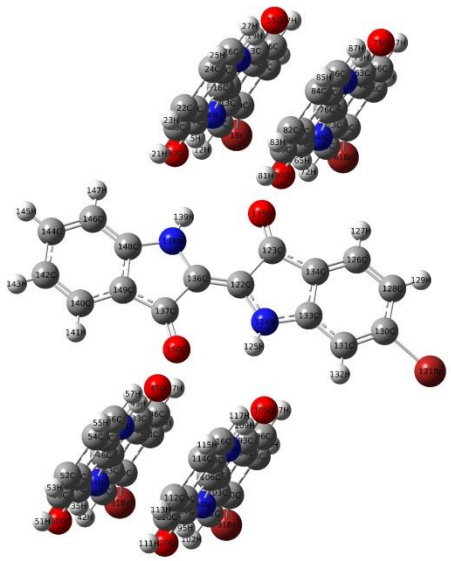

Figure 6.8. 5-molecule, II (end), cluster: crystal

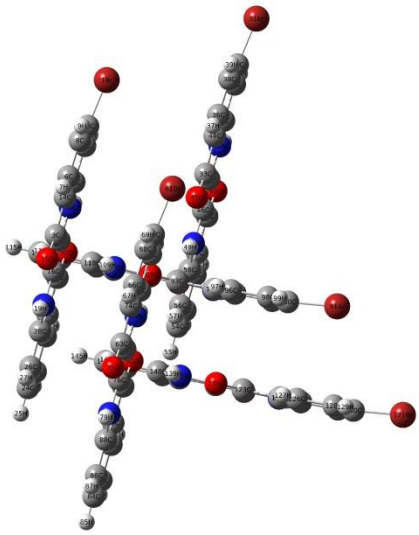

Figure 6.9. 6-molecule cluster: crystal

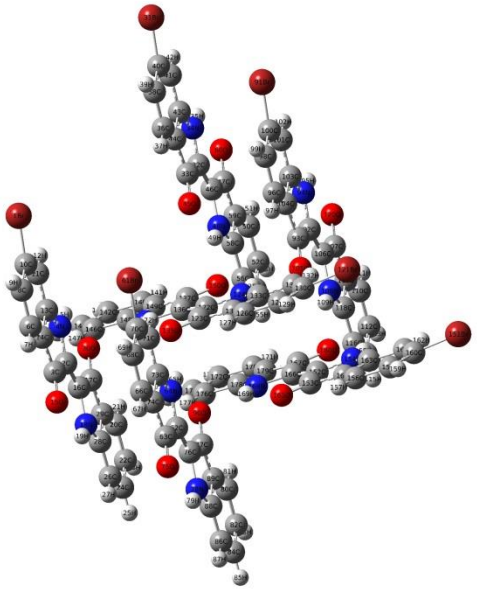

6.2.2. Results

From the excitation calculations of different size of clusters, I found that the excitation wavelengths shift continuously up towards the higher region, where most of the absorption peaks concentrated on at the end.

The magnitude of λ_{max} of MBI clusters keeps increasing, as the number of molecules in a cluster increases, until around 630 nm, where majority of absorption peaks are concentrated as well as the second populated peaks concentrated in the region of around 570 nm (see Figure 6.10 to 6.15).

These 2 wavelengths regions indeed give purple and blue colors, which we observe from MBI.

For major excitation transitions, the transitions were grouped into different colors. The occupied (OM) and unoccupied (UOM) orbitals transitions were then inspected for each color. Though this is not strictly true to all the cases, this is the correlation between the color and the pattern of molecular orbital transitions:

1) For red, molecular orbitals OM and UOM are most likely overlapped greatly. OM and UOM are most likely on the same molecule, and/or overlapping and seeping onto the next molecule. Majority of density is on the same species.

2) For purple, OM and UOM are close, but usually on the adjacent 2 molecules aligned parallel. The density is delocalized into a newer neighboring molecule, compared to the "red" transitions.
3) For blue, as the color becomes bluer, the space that these orbitals occupy expands by spreading the orbitals into both parallel and crossing positions. So the OM and UOM are positioned in like "chairs" and the directions of these "chairs" often changes after the transitions.
4) For Green/Blue, often the distance between the OM and UOM are much further than other colors. Sometimes these orbitals are at the end of each side. I am not sure if this is simply the fact that I use a crystal structure and these ends-orbitals actually interacting with the orbitals in the next unit in reality, nevertheless, it seems fair enough to consider that for this color, OM and UOM occupy the most spaces for the transition among other colors. Orbitals use mainly crossing positions, but instead of having "chair" like positions, OM occupies one site with angle and UOM occupies another site with angle completely different.

Major excitation wavelengths are summarized in Table A.1 and an example of this trend is in Figure 6.33.

Table 6.1. Major Excitations (nm) with MBI Cluster Systems (crystal structures)

Number of molecules in a cluster	1	2-I parallel	2-II cross	3-I Less crossing	3-II More crossing	4	5 center	5 end	6
Excitation Energy (eV)	1.9274	2.4048	2.3670	2.4531	2.4411	2.1655	2.2029	0.0288	1.9274
Wavelengths (nm)	643.27	515.57	523.81	505.41	507.89	572.55	562.83	593.20	641.27
Oscillation Strength	0.0090	0.533	0.3656	0.3930	0.3282	0.0259	0.0699	0.0288	0.0090
Excitation Energy (eV)	1.9306	2.4216	2.3402	2.3453	2.2993	2.1026	2.1787	1.9303	1.9306
Wavelengths (nm)	642.22	512.00	529.81	528.65	539.24	589.66	569.07	642.29	642.22
Oscillation Strength	0.0057	0.0016	0.1145	0.1666	0.1307	0.0187	0.0252	0.0084	0.0057
Excitation Energy (eV)	1.9147		2.8828	2.1301	2.3105	2.2796	1.7894	1.9034	1.9147
Wavelengths (nm)	647.54		430.08	582.04	536.61	543.89	692.88	651.39	647.54
Oscillation Strength	0.0041		0.0242	0.0215	0.0437	0.0105	0.0084	0.0082	0.0041
Excitation Energy (eV)	1.8814		2.8072	2.0154	2.1849	1.9201	1.9230		
Wavelengths (nm)	659.01		441.67	615.18	567.47	645.72	644.73		
Oscillation Strength	0.0019		0.0116	0.0125	0.0276	0.0089	0.0055		
Excitation Energy (eV)	1.7443				1.9172	1.9431	1.9481		
Wavelengths (nm)	710.78				646.69	638.07	636.44		
Oscillation Strength	0.0003				0.0058	0.0058	0.0020		
Excitation Energy (eV)						1.9659			
Wavelengths (nm)						630.68			
Oscillation Strength						0.0031			

*Refer to (Figure 6.1– 24) for the structures

Calculated absorption spectra from MBI cluster systems

Figure 6.10. Monomer: Only red and uv peaks are present

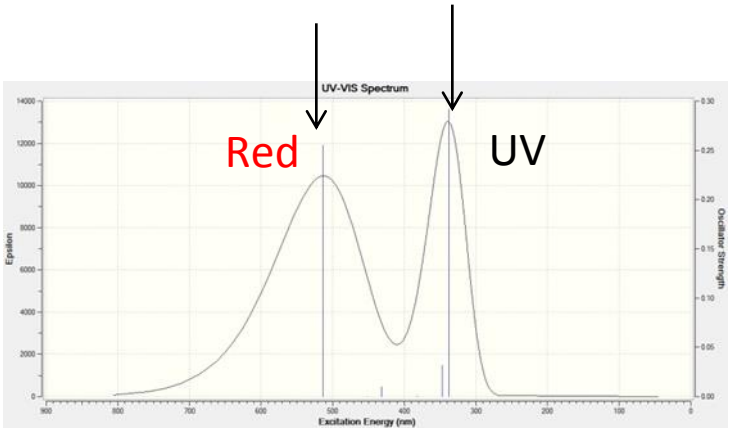

Figure 6.11. Dimer: Blue/Green peaks start to appear. Uv peaks disappear.

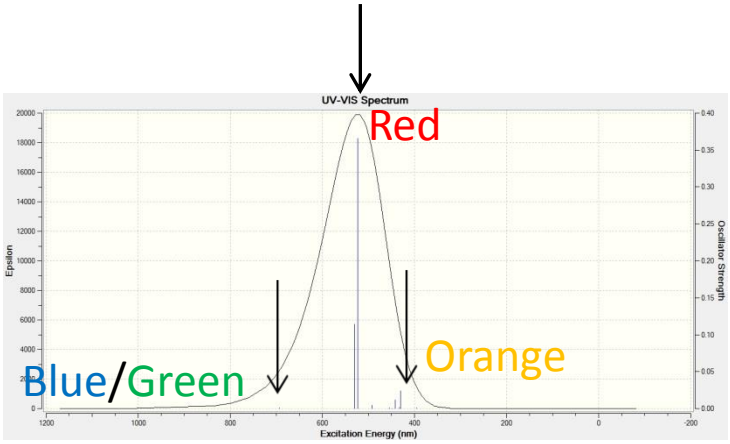

Figure 6.12. Trimer: Blue/Green peak become intensified.

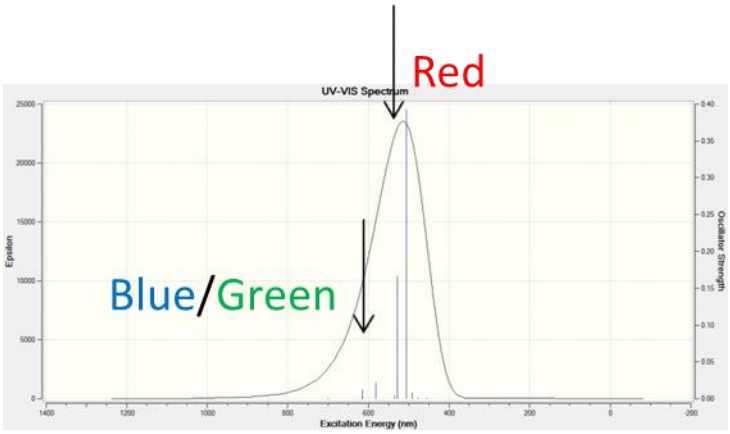

Figure 6.13. Four-molecule cluster: Blue/Green becomes intensified

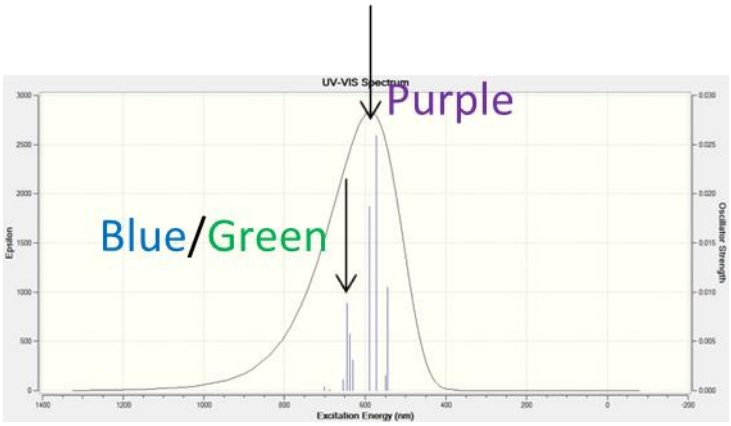

Figure 6.14. Five-molecule cluster: Blue/Green becomes intensified.

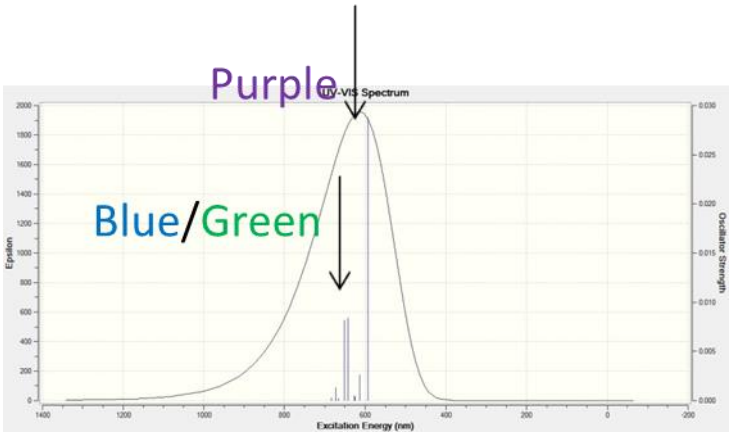

Figure 6.15. Six-molecule cluster: Signals concentrated around Purple and Blue/Green.

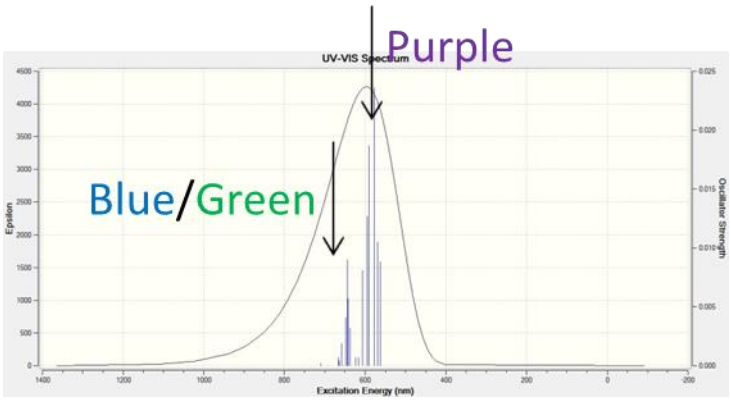

Example of a Purple Color Transition: MO and Absorption Spectra with a 6-Molecule Cluster

Figure 6.16. MBI 6-molecule-cluster: Purple color at 578 nm

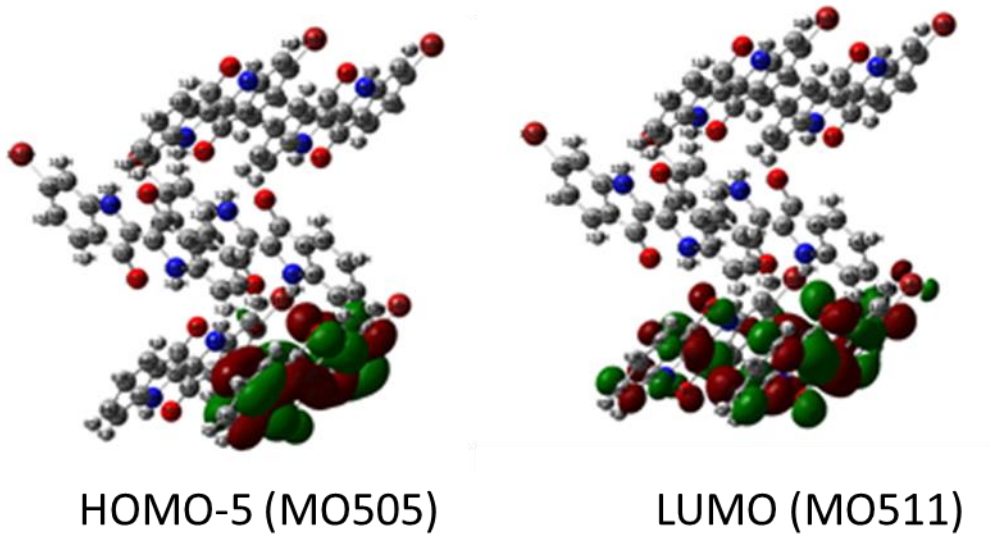

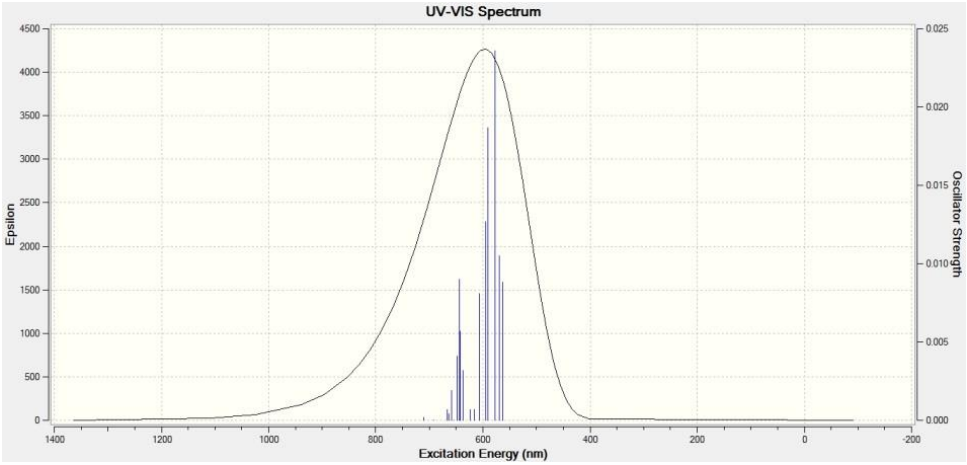

Figure 6.17. Uv-Vis spectra of MBI 6-molecule-cluster: Purple color at 578 nm by DFT calculation

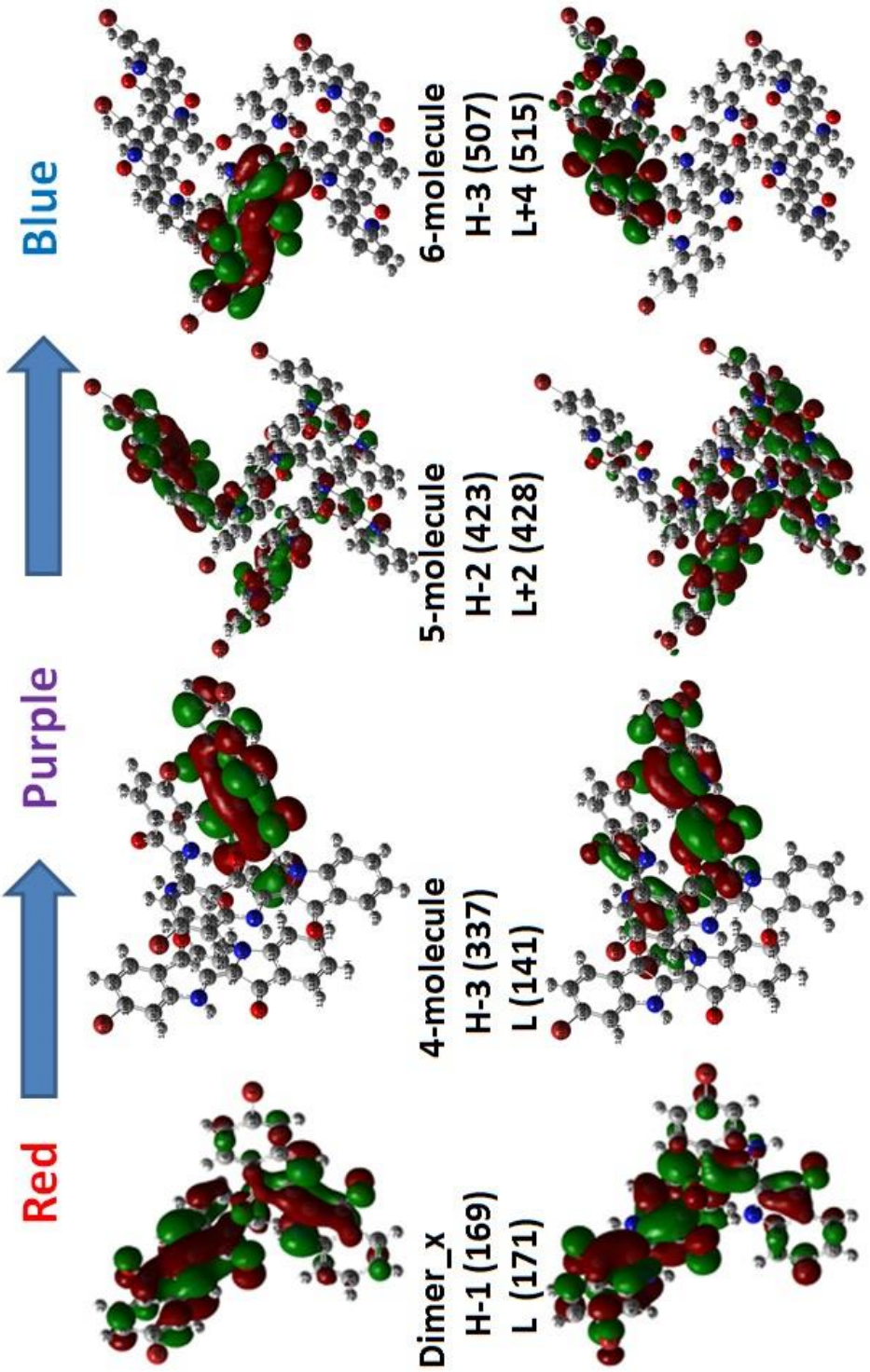

Figure 6.18. Pattern of Molecular Orbitals with Transition Colors

Table 6.2. Summary of MBI 6-molecule-cluster: Purple color at 578 nm

Wave-length (nm)	Observed color	Orbitals transitions (Occupied to Unoccupied)	Oscillation Intensity	Excitation Energy (eV)
578	Purple	505 - 511	0.0236	2.1461 S0 -> S18
591	Purple	509 – 515	0.0187	2.0971 S0 -> S17
595	Blue	507 - 515	0.0127	2.0842 S0 -> S16
570	Purple	508 – 515	0.01050	2.1759 S0 -> S19
643	Blue	510 - 515	0.00900	1.9274 S0 -> S8
606	Blue	507 - 512	0.00810	2.0445 S0 -> S14
692	Green	510 – 511 (HOMO-LUMO)	0.00000	1.7911 S0 -> S2

PART III

Discussion and Conclusion

7. Discussion

7.1. Color and Cluster Size

I now compare the theoretical calculation results and experimental results, especially excitation results to discuss the MBI's colors and its thermochromism property.

As mentioned in earlier chapters, MBI has a thermochromism property. The color changes from purple to blue on fabric when heated at around 60ºC when the chemical itself is considered to be exceptionally stable. Also, MBI' color varies depending on its phase: red in gaseous phase, purple on fabric or in solution, and dark blue in solid. The color difference with its phase change was unknown to us and was found in the process of studying about the thermochromism property. Also, the common color of indigo and MBI are much bluer than expected with the calculated results. That means the energy difference between HOMO and LUMO is much smaller than expected from its small conjugation system. The common assumptions for this smaller energy gap and therefore the bluer colors of the molecules are these [10,96]:

1) By stacking and/or aggregation of molecules
2) By stabilizing the LUMO structure, thus lowering the HOMO-LUMO gap

The mechanism of this color change and the color differences have been a mystery to color chemists.

Our first hypothesis toward the thermochromism property was that it is due to the structural change upon heating. Therefore, if we can find the crystal coordinate of MBI at room temperature and at above 60ºC, where the color changes, we can explain the color change.

The results were interesting. The crystal structures did not show differences in two different temperatures. When I took 13C solid state NMR at these two different temperatures, I was not able to find the significant differences either. Therefore, our first hypothesis of the thermochromism property caused by its structural change was not validated.

As we study about the thermochromism property, I found that the excitation calculation of monomers of MBI, indigo, and DBI are all red in its gaseous phase, which I first suspected it is due to the selection of calculation method and basis sets. There are about 100 nm differences between the calculated and observed colors. Therefore, I performed quick calculations with other methods and basis sets. Interestingly, the color was red, even redder with higher computational methods.

Then the results seemed strange. The three chemicals, especially indigo, seem to be much bluer than red, either purple or blue.

Yet after I found Christies's book and article[10,96], I found the color of indigo is actually red in its gaseous phase. I also found the color of MBI in its gaseous phase is red with a sublimation experiment of MBI by Lavinda and Ramig (Figure 7.1) [97].

Figure 7.1. MBI's result from sublimation experiment (http://www.youtube.com/watch?v=3oNw-khx30E). Note that the color is much redder than those purple colors of MBI.

I then, performed DFT calculations of optimized dimers, expecting the wavelengths shifting to higher regions.

The DFT calculations in gas phase were performed with dimers of cross-structures and parallel-structures of MBI and indigo (Figure 7.2), which shifted to higher wavelengths, but still did not give the observed color. Yet, with dimers, small peaks in ~620 nm (which cause blue-green colors) start to appear. Also, for monomers, the DFT calculations results show that the first excited state has the HOMO – LUMO transitions in which the electron transitions are happening

in both ways, which is common in conjugated benzene-type rings. This type of transition is not observed dimers and bigger systems.

Since when a molecule is excited, its structure is expected to be more like a charged one [10,96], a single point calculation of a resonance structure of MBI was also performed. MBI can have a few resonance structures and the one that has the most stability with symmetric charges was used for the calculation (Figure 7.3). The wavelengths around 600 nm became much more intense than other structures also with strong peaks in the UV region.

Figure 7.2. Dimers structures. Left: Cross, Right: Parallel

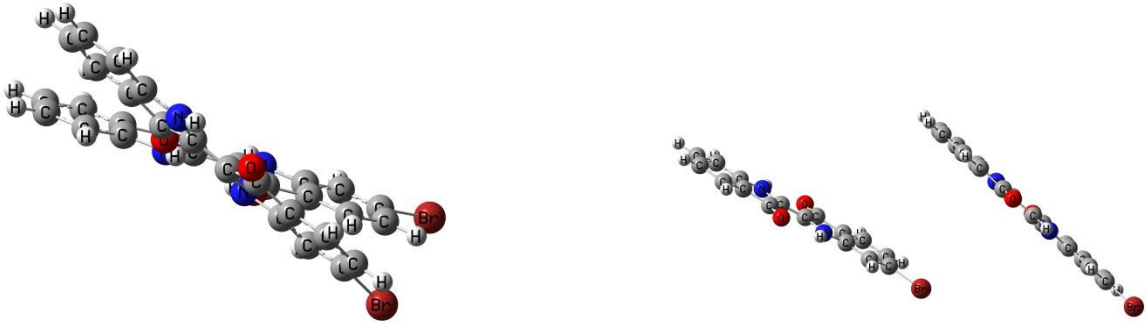

To see the stacking effect of crystal structures, the single point energy calculations and excitation calculations of MBI were performed without optimizations for the monomer. The result shows even lower wavelengths than optimized structure's results. Yet, as increasing the number of

molecules up to 6 in the clusters, the absorbed wavelengths shifted to the higher wavelengths, therefore the observed color becoming more purple and even shifted to bluer regions.

Up to 3-molecules clusters, the excitation energies all show the color is “red”, but wavelengths shift up in the same color region of the wavelengths. Dimers shifted to higher wavelengths, especially when the molecules are crossed each other’s than with parallel position. Trimer clusters shifted slightly lower than dimers. Except with monomer, transitions around 640nm appear in all clusters. With 4-molecules cluster calculation, the wavelengths shifted higher to the yellow region; therefore, the observed color is now purple. With 6-molecules cluster, the wavelength shifted even higher towards blue-green region. And with 6-molecules cluster, the peaks are getting concentrated around this blue-green peak and disappear in all red or purple regions.

These results show the color of MBI is red when the number of molecule (unit) is small, from 1

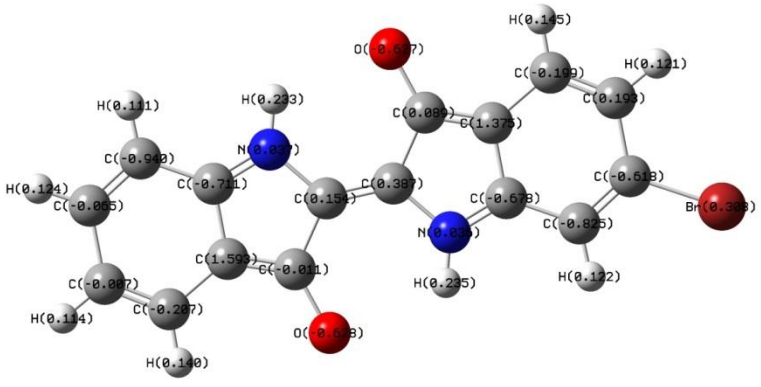

Figure 7.3. Resonance structure used for the calculation with Mulliken charges.

to 3. The color becomes purple when the number of molecule is around 4. The color becomes

bluer when the number of molecule is 6 and larger. In other words, when the molecules are highly ordered in crystal-like orientations with 4 or more units, MBI gives purple color or bluer colors.

From the observations of MBI' colors, it is red in its gaseous phase, purple on fabrics and in solution, and dark blue in its solid phase. In gaseous phase, it has more tendencies to be in smaller units because of high kinetic energy, therefore the molecules tend to be present as single units to give the redder colors. In solutions and on fabrics, which is from vat-dying, molecules have less kinetic energies and have more chance to come closer to form clusters with 4 or 5 units. In solid phase, it is structured in high order with many units coming close and forming large clusters, therefore MBI produces dark blue colors.

Although all three compounds, MBI, indigo, and DBI are conjugated, such small molecules are usually expected to absorb lower wavelengths, and therefore are perceived as redder colors than these three colorants. "Blue" molecules usually have much longer extended conjugated system of pi electrons and therefore small HOMO-LUMO energy gaps[98–100]. Absorbing higher wavelengths mean having smaller HOMO-LUMO energy gaps[91,93,101]. Diluting the solutions lowers intermolecular attractions between the molecules due to a colligative property of solutions. Heating the solutions lowers intermolecular attractions by increasing kinetic energy of molecules[101]. TEM results show slightly narrower spacing of molecules before the heating and aggregations of molecules into smaller nanoparticles after the heating[69]. All of these imply the

color differences come from the physical differences, rather than chemical differences. Moreover, indigo and MBI are noted to be perceived as “red” color in gaseous phase [10,96,97], which indicated when the effect of intermolecular forces is very low, the molecule indeed absorb the low wavelengths as expected by its structure. And when there exist enough intermolecular attractions causing the molecules to orient in highly ordered structures, these colorants’ colors become purple or blue.

7.2. Color and Particle Size

With TEM experiments[69] (ref. Ch.5), we found the size of aggregations becomes smaller upon heating, i.e., the size of aggregation becomes smaller when the color changes from purple to blue.

When the histogram was carefully inspected, I noticed that some population peaks with certain sizes disappear and/or appear upon heating (Figure 5.7). Then we can correlate these with the color differences.

Before heating, the most populated sizes can be found at around 12.5 nm, with the second populated size of ~27.5 nm and ~ 3nm in size. After the heating, the biggest particle size at 27.5 nm and the smallest size at from 0 to 2 nm completely disappeared, instead, the new populated peak at the size of ~5 nm appeared with the slight shift and decrease of the previously most populated peak at 12.5 nm. Then, the most populated peaks before the heating can be assigned to purple colors, which remain in almost the same place after heating. The disappearing peaks upon the heating at the largest size and smallest sizes can be assigned to red colors since the color becomes bluer, losing red components upon heating. And the appearing peaks upon the heating can be assigned to blue colors. These results are summarized in Table 7.1& Figure 7.4.

Table 7.1. Summary of the color-wavelengths & aggregation sizes

Color	Wavelength (nm)	Particle size (nm)
Purple	~ 420 reflected	12.5, 12
Red	~ 540 absorbed	27.5, 3
Blue/Green	~ 620 absorbed	6, 17.5

Figure 7.4. Peaks relationships between the reflectance and aggregations size

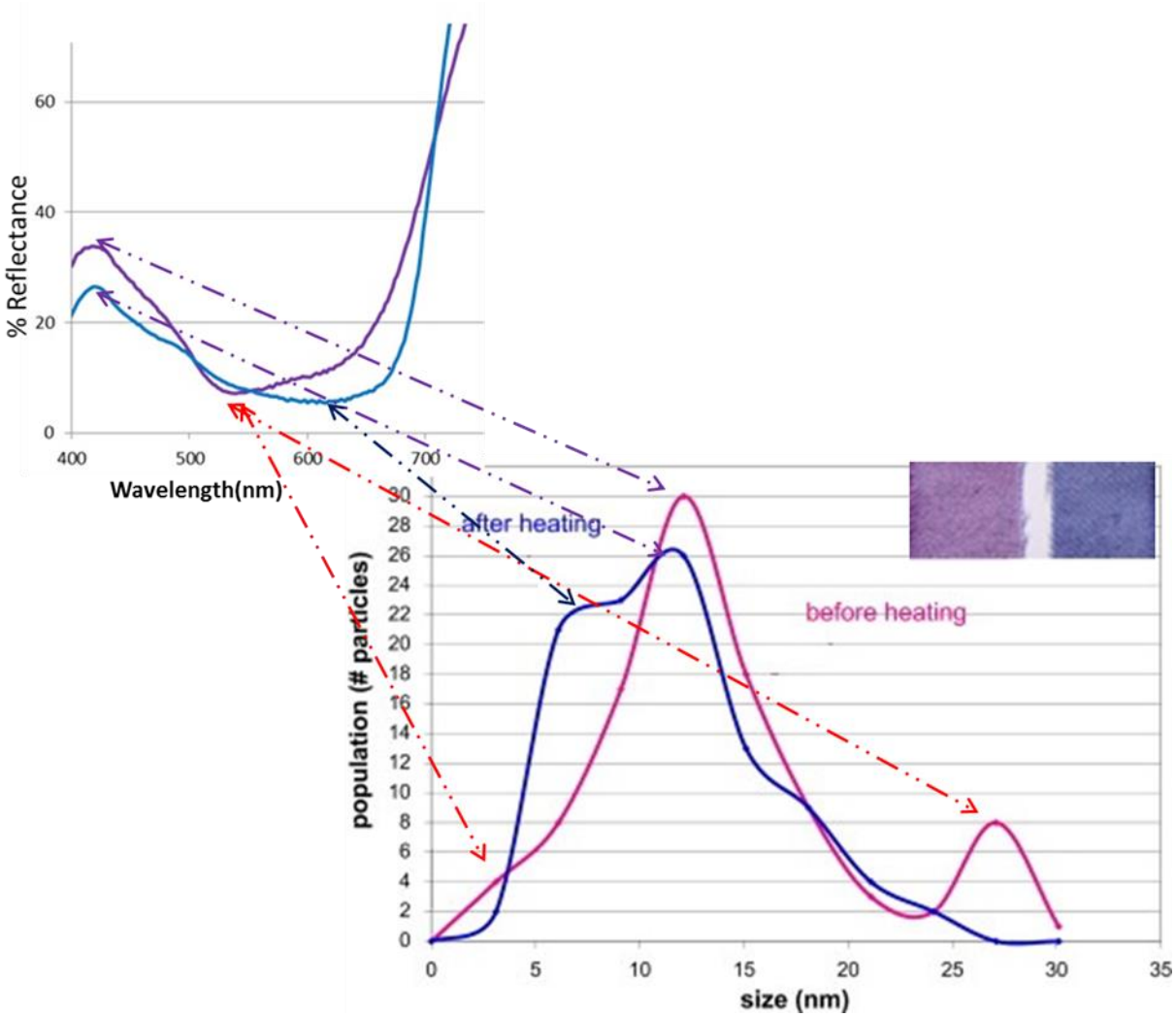

Lavinda, O.; Mironova, I.; Karimi, S.; Pozzi, F.; Samson, J.; Ajiki, H.; Massa, L.; Ramig, K. *Dyes Pigm.* **2013**, *96*, 581–589.

7.3. Particle and Cluster Size

In 7.1, I claimed that the color of MBI becomes bluer when the size of cluster becomes bigger. In 7.2, I claimed that the color of MBI becomes bluer when the size of particles becomes smaller.

Do these claims contradict to each other?

At beginning, that is what I thought, both deals with “size”, and one says the color becomes blue when the size gets big, the other says the color gets when the size gets small, does not make sense…

But when I examined the data carefully, with measuring the size of each molecule, I found that they are not talking about the same thing. The aggregation sizes from TEM histogram are far too big even the smallest size when compared to each of the MBI molecules.

One is talking about the aggregation sizes, which are all much larger than the size of MBI molecules. The other is talking about much smaller units of molecules.

In short, even though the size of cluster becomes bigger, the size of particles can be smaller and vice versa. It is because if a particle is constructed with small clusters, which are randomly oriented in the particle, it will more likely occupy more space than a particle which is constructed with one big cluster of the same number of molecules. An example is comparing two particles, one with constructed with 10 of one-molecule cluster (small, less ordered) and the

other particle is constructed with 1 of 10-molecule cluster (large, ordered). In this case, the latter will probably occupy less space, therefore is considered to be a smaller particle even though the cluster size is bigger. And this idea works well with the data.

The Table 7.1 and Figure 7.5 show the summary of color wavelengths, particle size and cluster size correlations. According to this, the Purple color is assigned to the size of 4 molecules and larger, major in 4+. Red is size from 1 to 3 molecules and Blue/Green is to 6 and larger, but start from 2+.

Smaller clusters with random orientation vs. larger cluster size with more ordered, crystal-like organizations.

The second populated size of 27 nm and 3 nm, which is related to smaller size of cluster, seems to be reasonable because in the dying solution, molecules have more tendencies to have smaller, but not the smallest number of molecules in a system because they are in solution. Therefore have more chance to have smaller size clusters (4+) deposited onto fabrics. Also, since the purple color is the "main" color when wool fabrics are dyed with MBI, that number of cluster systems are expected to be in the major amount. Therefore, the reflectance peaks with these will remain even when the passes are increased. When the number of passes is increased, the color of fabrics becomes bluer. When the reflectance spectra of these are examined[69], the differences are coming from the red-causing peaks around 530 nm. The blue-causing peaks do not change significantly after the second passes. This implies that smaller units are present in large amount in the initial dying solutions as expected from the nature's power law[102], which will be screened

out with the fabrics quickly. The remaining systems in the solutions will be the dominant 4+ systems and 6+ systems.

Table 7.2. Summary of the color-wavelengths, the cluster system sizes and aggregation sizes

Color	Wavelength (nm)	Particle size (nm)	**# of molecules in a system**
Purple	~ 420 reflected	12.5 12	**4 and larger (major in 4+)**
Red	~ 540 absorbed	27.5 3	**1 - 3**
Blue/Green	~ 620 absorbed	6 17.5	**6 and larger (start to appear from 2+)**

Figure 7.5. Reflectance Spectra and TEM Histogram: arrows show the correlations between red, purple and blue colors and the size of the aggregations (TEM) and the size of cluster systems (DFT calculations).

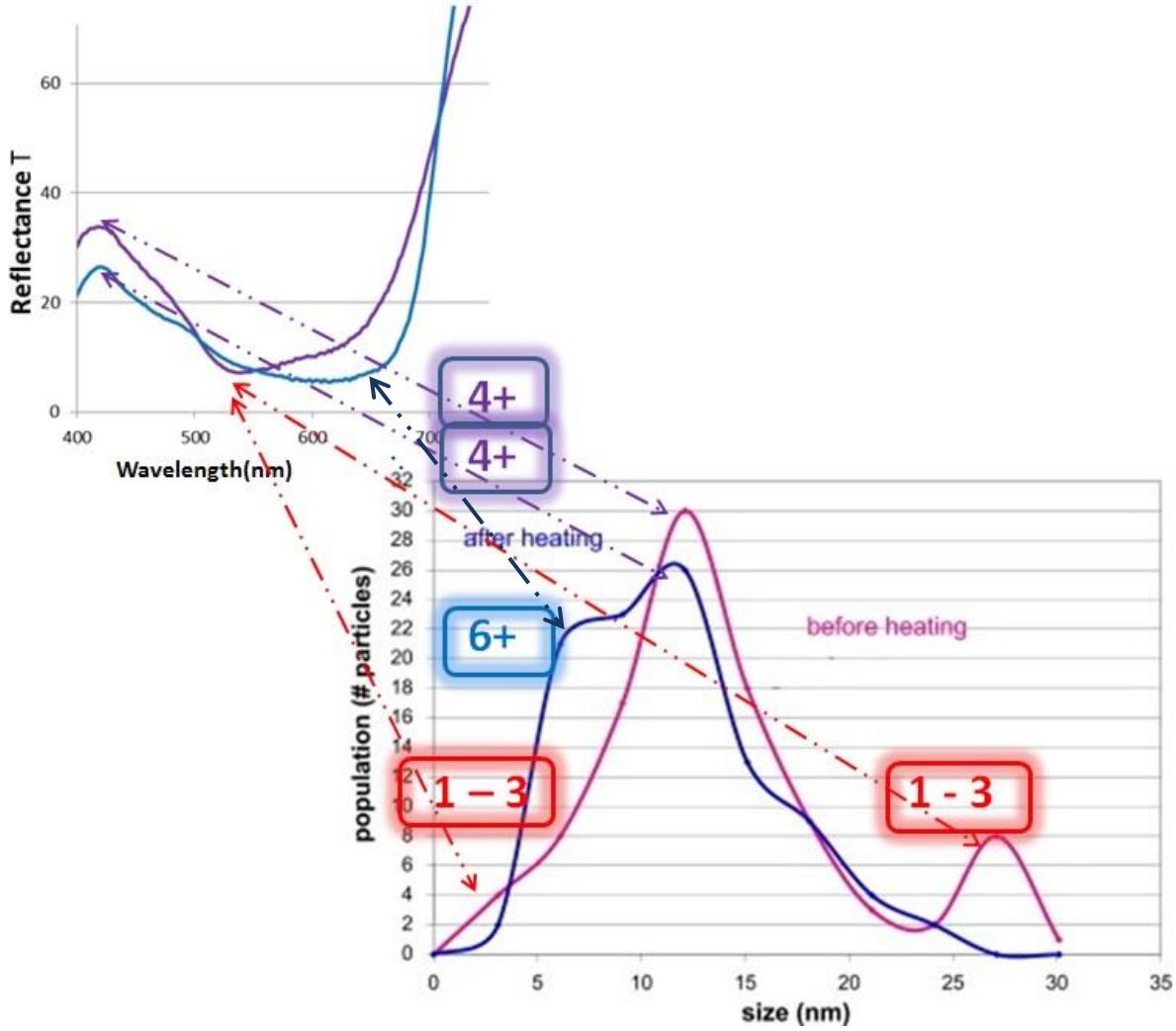

Lavinda, O.; Mironova, I.; Karimi, S.; Pozzi, F.; Samson, J.; Ajiki, H.; Massa, L.; Ramig, K. *Dyes Pigm.* **2013**, *96*, 581–589.

7.4. The Color and Thermochromism Color Change of MBI due to its Cluster Size

Having made the correlations of the color, particle sizes, and cluster sizes, I discuss here about the mechanism of the thermochromism property and the colors of MBI.

For the different colors in different phases can now be explained with the size of cluster sizes due to the kinetic energy available to the system. In gaseous phase, the color is red because there is enough kinetic energy available to the system so that molecules move fast enough to form smaller unit systems. In solutions, less kinetic energy is available so that compounds tend to form larger unit clusters of around 4 molecules. In solids, molecules stack and organize themselves in much larger units of clusters; therefore the color is dark blue.

For the thermochromism property, the color becomes blue from purple upon heating. That means the cluster size becomes larger upon the heating. The size of cluster becoming larger means that the orientation and organization of molecules are more ordered, becoming more like crystal. Then applying heat gives the energy needed for molecules to reorganize and reorient themselves to more ordered, crystal-like structures. Thus, the mechanism of the thermochromism property of MBI is the energy supplied in the form of heat cause the molecules to reorganize themselves to larger units of more ordered structures.

8. Conclusion

With these results, I believe I have done the most complete analysis of the chemistry of MBI, including synthesis, HPLC-PDA, x-ray single crystallography, Raman, NMR, UV-Vis spectroscopy, and quantum mechanical study and analysis.

I have shown the full investigation of 6-monobromo indigo, which is the least studied and known chemical among other components in the historically important colorant and has been gaining interests in technological purpose, Tyrian Purple.

I have concentrated on identifying MBI's chemistry and working on its color properties in this study. With the results from the DFT calculations for excited states, TEM analysis and visible reflectance analysis of dyed fabrics, its thermochromism color change from purple to blue and its "actual" different colors in different phases are described by the different size of cluster systems.

The color of MBI is red in its gaseous phase, purple in solutions and on fabrics, and dark blue in its solid phase. The color is red when the cluster size is small, from 1 to 3 molecules are present in a cluster system. The color is purple when the cluster system is middle sizes, with up to ~ 4 units of MBI are present in a cluster system. The color becomes dark blue when the cluster system becomes bigger than 6 units of MBI present in a cluster system.

The color of MBI changes from purple to blue upon heating because the heating gives MBI enough energy to reorient and reorganize themselves in bigger cluster systems with more ordered, compact crystal-like structures, which occupy less volume.

I have not observed the reversibility of this color change, but the research laboratory at JURAKU Corporation, Japan has observed the color reversibility with fabrics dyed with natural snail-extracted Tyrian Purple. And the interesting part is that they observed the color change-reversibility when they heated cotton and wool with "steam iron" and did not observe when they did the same thing to silk fabrics. The colors became bluer upon heating and went back to original-purple upon cooling, according to them. They also reported that the color change of Tyrian Purple seems to be physical rather than chemical. I have observed the wool fabrics which changed the color from purple to blue, but they stayed that color even when they were cooled. Using "steam" iron and using certain fabrics cause the reversibility of color change seems that it may be that MBI is a sort of vapochromism as well as thermochromism. And the spacing of the fabrics and the vaporizing water molecules causing the initial color change by the reorganization, and as vapor waters leave quickly, the spacing of molecules come back to the original and the color go back to the original. Steam may be giving some "phase" change temporarily. Of course, the results at Juraku Corporation is with natural Tyrian Purple and not with pure MBI, so I cannot conclude this is the same with the color change of MBI. Still this seems to be a strong supporting result for aggregation of molecules.

Further study is needed to fully conclude about MBI and other indigoids' color property because the study shown here have been completed with mainly gaseous phase for theoretical calculations and with single point calculations of MBI crystals. For further study, such as optimizations of clusters of MBI, indigo and DBI, simulation study with temperature differences is of the interests for future studies. Also, since the study was for gaseous phases, the electronic correlation properties exist in solid states have been ignored. If we can study these in near future, the property will be better understood.

Yet, these results make a good milestone to the history of the study of 6-monobromo indigo and Tyrian Purple.

Appendix A: Optimizations of Monomers and Dimers with Excitation Energy Calculations

A.1. Calculations

Optimizations of monomers and dimers of MBI, indigo and DBI were performed using the previously published crystal structures [37,52,95]. The structures were optimized by Density Functional Calculation (DFT) [71,87]method and then, the optimized structures were excited with Time-Dependent DFT (TD-DFT) method. The exchange correlation functional and orbital basis functions used for a minimum geometry of MBI were Becke, Three-parameter, Lee-Yang-Parr (B3LYP) [59,103] and 6-31G (2d, 2p)[61,62].

Two types of dimers coordinates were optimized, a crossed structure and a parallel structure (Figure A.2) for MBI and indigo.

Next, the monomers and dimers of MBI and indigo in solutions are calculated. The solvents used are chloroform and DMSO. The calculation method used are DFT for the optimizations and TD-DFT for the excitations with B3LYP 6-31G(2d,2p) CPCM[104,105]. This method creates the solute cavity via a set of overlapping spheres[106]. The Barone and Cossi's implementation of the polarizable conductor model continuum solvation method (CPCM) performs a Polarizable Continuum Model[107–113] (PCM) calculation using CPCM polarizable conductor calculation model[106].

Since when a molecule is excited, its structure is expected to be more like a charged one [10,96], a calculation of a resonance structure of MBI was also performed. MBI can have a few resonance structures and the one that has the most stability with symmetric charges was used for the calculation (Figure A.3). When the resonance structure was optimized, it is expected to become the same as the optimized crystal structure. Therefore the calculation was carried as single point energy and excitation energy calculations for the resonance structure.

A.2. Results

The optimized total energies of MBI, indigo and DBI are the following with single point energy of crystal structures in the following brackets; -3447.006 (-3446.848), -875.690 (-875.499), and -6018.327 (-6018.244) in atomic units (Table A.1). One of the major differences in the structures of these three molecules is the bond lengths of C-Br [37,52,114] , MBI being shorter than DBI. After the optimization, the bond lengths of MBI became longer for 0.007631 Å with optimization, same with indigo for 0.144405 Å, and for DBI, the optimized bond length became slightly shorter than the crystal structure for 0.00421 Å. The dihedral angle of N-C=C-N remains at 180º for all three indigoids despite of the expectation of distortion of the ring due to Br atoms (Figure A.1. Labelling of bonds with Indigo & Table A.2).

The shape of molecular orbitals of indigo and DBI are slightly different from the previous reported one, especially the one for with DBI (see Figure A.8. to A.13). The MOs are more delocalized with indigo and DBI's MOs show more influence of Br atoms attached to the both sides, which shows up with MBI in the same manner, but asymmetrically[19].

Also, the excitation energy between $S_0 \rightarrow S_1$ for indigo and DBI are lower than the previously reported[19] (see Table A.1). These calculated values are: 2.3169 for MBI, 2.2416 for indigo, and 2.2830 for DBI, all in the unit of eV.

Excitation wavelengths of these indigoids resulted in the region of around 535 to 550 nm (Table A.3). This is green-absorbing region, therefore cause red colors to our eye, which seems to be strange because all the three chemicals give purple to blue colors.

The optimizations in gas phase were performed with 2 types of dimers structures, one for a cross-structures and the other for a parallel-structures (Figure A.2) of MBI and indigo. These spectra show the absorption peaks shifted to higher wavelengths with MBI, but slightly downward with indigo dimer. In any cases, the absorption peaks remain in the red-causing regions.

The results from excitation calculations with solvents give much higher wavelength absorptions. All the results shifted to the yellow region of the EM, therefore they cause purple colors to our eyes (Table A.3)

Surprisingly, the absorption maxima of the resonance structure of MBI in gaseous phase showed up in much lower region. The maxima showed up in the UV-region with almost double intensity of other structures. Moreover, the wavelengths around 600 nm became much more intense than other structures also.

Table A.1. Total Energy of Optimized MBI, Indigo, and DBI Monomers

Monomers	Total Optimized Energy (a.u.)	Total Energy of Crystal Structure (a.u.)
MBI	-3447.006	-3446.848
Indigo	-875.690	-875.499
DBI	-6018.327	-6018.244

Figure A.1. Labelling of bonds with Indigo

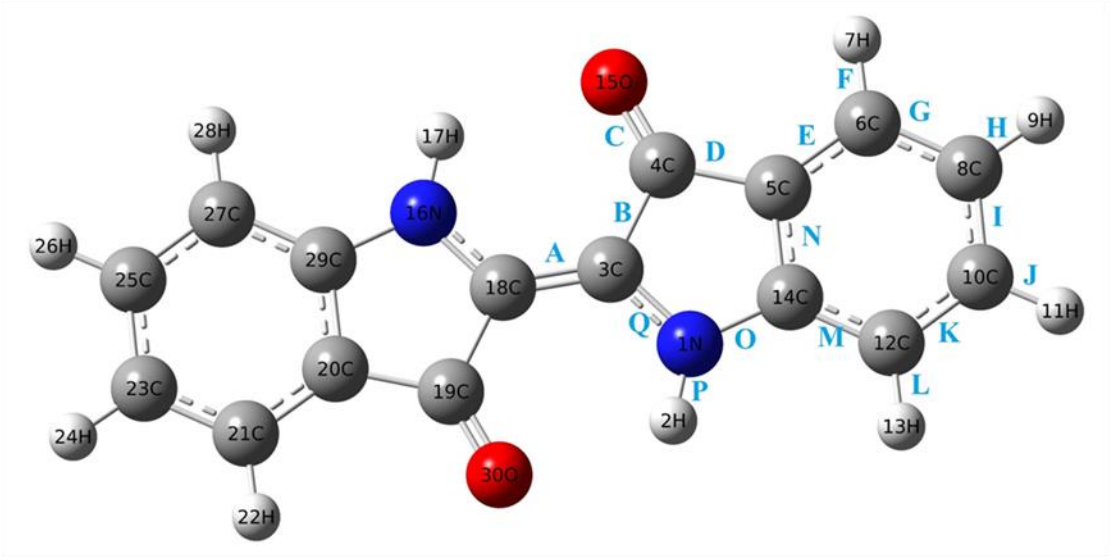

A: C=C double bond

B: C-N bond

C: N-H bond

D: N-C bond

E, G, K, M: C-C bond

F, H, L: C-H bond

J: C-Br bond for MBI and DBI, C-H bond for Indigo

I, N: C-C bond

O, Q: C-C bond

P: C=O bond

Table A.2. Dihedral angle and bond lengths for monomers (MBI, Indigo, and DBI). The optimized bond length of C-Br for MBI is longer than crystal structure's lengths [52,95,114]. C-Br bonds are labelled in red

Dihedral Angle (º) and Bond Lengths (Å) *1	MBI	Indigo	DBI
Dihedral Angle: N-C=C-N (º)	180.00	180.00	180.00
A	1.357	1.359	1.357
B	1.489	1.492	1.491
C	1.227	1.229	1.226
D	1.468	1.468	1.468
E	1.392	1.395	1.392
F	1.084	1.084	1.084
G	1.390	1.392	1.390
H	1.081	1.083	1.081
I	1.402	1.405	1.402
J	1.894	1.084	1.893
K	1.392	1.395	1.393
L	1.082	1.084	1.082
M	1.392	1.394	1.392
N	1.414	1.414	1.414
O	1.383	1.388	1.384
P	1.010	1.010	1.010
Q	1.381	1.379	1.379

*1: Refer to Figure A.1 for the labeling of bonds

Table A.3. Summary of Excitation Energy and Oscillation Strength from Optimizations

Molecule			Excitation Wavelengths	Oscillation Strength	Energy (eV) $S_0 \rightarrow S_1$
MBI	Monomer	Monomer	535.13	0.2782	2.3169
		Resonance Structure (single point)[*1]	398.24	0.2281	3.1133
			601.78	0.0464	2.0603
		DMSO	570.99	0.3458	2.1714
		$CHCl_3$	566.86	0.3489	2.1872
	Dimer	Dimer (cross)	545.27	0.4633	2.2738
		Dimer (parallel)	537.56	0.5689	2.3064
		DMSO (cross)	582.14	0.4155	2.1298
		$CHCl_3$ (cross)	579.80	0.4823	2.1384
Indigo		Monomer	553.10	0.2685	2.2416
		DMSO	573.73	0.3179	2.1610
		Dimer (parallel)	534.77	0.4501	2.3185
DBI		Monomer	543.07	0.3113	2.2830

*1: Data here are taken from visible regions only

Figure A.2. Dimers. Left: Parallel & Right: Cross

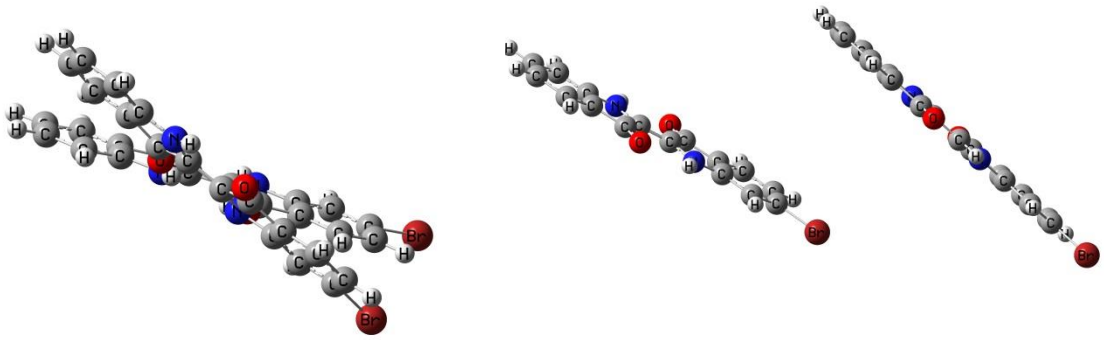

Figure A.3. Resonance structure used with Mulliken charges. MBI

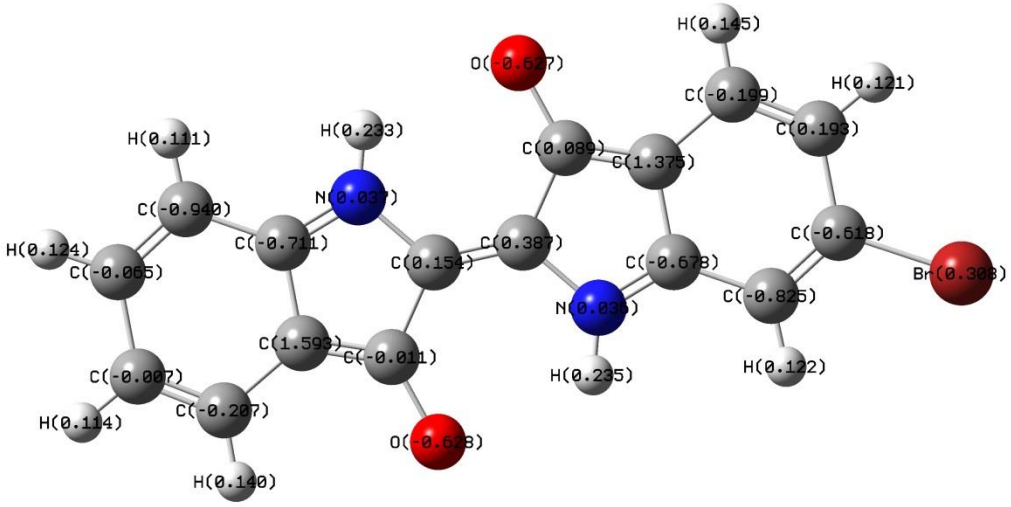

Figure A.4. MBI HOMO (85)

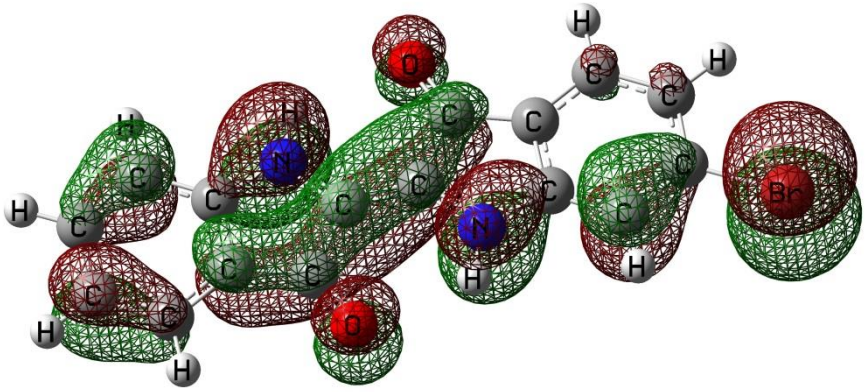

Figure A.5. MBI LUMO (86)

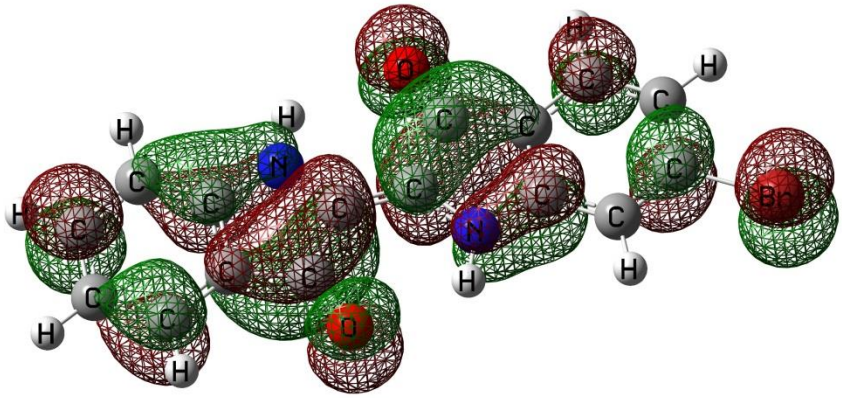

Figure A.6. MBI HOMO-1

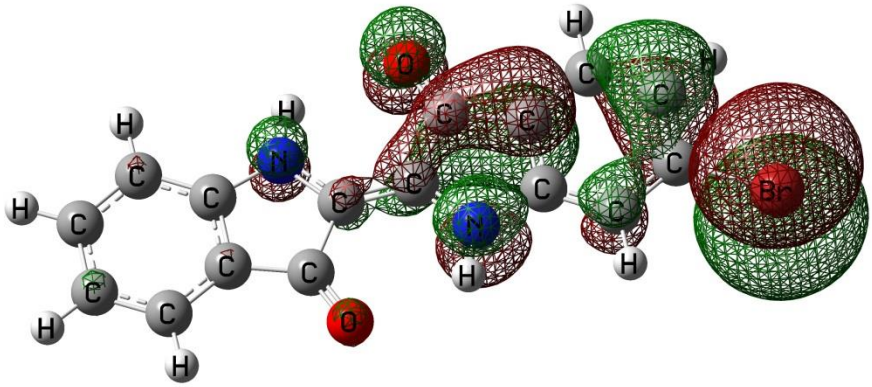

Figure A.7. MBI LUMO+1

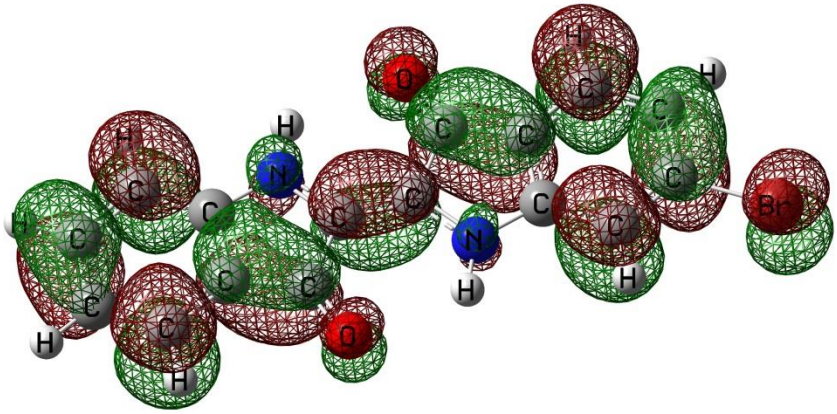

Figure A.8. Indigo HOMO (68)

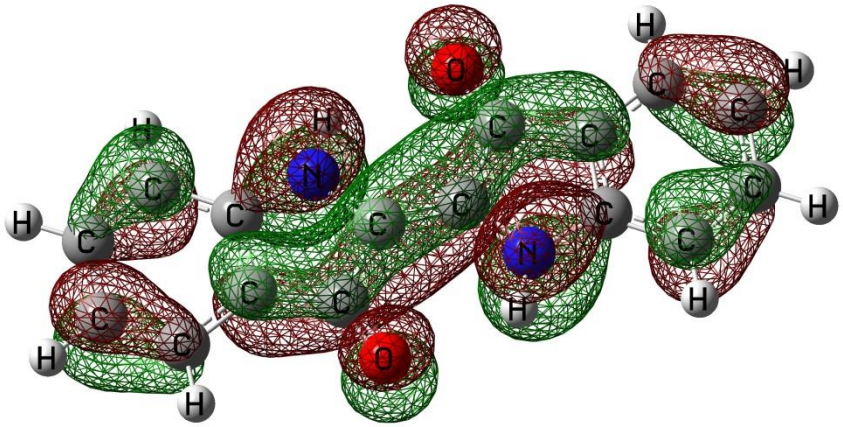

Figure A.9. Indigo LUMO (69)

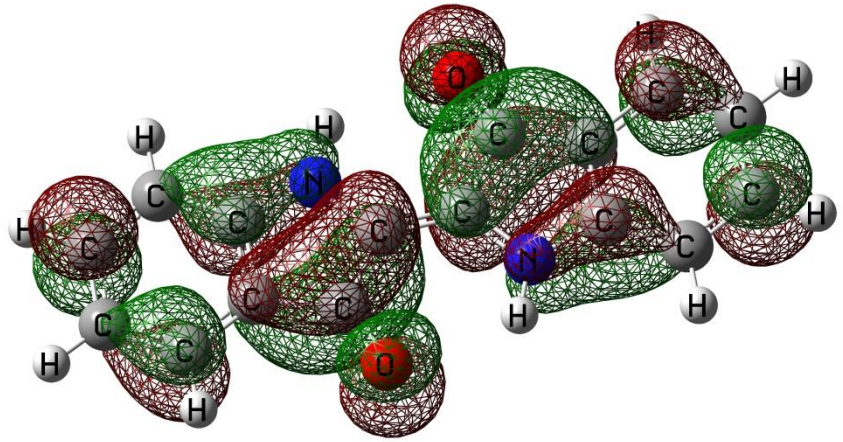

Figure A.10. Indigo HOMO-1

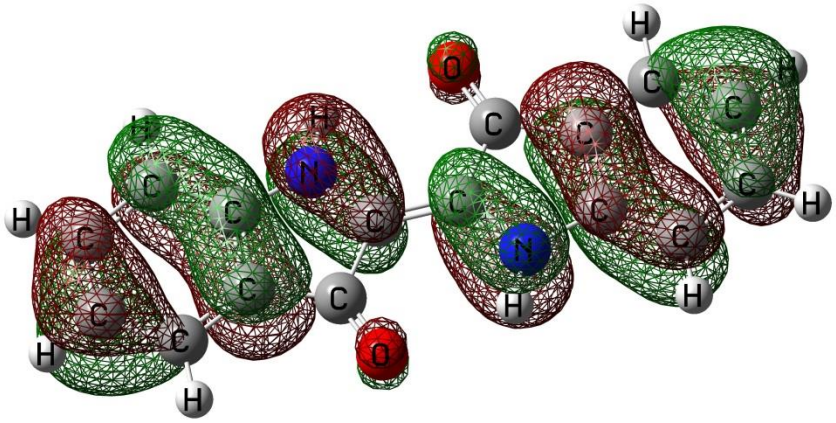

Figure A.11. Indigo LUMO+1

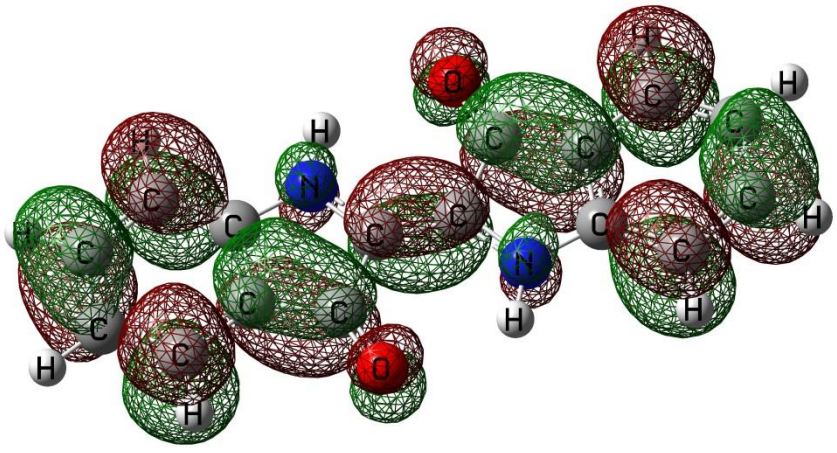

Figure A.12. DBI HOMO (102)

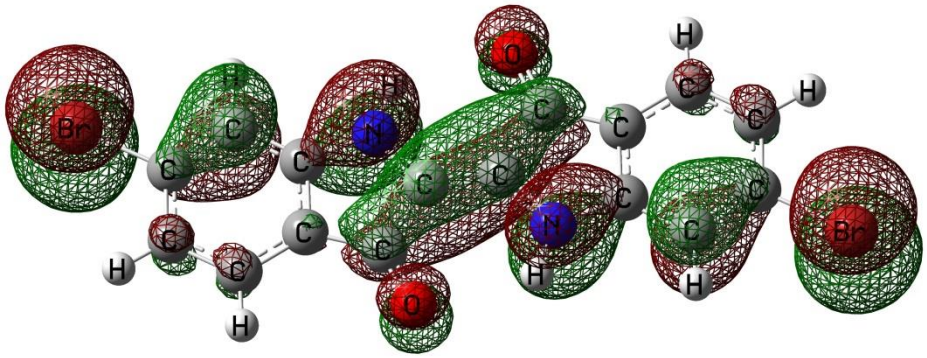

Figure A.13. DBI LUMO (103)

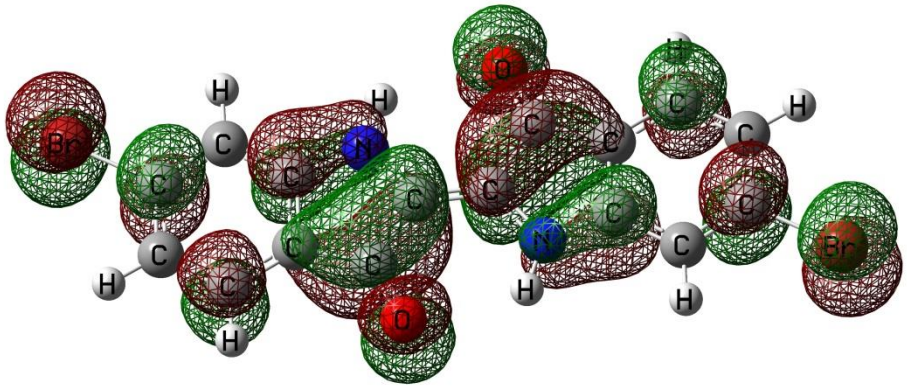

Figure A.14. DBI HOMO-1

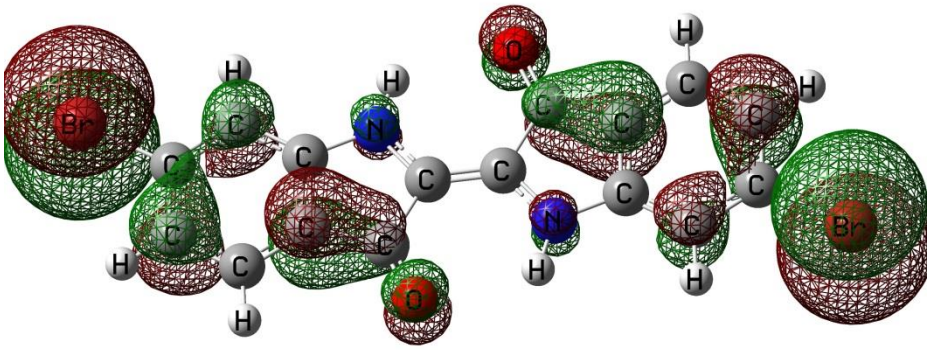

Figure A.15. DBI LUMO+1

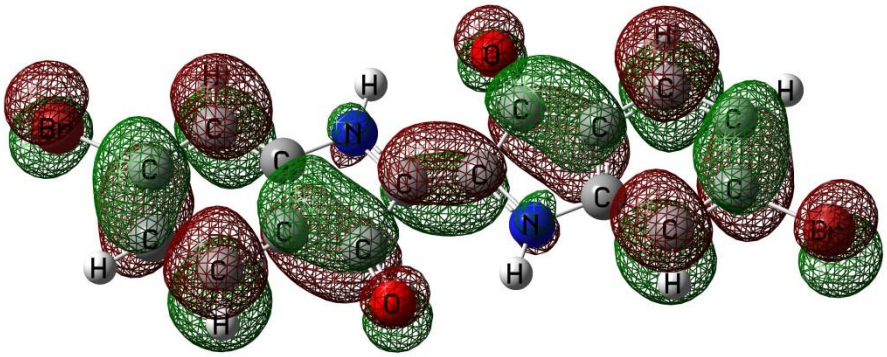

Appendix B: Pictures of objects dyed with snail purple

Figure B.1. Kimono-obi (belts) with Tyrian Purple by Juraku Corp., Japan

Figure B.2. Ama-san (Japanese female divers) with the ritual symbols (star: Seiman, mesh: Doman) written with snail purple on their thin towels and on the charms. Note how simple tools they use to dive in up to ~ 5 m.

Figure B.3. A part of the ritual fishing mesh (~5 m x 6 m in total size) from Peru, approximately AD 1 old. Dyed with Tyrian Purple, indigo, and cochineal. The actual color is much vivid and bright. Owned by Juraku Corp., Japan

Figure B.4. Snail dyeing at TOBA Sea Folk Museum. Note how the color changes from yellow (from the left to right and to the bottom), green to purple under the sun. The time differnce is approximately 30 minutes between the first picture and the last picture.

Appendix C: Molecular Orbital Pictures

Figure C.1. MBI Resonance HOMO (85)

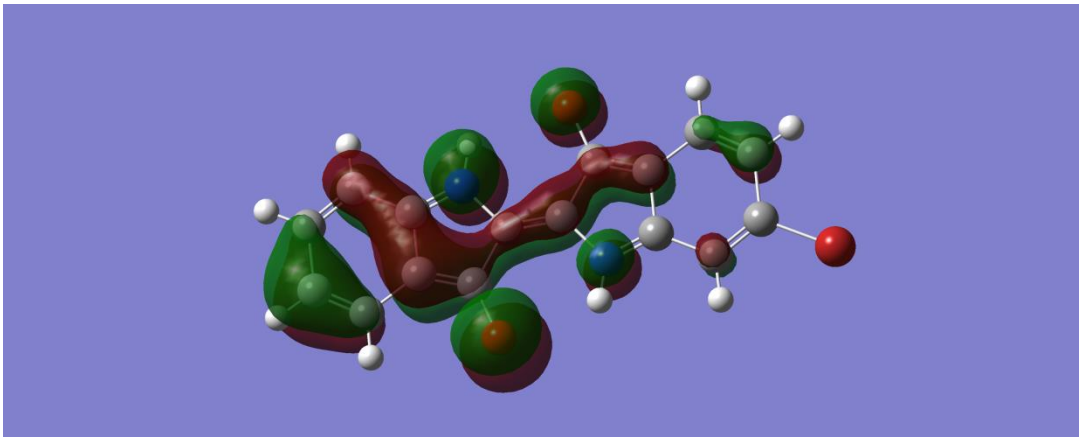

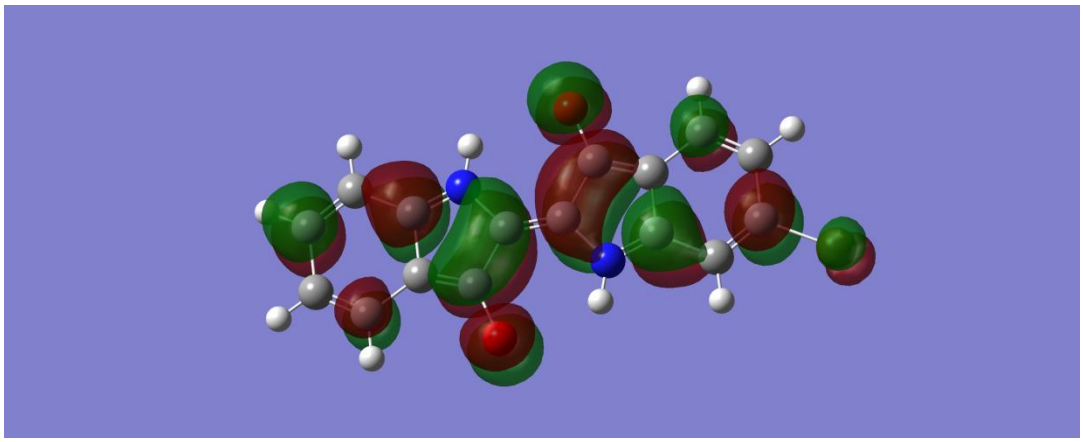

Figure C.2. MBI Resonance LUMO (86)

Figure C.3. MBI Resonance HOMO-1

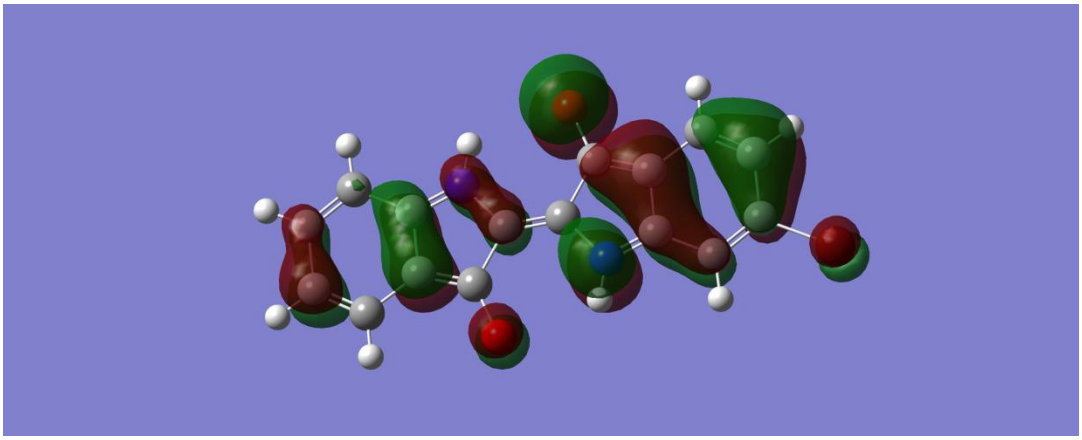

Figure C.4. MBI Dimer, cross in DMSO, HOMO (170)

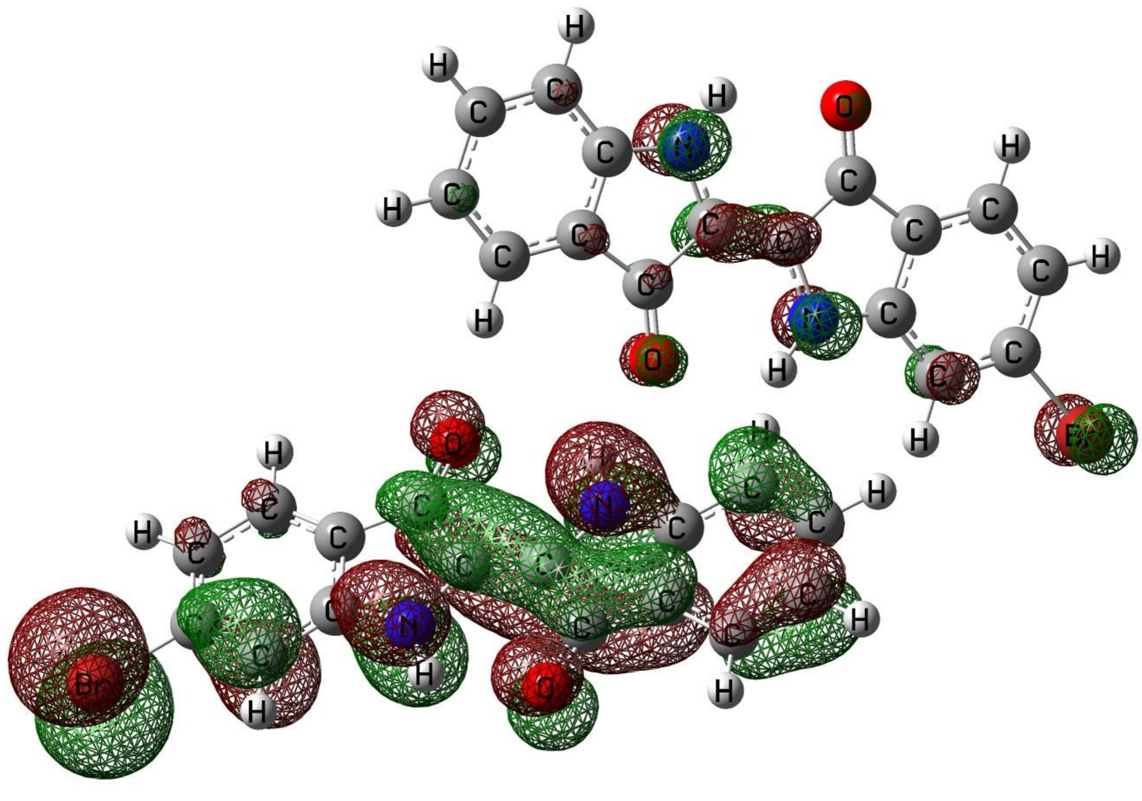

Figure C.5. MBI Dimer cross in DMSO, LUMO (171)

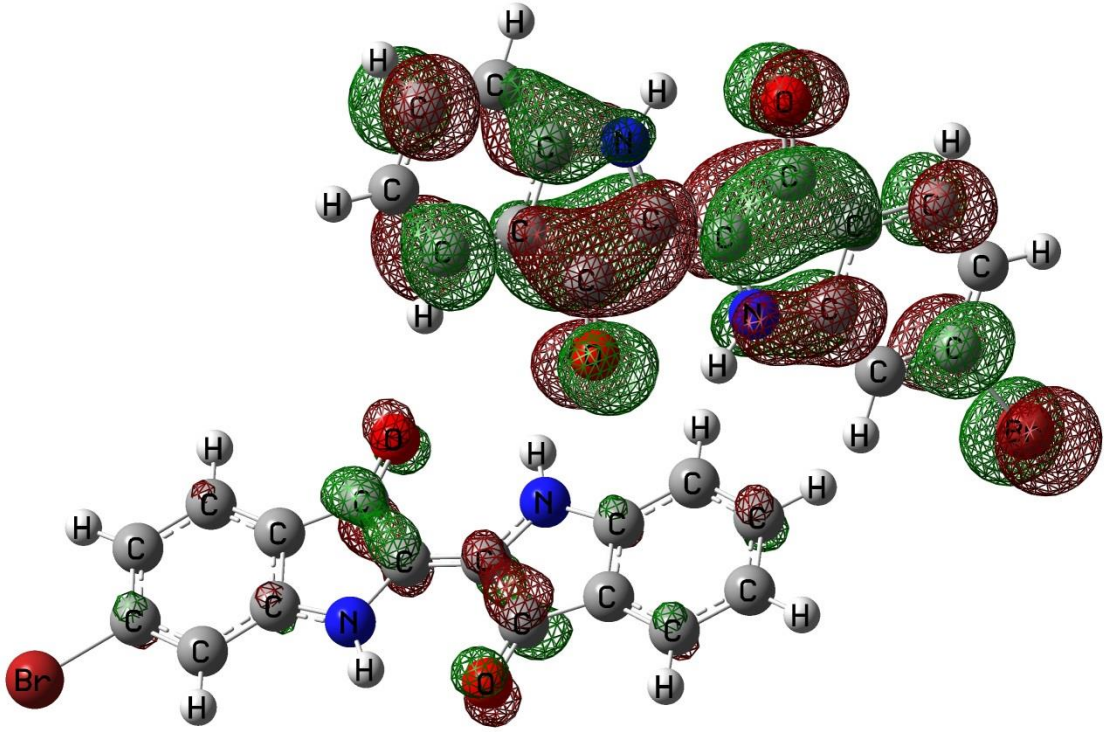

Figure C.6. MBI Dimer cross in DMSO, HOMO-1

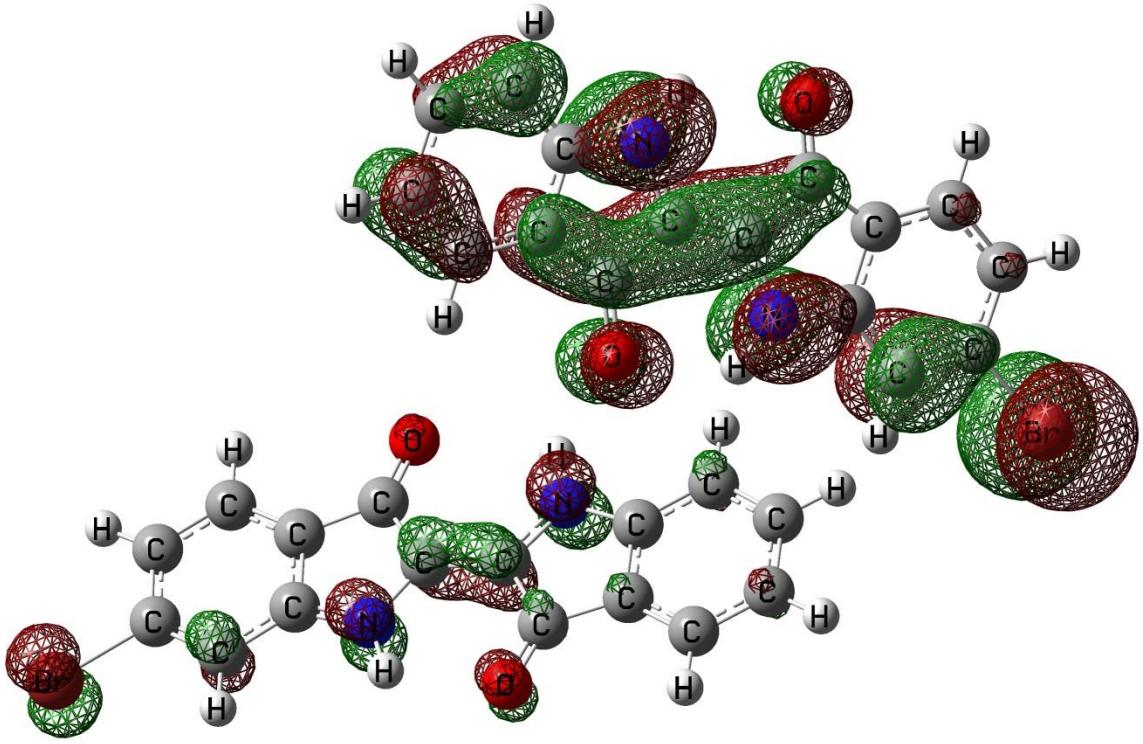

Figure C.7. MBI Dimer cross in DMSO, LUMO+1

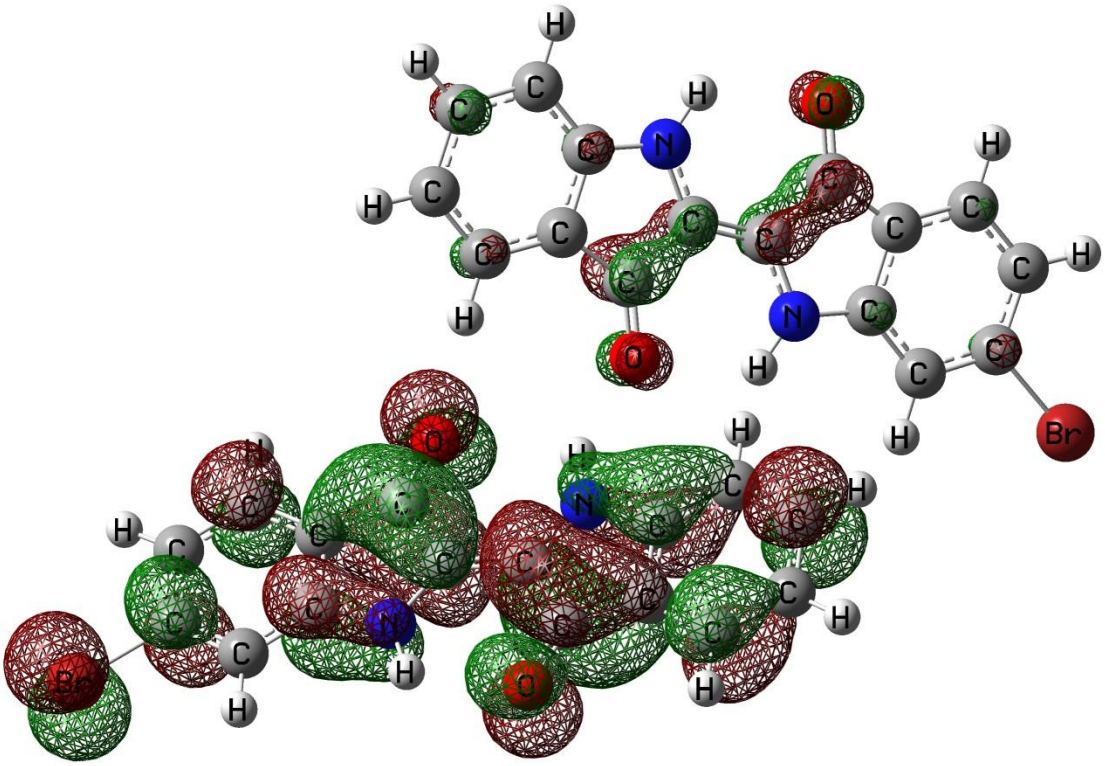

Figure C.8. MBI Dimer cross CHCl3, HOMO (170)

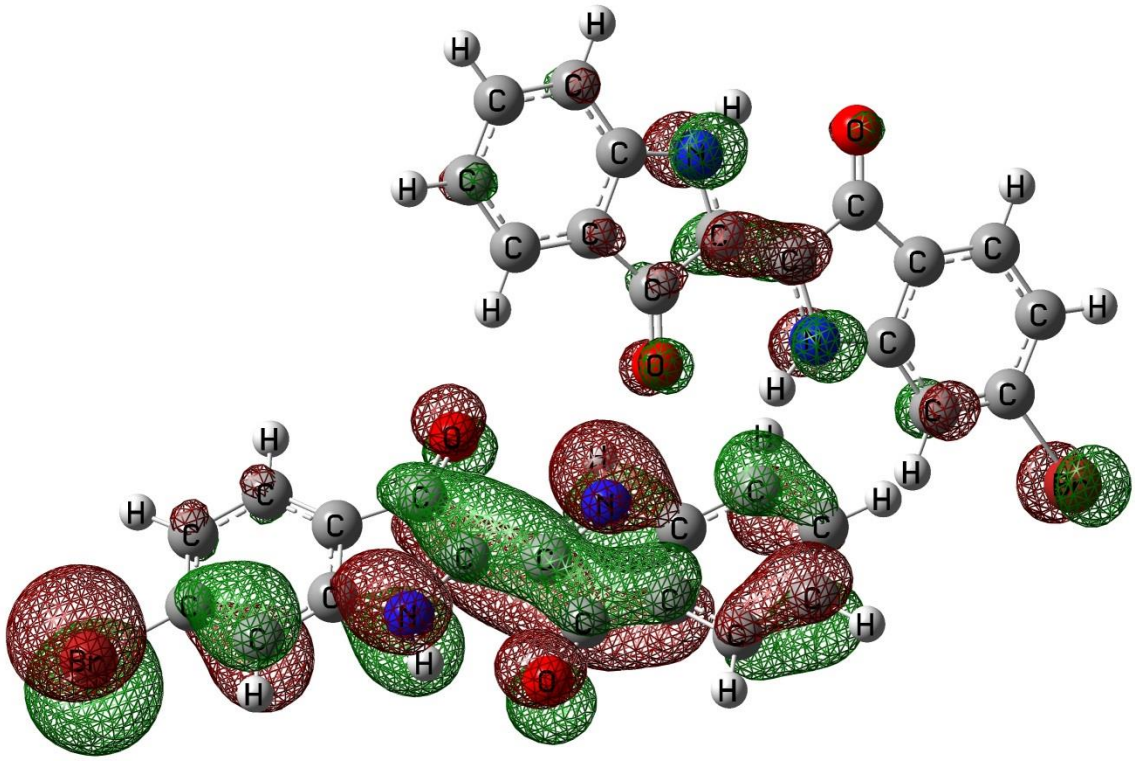

Figure C.9. MBI Dimer cross CHCl3, LUMO (171)

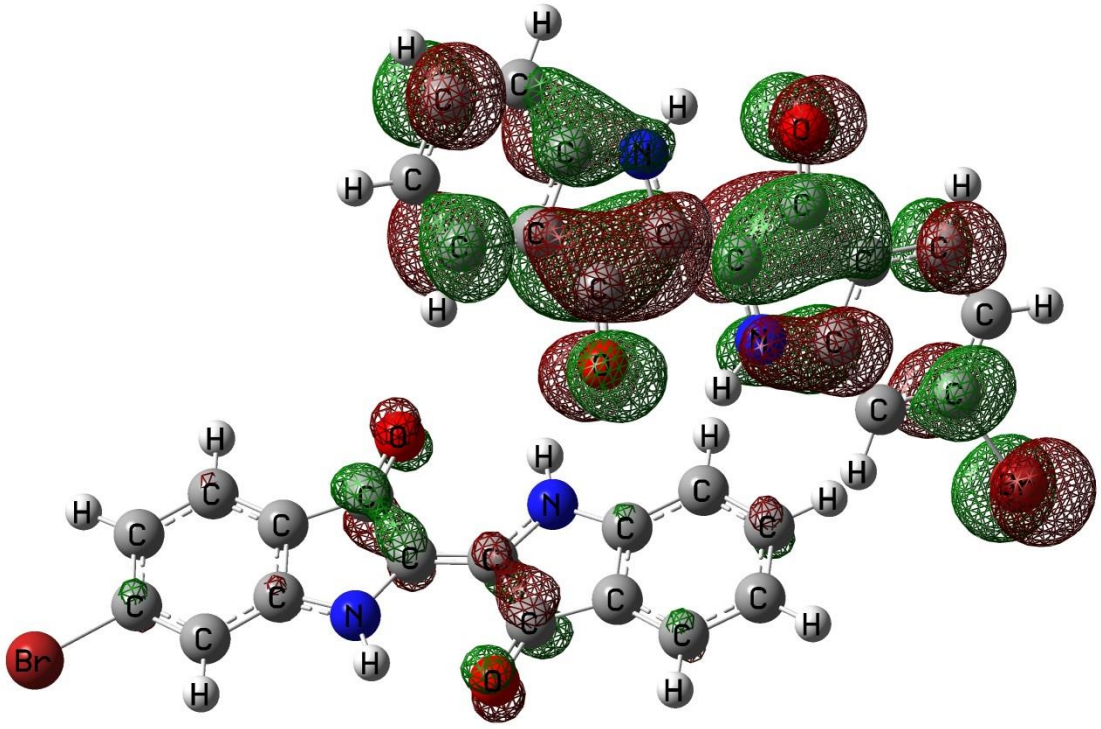

Figure C.10. MBI Dimer cross CHCl3, HOMO-1

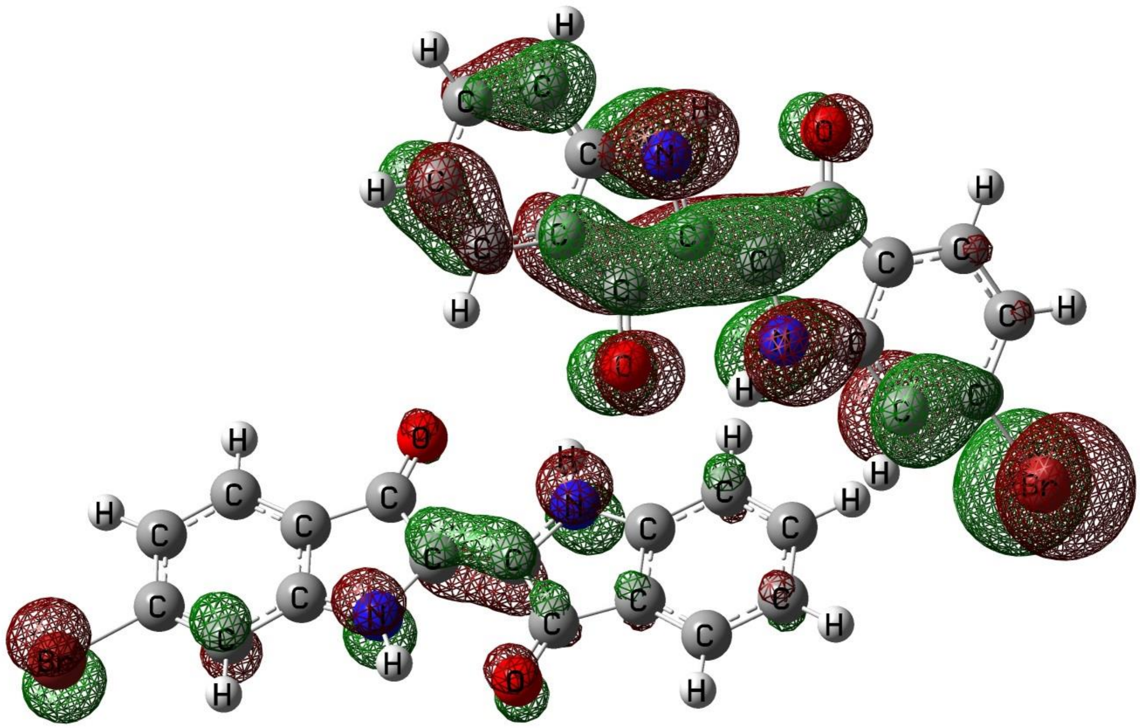

Figure C.11. MBI Dimer cross CHCl3, LUMO+1

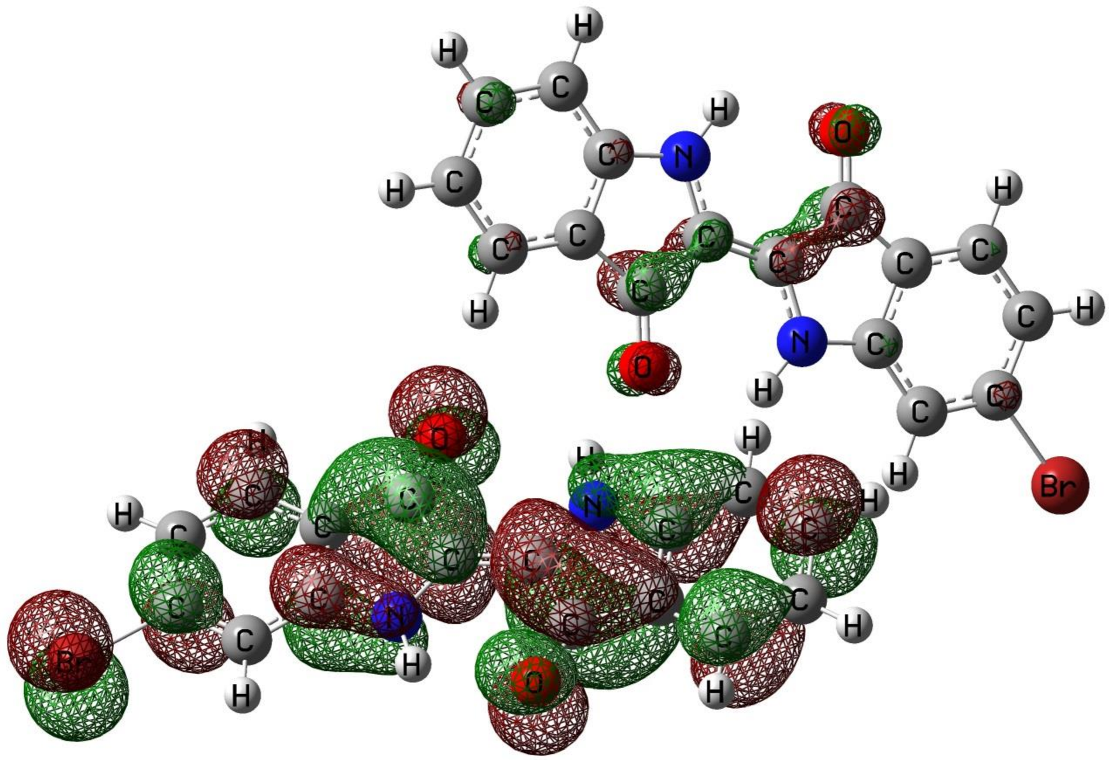

Figure C.12. Indigo Dimer parallel Optimized, HOMO (170)

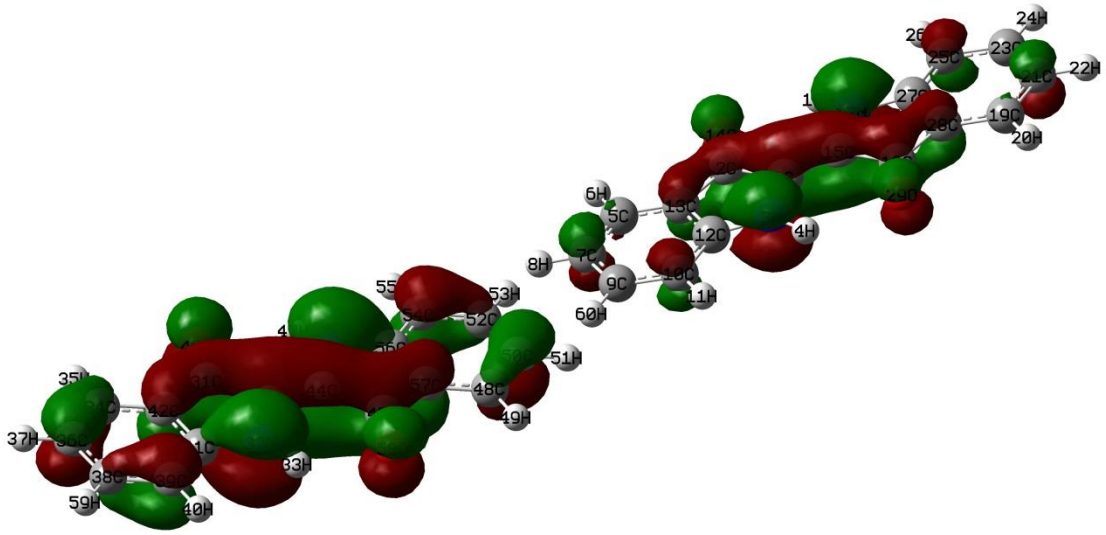

Figure C.13. Indigo Dimer parallel Optimized, LUMO (171)

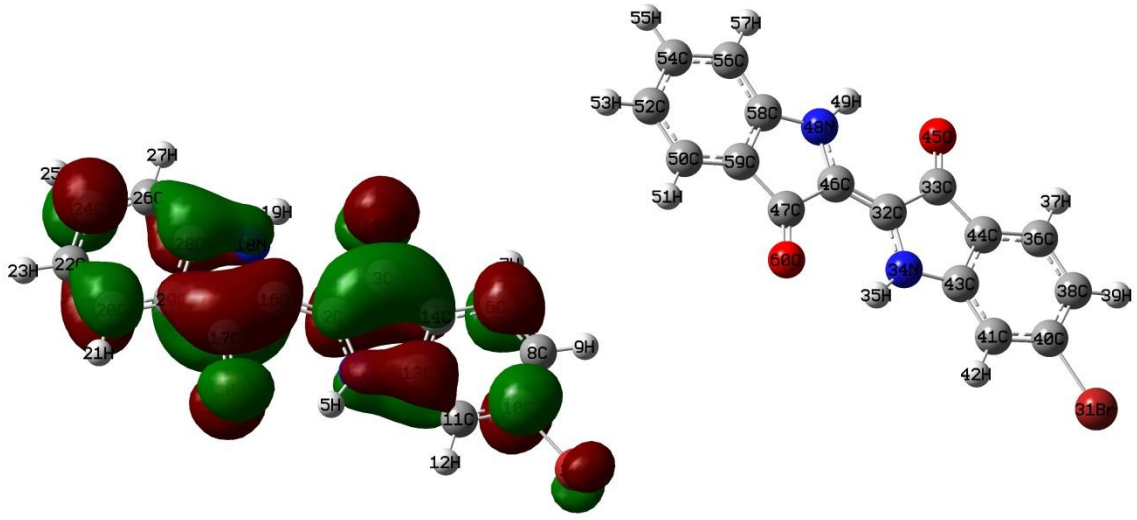

Figure C.14. MBI Dimer parallel Optimized, HOMO (170)

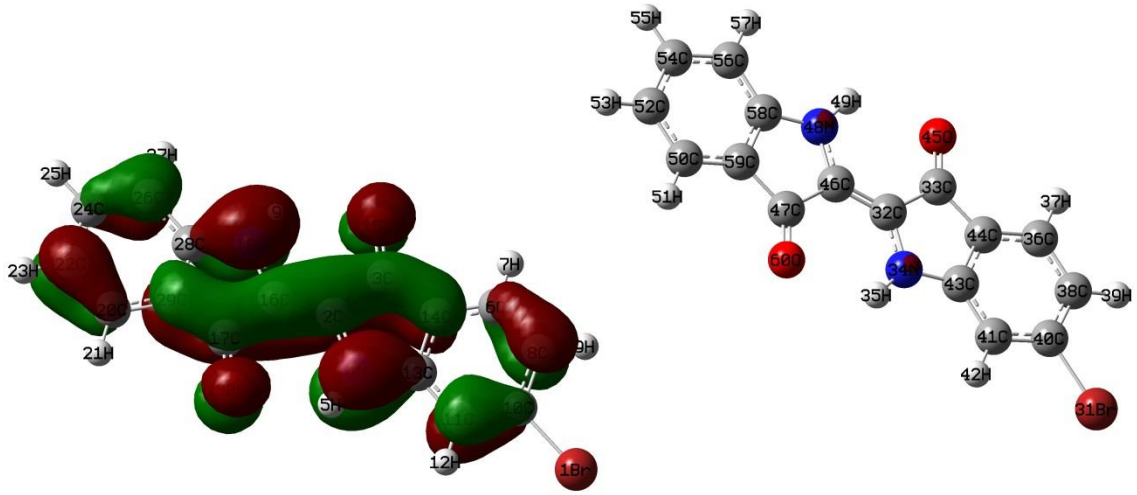

Figure C.15. MBI Dimer parallel Optimized, LUMO (171)

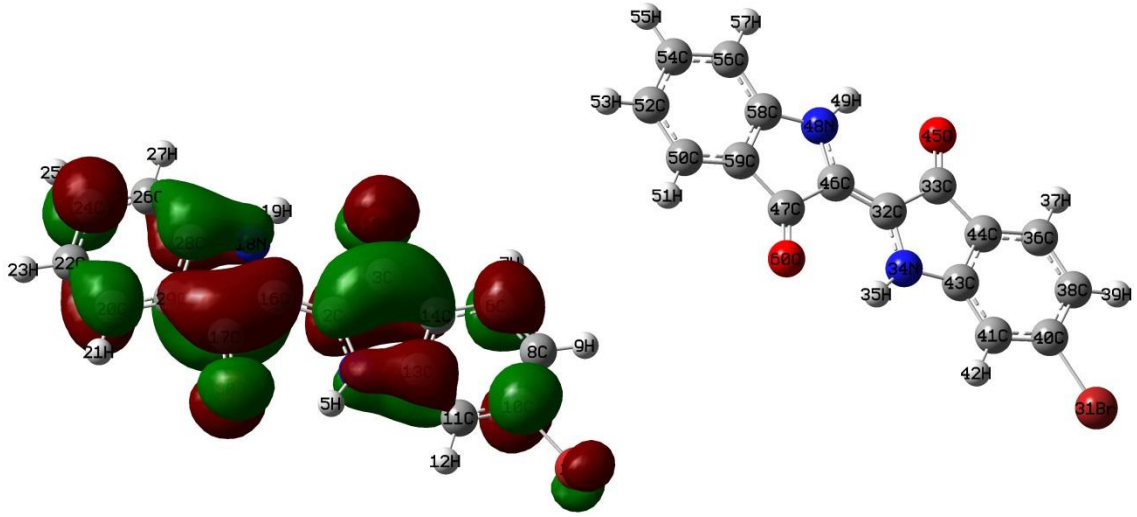

Figure C.16. MBI Trimer (less crossing), HOMO (255)

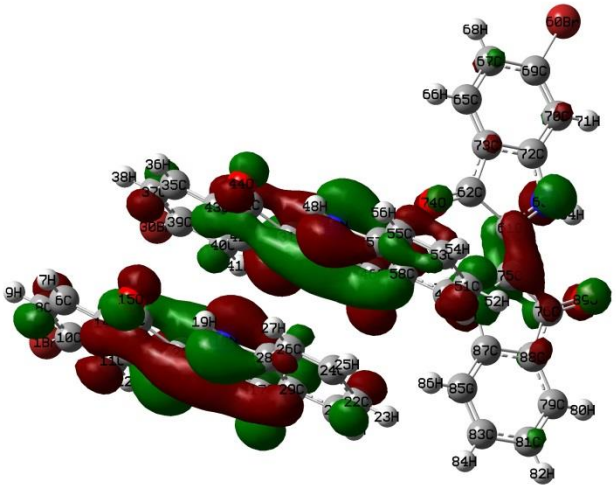

Figure C.17. MBI Trimer (less crossing), LUMO (256)

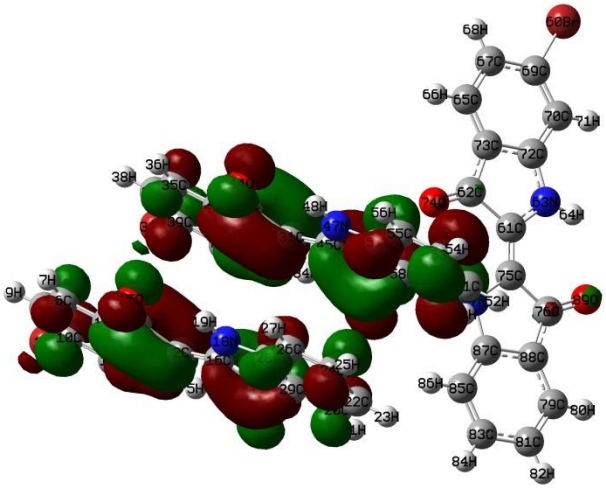

Figure C.18. MBI Trimer (less crossing), HOMO-1

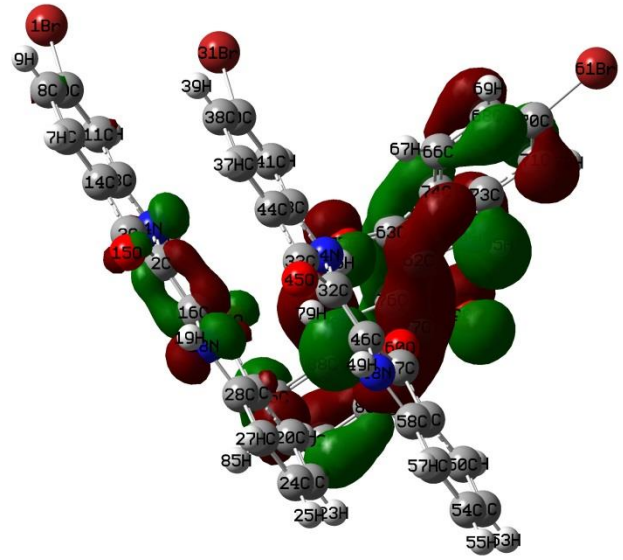

Figure C.19. MBI Trimer (less crossing), LUMO+1

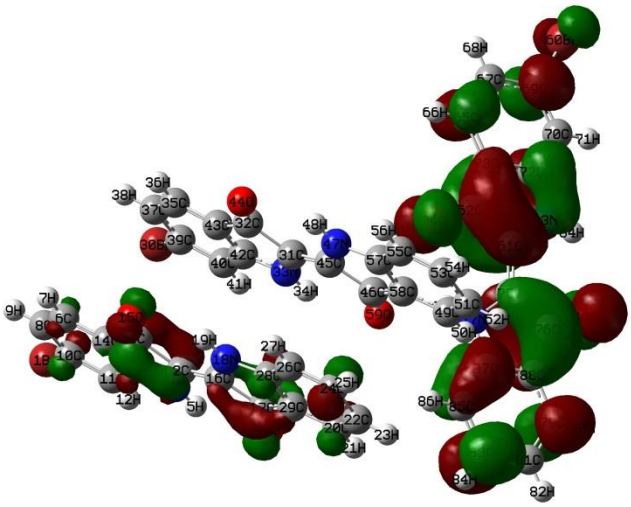

Figure C.20. MBI Trimer (more crossing), HOMO (255)

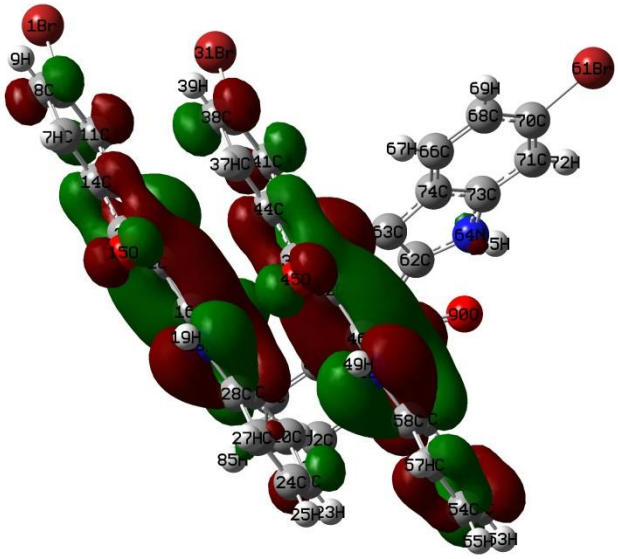

Figure C.21. MBI Trimer (more crossing), LUMO (256)

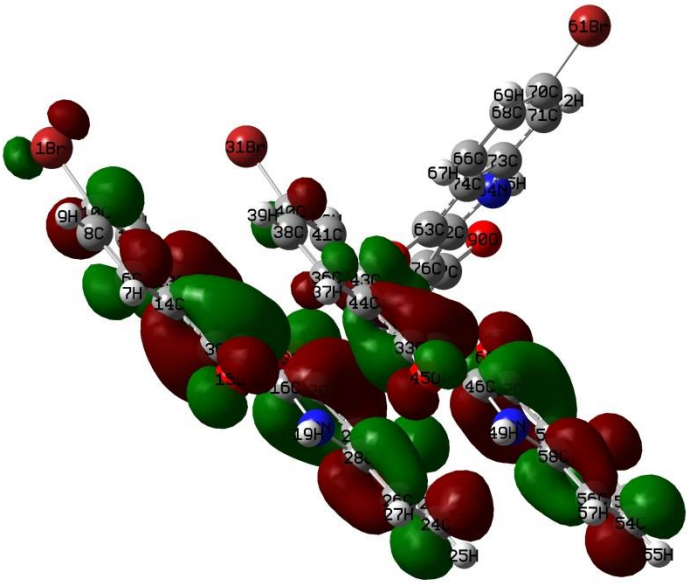

Figure C.22. MBI Trimer (more crossing), HOMO-1

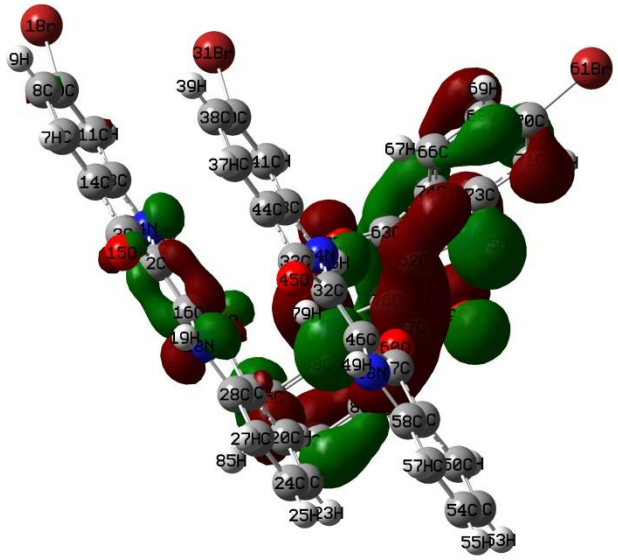

Figure C.23. MBI Trimer (more crossing), LUMO+1

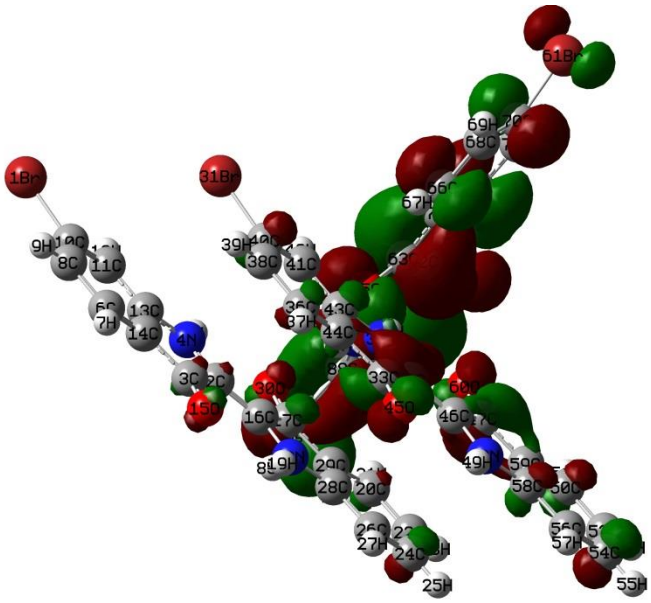

Figure C.24. MBI 4-Molecule Cluster, HOMO (340)

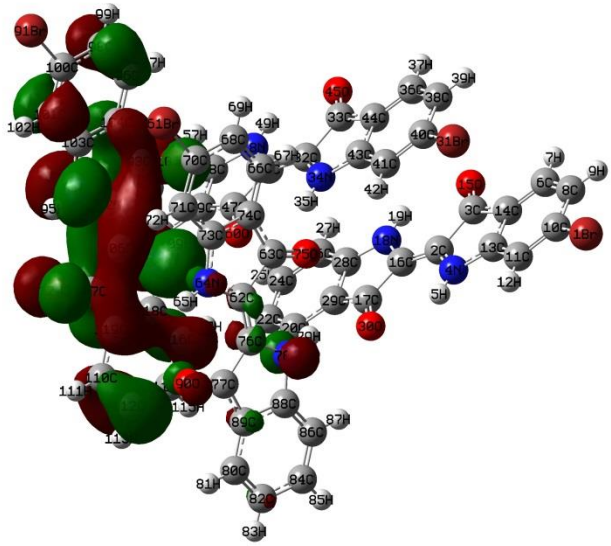

Figure C.25. MBI 4-Molecule Cluster, LUMO (341)

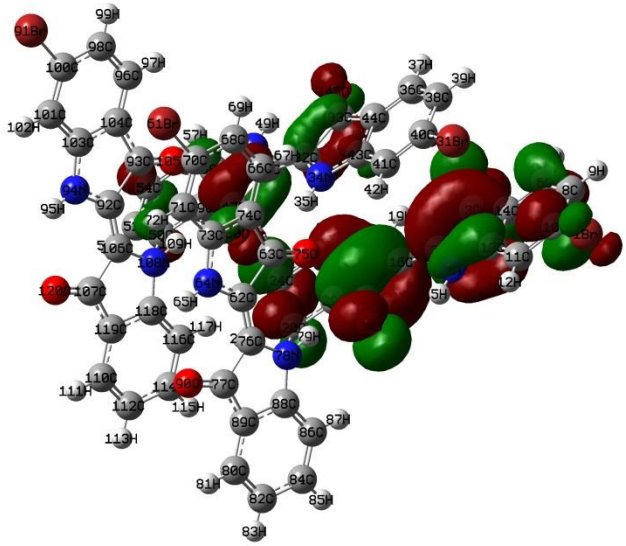

Figure C.26. MBI 5-Molecule Cluster I (center), HOMO (425)

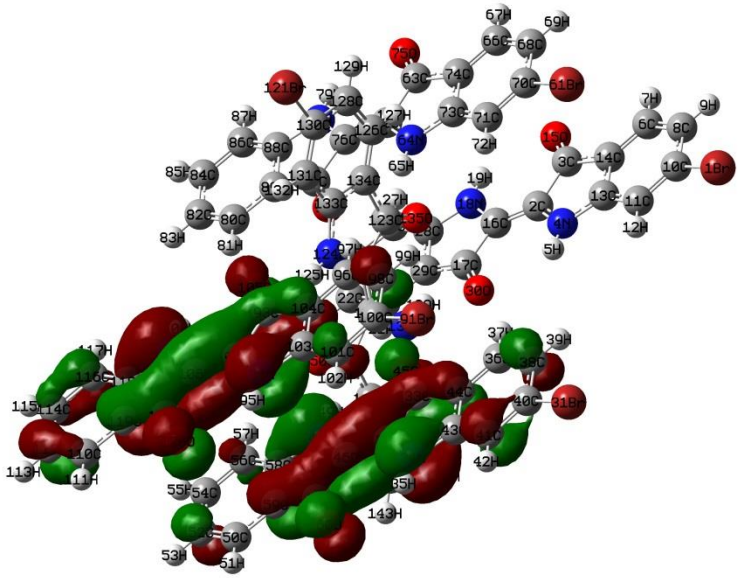

Figure C.27. MBI 5-Molecule Cluster I, LUMO (426)

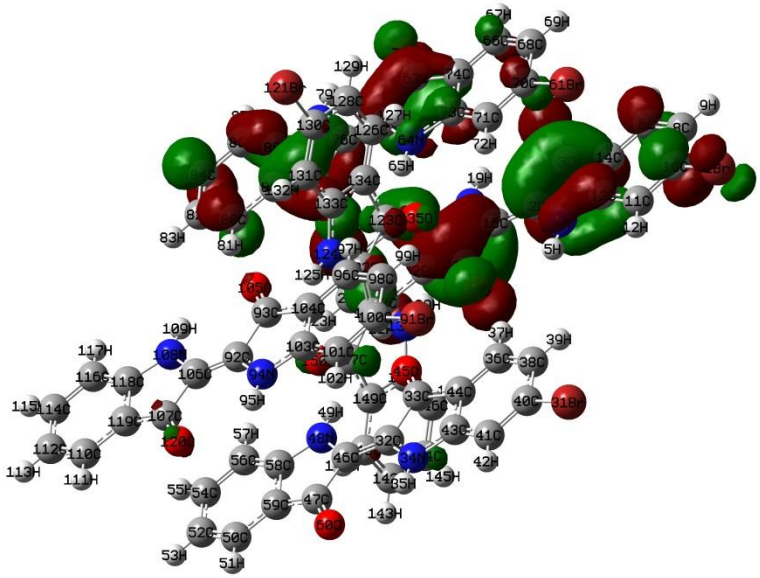

Figure C.28. MBI 5-Molecule Cluster I (center), HOMO-1

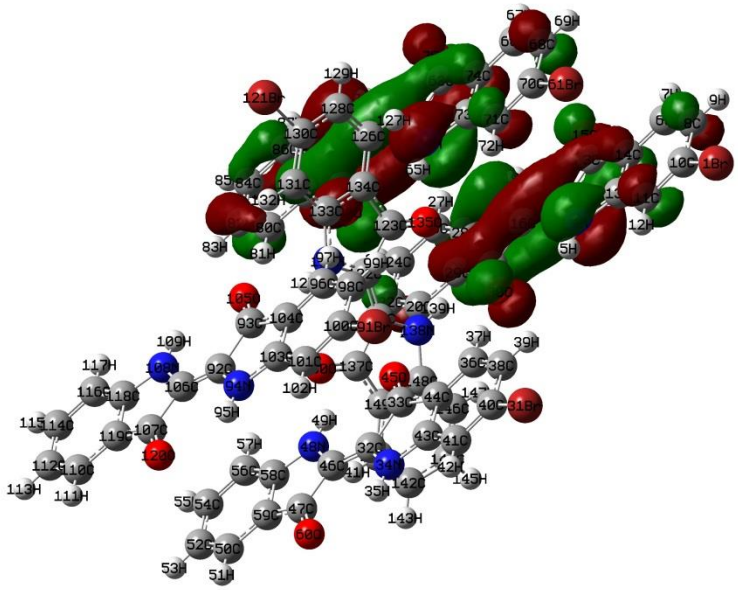

Figure C.29. MBI 5-Molecule Cluster I (center), LUMO+1

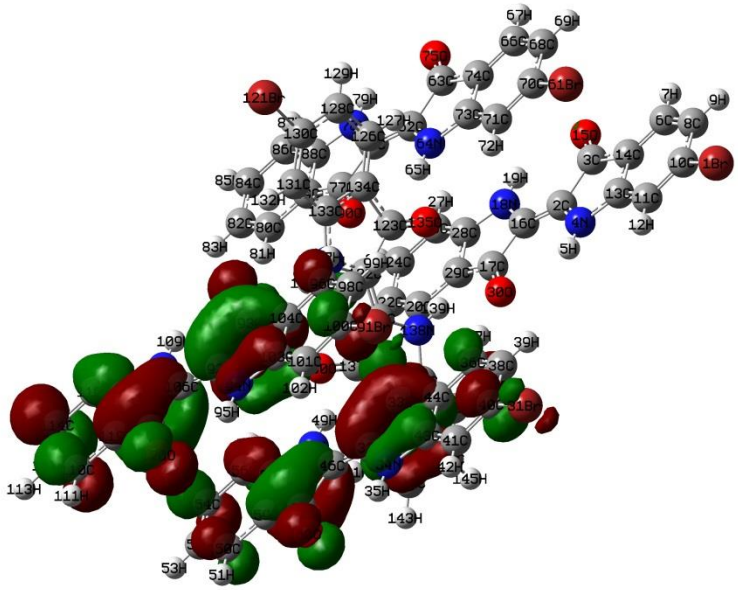

Figure C.30. MBI 5-Molecule Cluster II (end), HOMO (425)

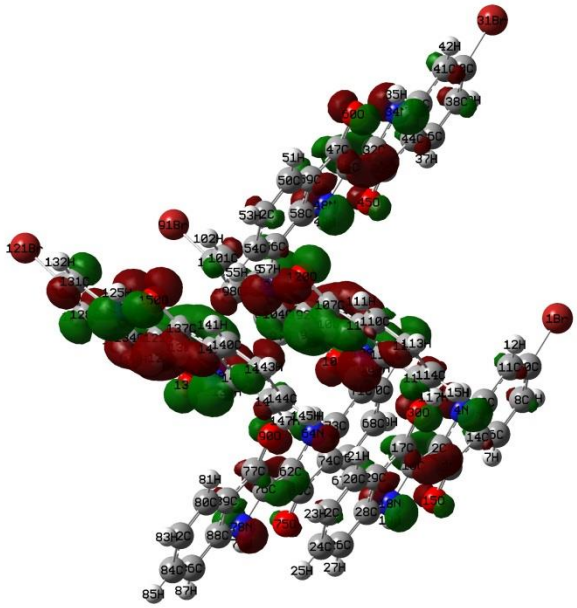

Figure C.31. . MBI 5-Molecule Cluster II (end), LUMO (426)

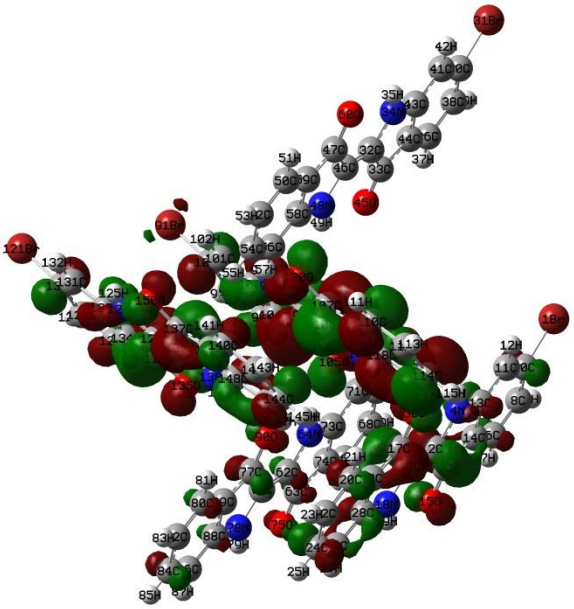

Figure C.32. . MBI 5-Molecule Cluster II (end), HOMO-1

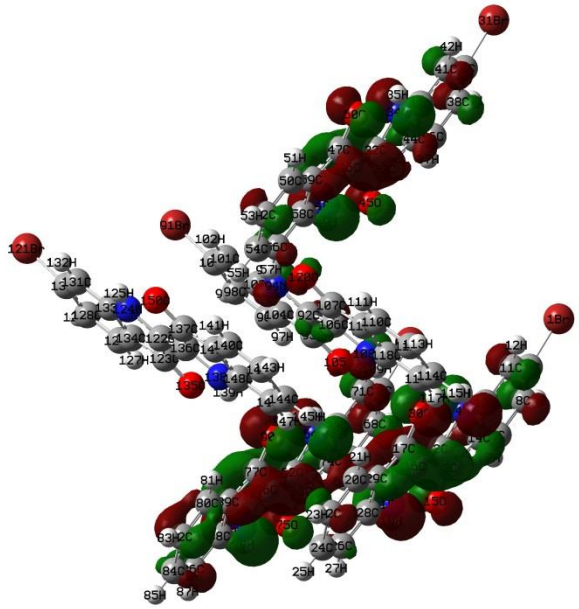

Figure C.33. . MBI 5-Molecule Cluster II (end), LUMO+2

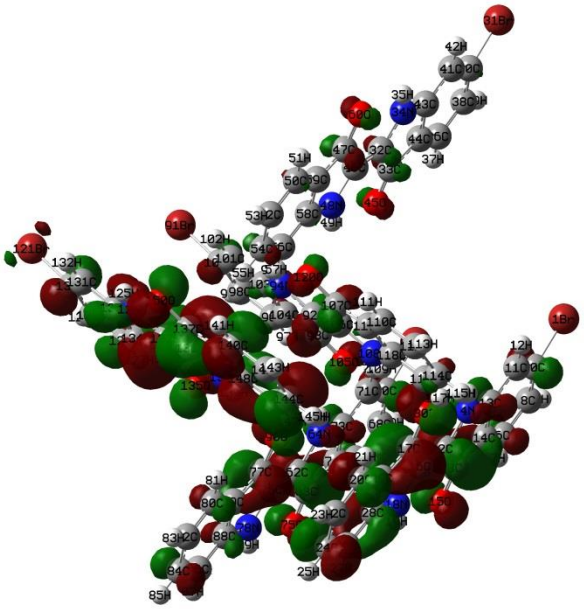

Figure C.34. . MBI 6-Molecule Cluster, HOMO (510)

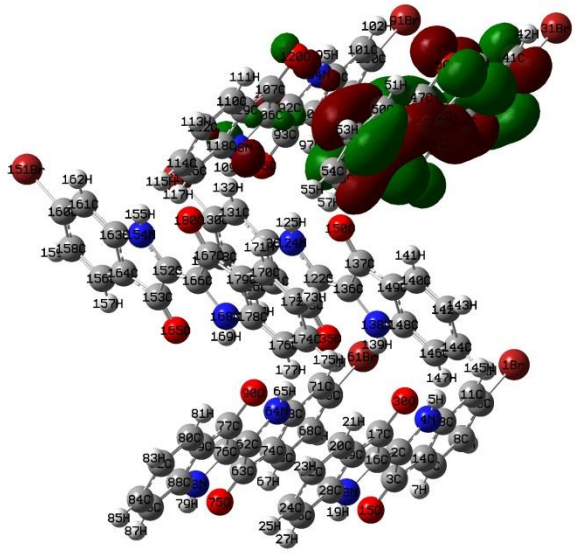

Figure C.35. MBI 6-Molecule Cluster, LUMO (511)

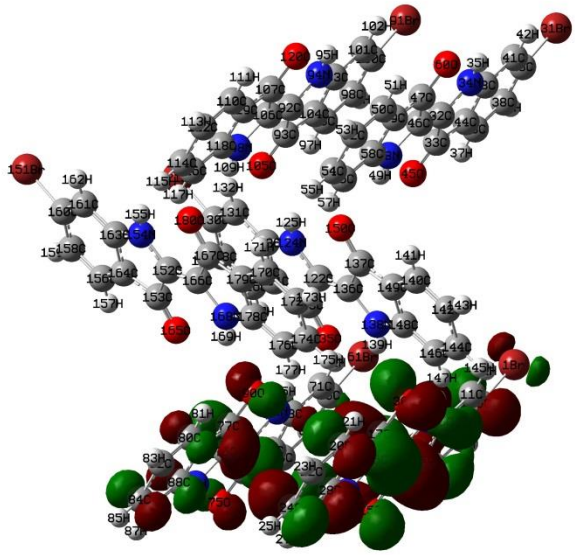

Figure C.36. MBI 6-Molecule Cluster, HOMO-1

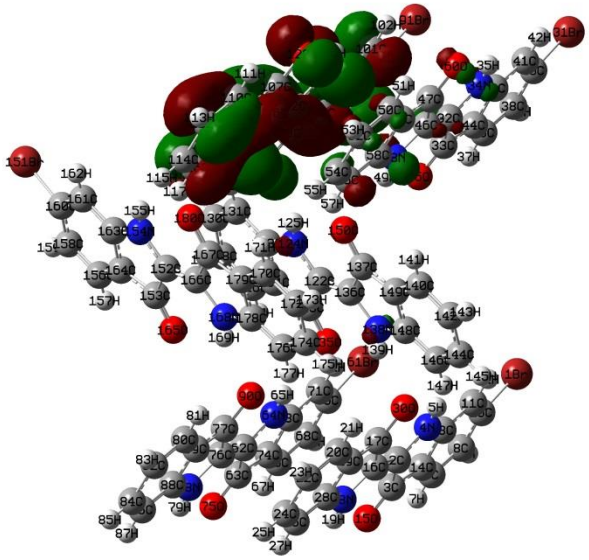

Figure C.37. MBI 6-Molecule Cluster, LUMO+1

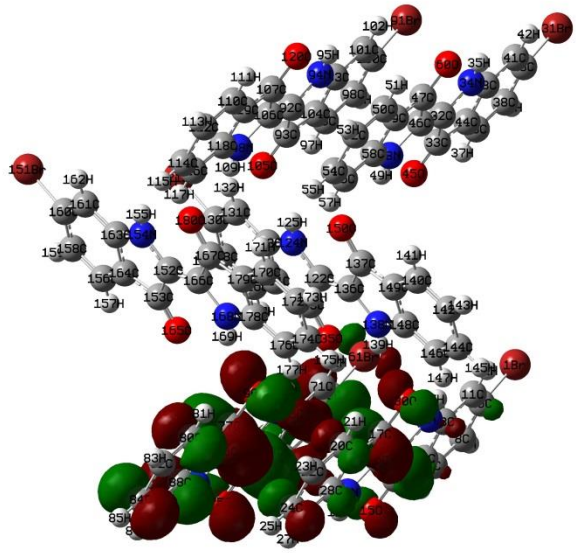

Appendix D: Pictures of dyed fabrics under the microscope (x 50)

Figure D. 16. Under the microscope: Wool Fabrics with MBI (Left: unheated Right: heated)

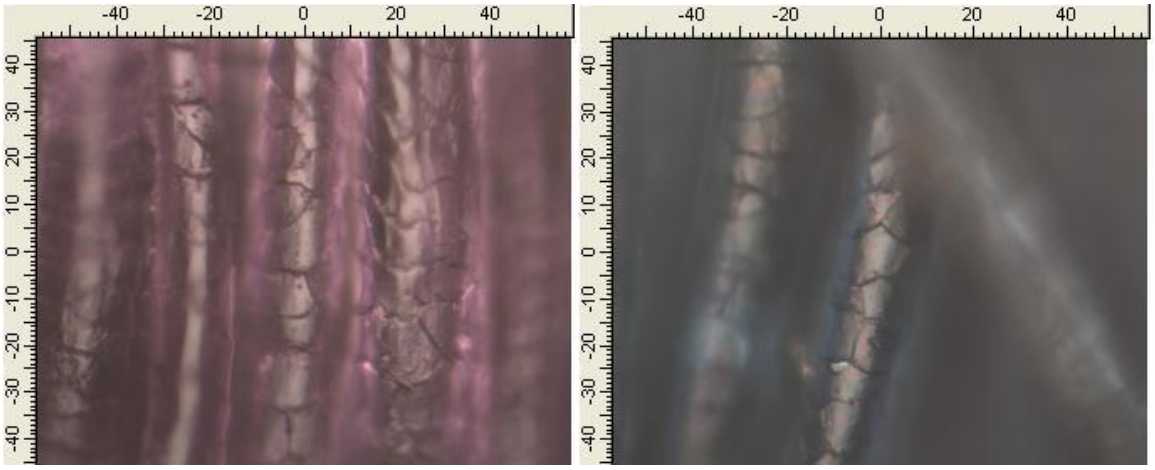

Figure D. 217. Under the microscope: Polyester Fabrics with MBI (Left: unheated Right: heated)

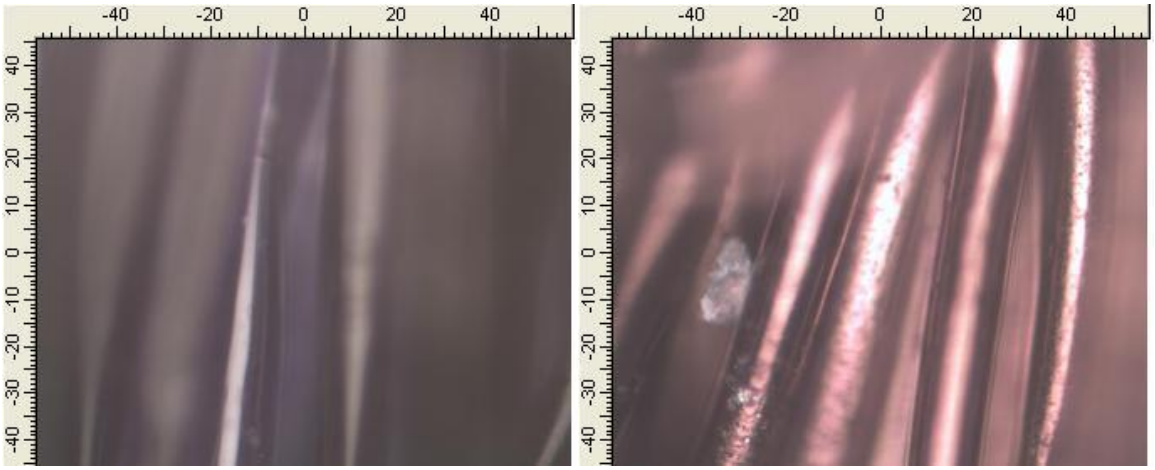

Figure D. 3. Under the microscope: Wool Fabrics with DBI (Left: unheated Right: heated)

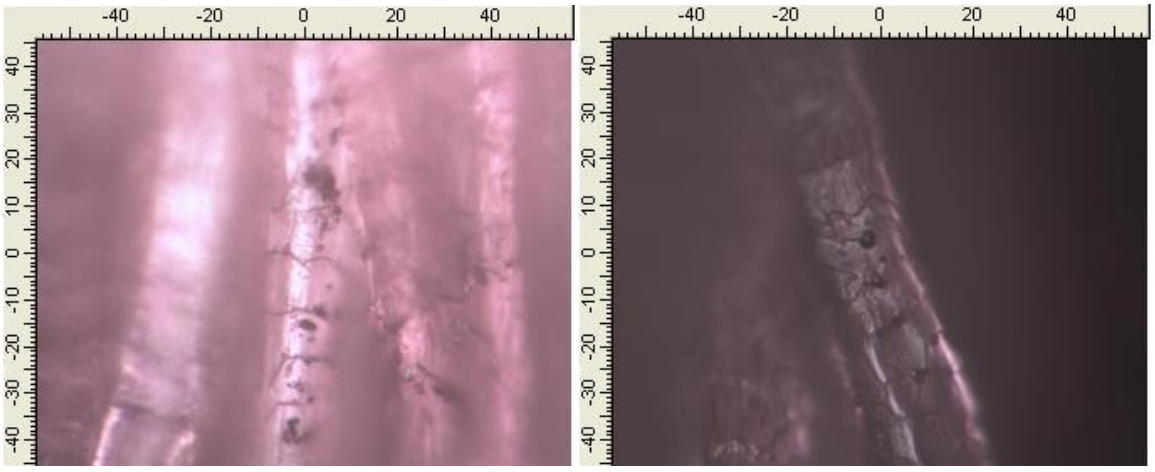

Figure D. 4. Under the microscope: Polyester Fabrics with DBI (Left: unheated Right: heated)

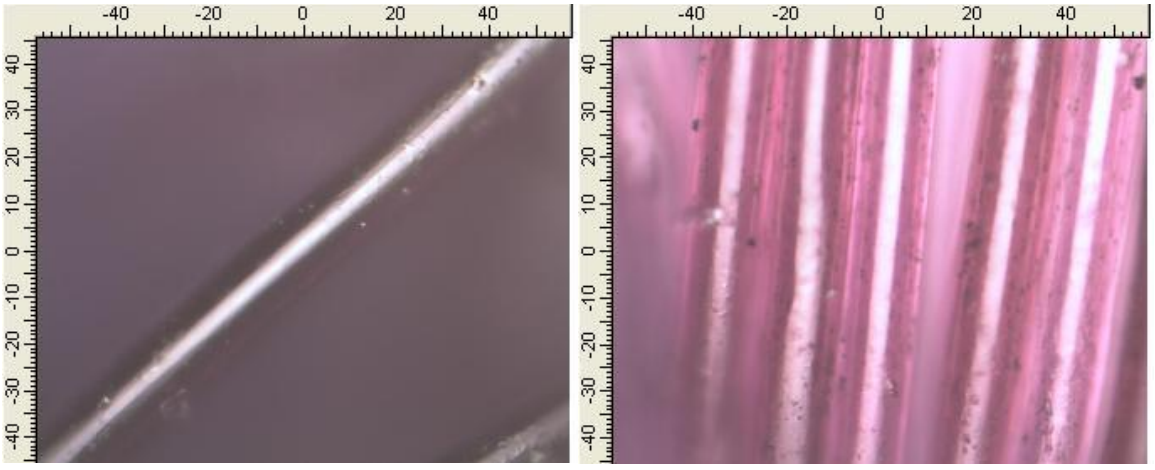

Figure D. 5. Under the microscope: Wool Fabrics with Indigo (Left: unheated Right: heated)

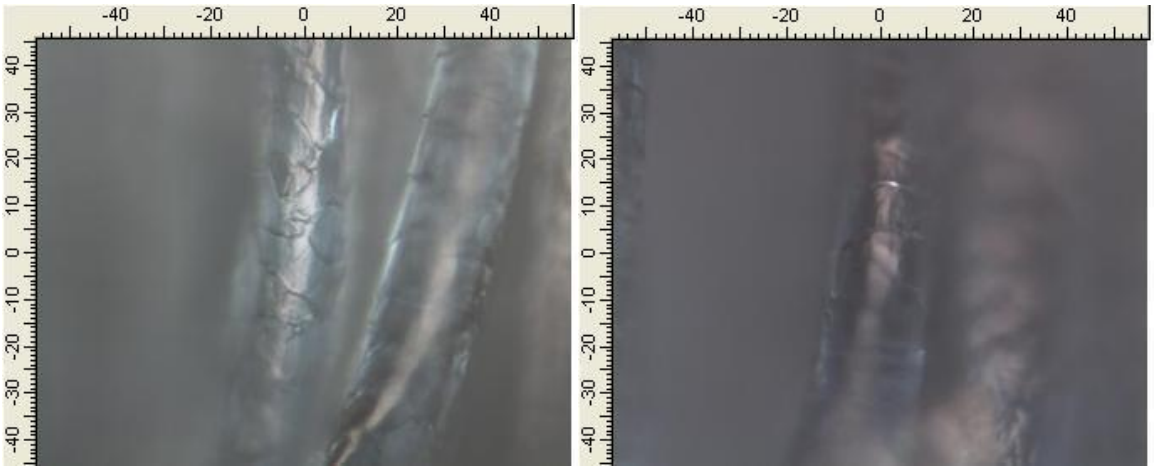

Figure D. 6. Under the microscope: Polyester Fabrics with Indigo (Left: unheated Right: heated)

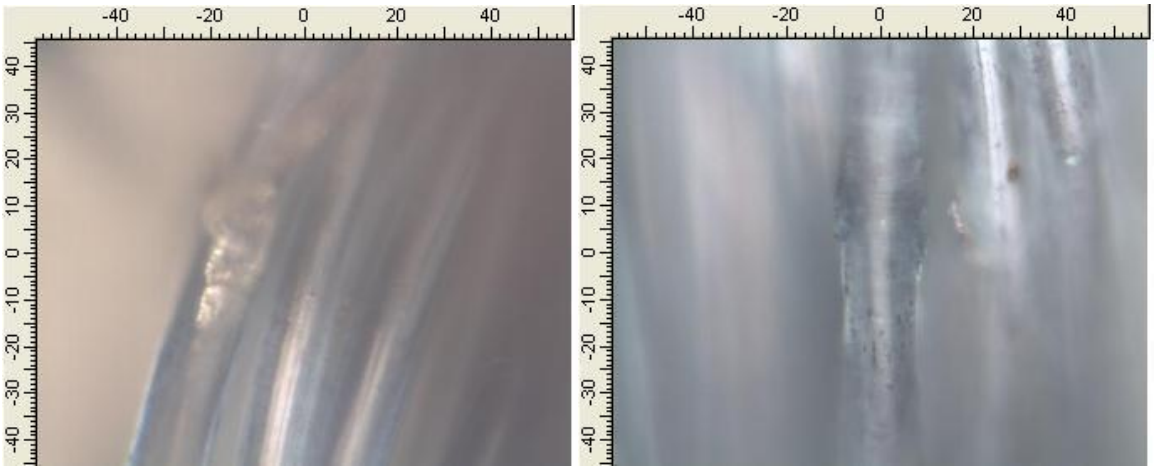

Bibliography

(1) Cooksey, C. *Sci. Prog.* **2013**, *96*, 171–186.
(2) Clark, R. J. H.; Cooksey, C. J. *New J. Chem.* **1999**, *23*, 323–328.
(3) Cooksey, C. J. *Mol. Online Comput. File* **2001**, *6*, 736–739.
(4) Yoshioka, T. *帝王紫探訪 : Teioumurasaki Tanbou (Searching for Royal Purple)*; Shikousha, 1988.
(5) Koren, Z. American Chemical Society, 2006; p. HIST–016.
(6) Koren, Z. *Microchim. Acta* **2007**, *162*, 381–392.
(7) Koren, Zvi Personal Communication.
(8) Ramig, Keith. Personal Communication.
(9) Juraku Corporation, S. R. D. Personal Communication.
(10) Christie, R. M. *Colour Chemistry*; Royal Society of Chemistry, The.
(11) Clark, R. J. H.; Cooksey, C. J.; Daniels, M. A. M.; Withnall, R. *Endeavour* **1993**, *17*, 191–199.
(12) Koren, Z. *Microchim. Acta* **2008**, *162*, 381–392.
(13) Yoshioka, T. *天平の赤・帝王の紫　幻の色を求めて : Tenpei no Aka, Teiou no Murasaki Maboroshi no Iro wo motomete - Yoshioka Tsuneo no Shigoto*; Shikousha, 1989.
(14) Murayama, Sadaya. *人はなぜ色にこだわるか　(Hito ha naze iro ni kodawaruka)*; KK Bestsellers, 1988.
(15) Glowacki, E. D.; Voss, G.; Leonat, L.; Irimia-Vladu, M.; Bauer, S.; Sariciftci, N. S. *Isr. J. Chem.* **2012**, *52*, 540–551.
(16) Eric Daniel Glowacki et al. *J. Mater. Chamistry B 1*, 3742.
(17) Irimia-Vladu, M.; Glowacki, E. D.; Monikowius, U.; Leonat, L.; Schwabegger, G.; Bozkurt, Z.; Sitter, H.; Bauer, S.; Sariciftci, S. American Chemical Society, 2012; p. ENVR–110.
(18) Glowacki, E. D.; Voss, G.; Demirak, K.; Havlicek, M.; Suenger, N.; Okur, A. C.; Monkowius, U.; Gasiorowski, J.; Leonat, L.; Sariciftci, N. S. *Chem. Commun. Camb. U. K.* **2013**, *49*, 6063–6065.
(19) Hirotaka Kojima et al. *Chem Lett* **68 - 70**, *42*, 68 – 70.
(20) Gerlach, H. J. Manufacture of 2-nitrobromobenzaldehydes for the one-step manufacture of 6,6’-dibromoindigo., October 4, 1990.
(21) Sawada, T.; Ishii, H. Method for preparation and storage of 6,6’-dibromoindigo vat dye solutions, and manufacture of goods dyed with the dye solutions., June 19, 2008.
(22) Sawada, T.; Ishii, H. Manufacture of 6,6’-dibromoindigo in good yield., October 4, 2012.
(23) Benkendorff, K.; Westley, C. B.; Gallardo, C. S. *Invertebr. Reprod. Dev.* **2004**, *46*, 93–102.
(24) Benkendorff, K.; Bremner, J. B.; Davis, A. R. *J. Chem. Ecol.* **2000**, *26*, 1037–1050.
(25) Benkendorff, K. *Mar. Drugs* **2013**, *11*, 1370–1398.

(26) Koren, Z. *Isr. J. Chem.* **1995**, *35*, 117 – 124.
(27) Ancient History Encyclopedia. http://www.ancient.eu.com/article/196/.
(28) Cooksey, C. J.; Sinclair, R. S. *Dyes Hist. Archaeol.* **2005**, *20*, 127–135.
(29) Maeda, U. *Kokuritsu Rekishi Minzoku Hakubutukan Kenkyu Houkoku* **1994**, *62*, 61 – 76.
(30) TOBA Sea Folk Museum. Personal Communication, 2012.
(31) *Me de Miru TOBA/SHIMA no Ama*; Umi no Hakubutukan, Ed.; Mie-prefecture, Japan, 2009.
(32) Elsner, O. *Dyes Hist. Archaeol.* **1992**, *10*.
(33) Wikipedia. http://en.wikipedia.org/wiki/Tyrian_purple.
(34) Valdez, P. *J. Exp. Psychol. Gen.* **1994**, *123*, 394 – 409.
(35) Ajiki, H.; Pozzi, F.; Huang, L.; Massa, L.; Leona, M.; Lombardi, J. R. *J. Raman Spectrosc.* **2012**, *43*, 520–525.
(36) Jacquemin, D.; Preat, J.; Wathelet, V.; Perpète, E. A. *J. Chem. Phys.* **2006**, *124*, 074104.
(37) Szalda et al., D. J. *Acta Crystallogr. Sect. C* **2012**, *68*, 160 – 163.
(38) Koren, Z. American Chemical Society, 2008; p. ANYL–081.
(39) Campagna, F.; Palluotto, F.; Carotti, A.; Maciocco, E. *Il Farm.* **2004**, *59*, 849–856.
(40) Campagna, F.; Palluotto, F.; Mascia, M. P.; Maciocco, E.; Marra, C.; Carotti, A.; Carrieri, A. *Il Farm.* **2003**, *58*, 129–140.
(41) Katritzky, A. R. *J Heterocycl. Chem* **1989**, *26*, 821 – 828.
(42) Tahara, R. *Kankyo Kagaku Kenkyu Senta Shoho* **2011**, *1*, 33–37.
(43) Skoog; Holler; Crouch. *Instrumental Analysis*; 6th ed.; Cengage Learning, 2007.
(44) Koren, Z. *Dyes Hist. Archaeol.* **2008**, *21*, 23 – 35.
(45) Koren, Z. *Dyes Pigments* **2012**, *95*, 491–501.
(46) Koren, Z. *MRS Online Proc. Libr.* **2011**, *1374*, 29–47.
(47) Sands, D. E. *Introduction to Crystallography*; Dover.
(48) Haase-Wessel, W.; Ohmasa, M.; Suesse, P. *Naturwissenschaften* **1977**, *64*, 435.
(49) Suesse, P.; Wolf, A. *Naturwissenschaften* **1980**, *67*, 453.
(50) Suesse, P.; Krampe, C. *Naturwissenschaften* **1979**, *66*, 110.
(51) Suesse, P.; Waesche, R. *Naturwissenschaften* **1978**, *65*, 157.
(52) Kettner et al., F. *Acta Cryst* **2011**, *E67*, 2867 –.
(53) *Gaussian 09*; Gaussian, Inc.: Wallingford CT, 2009.
(54) A. Frisch; M. J. Frisch; F. R. Clemente; G. W. Trucks. *Gaussian 09 User's Reference*; 2009.
(55) E. B. Wilson; J. C. Decius; P. C. Cross. *Molecular Vibrations*; McGraw-Hill: New York, 1955.
(56) Ochterski, J. W. Vibrational Analysis in Gaussian help@gaussian.com.
(57) S. Ajith Perera; R. J. Bartlett. *Chem. Phys. Lett.* **1999**, *314*, 381 – 387.
(58) M. J. Frisch; Y. Yamaguchi; J. F. Gaw; H. F. Schaefer III. *J Chem Phys* **1986**, *84*, 531 – 532.
(59) A. D. Becke. *J Chem Phys* **1993**, *98*, 5648 – 5652.
(60) B. Miehlich; A. Savin; H. Stoll; H. Preuss. *Chem Phys Lett* **1989**, *157*, 200 – 206.
(61) McLean, A. D.; Chandler, G. S. *J. Chem. Phys.* **1980**, *72*, 5639–5648.
(62) Clark, T.; Chandrasekhar, J.; Spitznagel, G. W.; Schleyer, P. v. R. *J. Comput. Chem.* **1983**, *4*, 294–301.

(63) Tomkinson, J.; Bacci, M.; Picollo, M.; Colognesi, D. *Vib. Spectrosc.* **2009**, *50*, 268–276.
(64) Teslova, T.; Corredor, C.; Livingstone, R.; Spataru, T.; Birke, R. L.; Lombardi, J. R.; Canamares, M. V.; Leona, M. *J. Raman Spectrosc.* **2007**, *38*, 802–818.
(65) Corredor, C.; Teslova, T.; Canamares, M. V.; Chen, Z.; Zhang, J.; Lombardi, J. R.; Leona, M. *Vib. Spectrosc.* **2009**, *49*, 190–195.
(66) Chang, J.; Canamares, M. V.; Aydin, M.; Vetter, W.; Schreiner, M.; Xu, W.; Lombardi, J. R. *J. Raman Spectrosc.* **2009**, *40*, 1557–1563.
(67) Karapanayiotis, T.; Jorge, V., Susana E.; Bowen, R. D.; Edwards, H. G. M. *Anal. Camb. U. K.* **2004**, *129*, 613–618.
(68) J. B. Lambert; E. P. Mazzola. *Nuclear Magnetic Resonance Spectroscopy*; Pearson/Prentice-Hall: NJ, 2004.
(69) Lavinda, O.; Mironova, I.; Karimi, S.; Pozzi, F.; Samson, J.; Ajiki, H.; Massa, L.; Ramig, K. *Dyes Pigments* **2013**, *96*, 581–589.
(70) W. Kohn; L. J. Sham. *Phys Rev* **1965**, *140*, A1133–A38.
(71) P. Hohenberg; W. Kohn. *Phys Rev* **1964**, *136*, B864–B71.
(72) J. A. Pople; P. M. W. Gill; B. G. Johnson. *Chem Phys Lett* **1992**, *199*, 557 – 60.
(73) Georg Schreckenbach; Tom Ziegler. *J Phys Chem* **1995**, *99*, 606 – 611.
(74) R. McWeeny. *Phys Rev* **1968**, *49*, 4852.
(75) R. Ditchfield. *Mol Phys* **1974**, *27*, 789 – 807.
(76) K. Wolinski; J. F. Hilton; P. Pulay. *J Am Chem Soc* **1990**, *112*, 8251 – 60.
(77) J. R. Cheeseman; G. W. Trucks; T. A. Keith; M. J. Frisch. *J Chem Phys* **1996**, *104*, 5497 – 509.
(78) Antonio Doménech. *J. Phys. Chem. C* **2009**, *113*, 12118 – 12131.
(79) Giuliano Malloci et al. *Mater Res Soc Symp Proc 854*.
(80) Wikipedia. Uv-Vis Reflectance Spectroscopy en.wikipedia.org/wiki/Ultraviolet-visible_spectroscopy.
(81) Pauling. *General Chemistry*; Dover.
(82) *A Dictionary of Science*, 2000.
(83) Judd, D. B. *Goethe's Theory of Colors*; MIT Publisher, 1970.
(84) Rossotti, H. *Color*; Princeton University Press, 1983.
(85) *CRC Handbook of Chemistry and Physics*; 1966.
(86) Tomkinson, J.; Bacci, M.; Picollo, M.; Colognesi, D. *Vib. Spectrosc.* **2009**, *50*, 268–276.
(87) Pople, J. A. *Chem Phys Lett* **1992**, *199*, 557 – 560.
(88) A. Frisch; M. J. Frisch; F. R. Clemente; G. W. Trucks. In *Gaussian 09 User's Reference*; 2009.
(89) G09 Keywords: DFT Methods http://gaussian.com/g_tech/g_ur/k_dft.htm (accessed Dec 12, 2013).
(90) *An Easy Guide to Quantum Chemistry Calcualtions*; Kimihiko Hirao; Tetuya Takeji, Eds.; Koubunsha Scientific: Tokyo, Japan.
(91) Lavine, I. N. *Quantum Chemistry*; 5th ed.; Prentice Hall.
(92) Jensen, F. *Introduction ot Computational Chemistry*; Wiley.
(93) Szabo, A.; Ostlund, N. S. *Modern Quantum Chemistry*; Dover.
(94) James B. Foresman et al. *Exploring Chemistry with Electronic Structure Methods*; Gaussinan Inc,: Pittsburgh, PA.

(95) Suesse, P.; Krampe, C. *Naturwissenschaften* **1979**, *66*, 110.
(96) Christie, R. *Biotech. Histochem.* **2007**, *82*, 51–56.
(97) Lavinda, O. MVI 3256 - YouTube http://www.youtube.com/watch?v=3oNw-khx30E (accessed Dec 10, 2013).
(98) Zollinger, H. *Color chemistry: syntheses, properties, and applications of organic dyes and pigments*; Wiley. com, 2003.
(99) Lewis, G. N.; Calvin, M. *Chem. Rev.* **1939**, *25*, 273–328.
(100) Zollinger, H. *Textilveredlung* **1989**, *24*, 207–212.
(101) Brown, T. E. *Chemistry*; 12th ed.; Prentice Hall.
(102) Graham, B. *Nature's Patterns - Ther Arts, Soul and Science of Engaging Her*; Amazon Digital Services, Inc.
(103) Miehlich, B.; Savin, A.; Stoll, H.; Preuss, H. *Chem. Phys. Lett.* **1989**, *157*, 200–206.
(104) V. Barone; M. Coss. *J Phys Chem A* **1998**, *102*, 1995.
(105) M. Cossi et al. *J Comput Chem* **2003**, *24*, 669 – 81.
(106) G09 Keyword: SCRF http://www.gaussian.com/g_tech/g_ur/k_scrf.htm (accessed Dec 11, 2013).
(107) B. Mennucci; J. Tomasi. *J Chem Phys* **1997**, *106*, 5151 – 58.
(108) E. Cancès et al. *Chem Phys* **1997**, *107*, 3032 – 41.
(109) V. Barone et al. *J Chem Phys* **1997**, *107*, 3210 – 21.
(110) M. Cossi et al. *Chem Phys Lett* **1996**, *255*, 327 – 35.
(111) J. L. Pascual-Ahuir et al. *J Comput Chem* **1994**, *15*, 1127 – 38.
(112) S. Miertuš et al. *Chem Phys* **1981**, *55*, 117 – 29.
(113) S. Miertuš et al. *Chem Phys* **1982**, *65*, 239 – 45.
(114) Larsen, S.; Watjen, F. *Acta Chem. Scand. A* **1980**, *A34*, 171–176.